Photocopy and Use Authorization

In presenting this thesis in partial fulfillment of the requirements for an advanced degree at Idaho State University, I agree that the Library shall make it freely available for inspection. I further state the permission for extensive copying of my thesis for scholarly purposes may be granted by the Dean of Graduate Studies, Dean of my academic division, or by the University Librarian. It is understood that any copying or publication of this thesis for financial gain shall not be allowed without my written permission.

Signature ___________________________

Date _______________________________

Understanding the Radiological Hazards of Generation IV Synchrotron Particle Accelerators and the Novel Technologies that Enable Them

By

Zachary R. Harvey

A dissertation

submitted in partial fulfilment

of the requirements for the degree of

Doctor of Philosophy in Applied Physics

Idaho State University

Spring 2023

To the Graduate Faculty:

The members of the committee appointed to examine the dissertation of Zachary R. Harvey find it satisfactory and recommend that it be accepted.

Dr. Richard Brey,
Committee Chair

Dr. DeWayne Derryberry,
Graduate Faculty Representative

Dr. Thomas Gesell,
Committee Member

Dr. George Imel,
Committee Member

Dr. Chad Pope,
Committee Member

ACKNOWLEDGMENTS

For Melanie and Logan.

There are many people I need to thank for allowing me to complete this work, but I will keep it brief. Thank you, Dr. Richard Brey, for your unwavering support and patience over the last several years. I have no doubt that without your support, I would not have completed this research. Thank you, my committee, for providing insightful comments and helping to increase the quality of my work. A thank you to my bosses over the years and Lawrence Berkeley National Laboratory who have provided me the support to pursue this work and the resources to do so. Lastly, a thank you to my wife for providing encouragement and the time to see it through.

TABLE OF CONTENTS

List of Figures

List of Tables

Understanding the Radiological Hazards of Generation IV Synchrotron Particle Accelerators and the Novel Technologies that Enable Them

Dissertation Abstract – Idaho State University (2023)

New fourth-generation synchrotrons are anticipated to increase the light source brightness by multiple orders of magnitude providing highly coherent x-ray sources. Common to the design of fourth generation ring synchrotrons is the use of swap-out injection of electron bunches. This injection technique and associated issues are examined.

Having a lower beam emittance than ALS results in more electron losses and hence lower beam lifetime, requiring more frequent injection of electrons into the system to maintain current. During operation of the upgraded ALS, the storage ring will contain 11 bunch trains, and the accumulator ring will contain one bunch train. A storage-ring bunch train, approximately once a minute, will trade places with the accumulator-ring train. Each injection of electrons from the booster ring, and each swap of the electron trains has an efficiency and loss which lowers beam lifetime. The anticipated dose and dose rates associated with different beam loss scenarios of the Booster-to-Accumulator, Accumulator-to-Storage, and Storage-to-Accumulator transfer lines have been estimated. The loss rates associated with their respective efficiencies were derived. The decrease of electron beam lifetimes displays an inverse-linear relationship with dose.

Gas bremsstrahlung (GB) will exist throughout the accumulator ring system as electrons collide with molecules of air within the vacuum chamber. MCNP6 BBREM was used to generate more high-energy photons by biasing each sampling of a bremsstrahlung photon toward a larger fraction of the available electron energy. A BBREM:1/*k* source spectra comparison of energy, flux, and error indicated the Monte-Carlo simulation approached the analytical expression's but only to 79.9% of the magnitude of the average bin value. The 1/*k* spectrum included both higher flux and the decreased angular distribution of GB in contrast to the direct generation method of MCNP6.

The temperature inside the storage-ring tunnel will be carefully controlled and the temporal variation limited if the ALS-U is to meet its designed beam emittance. This necessitates several new HVAC penetrations being made inside the inner storage-ring wall. Based upon these analyses, additional shielding will be necessary near all new HVAC penetrations to reduce the photon and neutron dose rates upon upgrade from the current ALS.

Key Words: MCNP, synchrotron, bremsstrahlung, bbrem, bunch swapping

1 INTRODUCTION

To advance the science made possible by synchrotron particle accelerators, new fourth generation machines are currently in the planning stages. These machines are anticipated to increase the light source brightness by multiple orders of magnitude providing highly coherent x-ray sources. Common to the design of fourth generation ring synchrotrons is the use of swap-out injection of electron bunches. Three anticipated problems associated with the new generation of synchrotron accelerators using this injection technique are presented here with insights into a comparison of models, and their solutions that may be applied at other facilities.

1.1 Research Motivation Overview

There are approximately 70 synchrotrons around the world in various stages of development. There are technical differences between the use and capabilities of synchrotrons, with some being used for appliance and others for fundamental/theoretical research. A list of the main large synchrotrons can be found on the lightsources.org website. There are currently more than twenty fourth-generation synchrotron facilities being studied or beginning construction, and one fourth-generation synchrotron facility is operational (MAX IV Sweden). Approximately half of those currently being studied will replace third-generation machines and occupy their physical space, which bring inherent challenges and limitations to radiation mitigation techniques.

The work presented here is tailored to a specifically designed synchrotron facility with its own parameters, however the methods to characterize and mitigate anticipated problems are applicable to any fourth-generation, ring-type synchrotron facility. In addition to characterizing this synchrotron facility, this work:

- Compares MCNP6 gas bremsstrahlung models and variance reduction source terms against analytical derivations of the fraction of the electron beam power that is converted to photons combined with a conservative spectrum assumption of $1/k$. The most conservative spectrum was used to produce dose equivalent rates during early operations when outgassing of components is highest and of the most concern to health and safety
- Addresses the reality of spatial limitations associated with existing facilities and the placement of new accelerators that carry additional physical operational requirements for cooling and electrical penetrations beyond third-generation facilities
- Derives and quantifies charge loss scenarios associated with the complex electron bunch swapping techniques of new fourth-generation facilities and demonstrates the inverse-linear relation of dose rates with beam lifetime due to those charge losses.

1.2 Description and Statement of Problem

LBNL is designing a new electron synchrotron for scientific research using synchrotron radiation. ALS-U is an ongoing upgrade of the ALS at Berkeley Lab that will endow the ALS with new x-ray capabilities. These new capabilities enable the production of highly focused beams of soft x-ray light that are at least 100 times brighter than those of the existing ALS. The ALS is a 1.9-GeV storage ring operating at 500 mA of beam current. It is optimized to produce intense beams of soft x-rays, which offer spectroscopic contrast, nanometer-scale resolution, and broad temporal sensitivity.

Upgrading the ALS from a triple-bend-achromat to a multibend-achromat (MBA) lattice design will provide a soft x-ray source that is 100 to 1,000 times brighter than today's ALS and will provide a significantly higher fraction of coherent light in the soft x-ray region than is currently available at the ALS. The upgraded ALS will offer the highest coherent flux of any existing or planned storage-ring facility, worldwide, and this will span up to a photon energy of 3.5 keV. The addition of an accumulator ring that enables on-axis, swap-out and recovery and exchange of bunch trains is required to achieve this coherence and brightness.

The accumulator ring is novel equipment relative to the ALS that will enable new science, as such characterization of the radiation generated by the addition of this new component and the complex nature of bunch swapping is required. The accumulator ring has two main functions (LBNL 2018):

1. To dampen the beam emittance before injection into the small storage-ring dynamic aperture.
2. To store the beam for top-off in between swap-outs.

During operation of the upgraded ALS, the storage ring will contain about 11 bunch trains (each in turn containing about 26 bunches) and the associated accumulator ring will contain one bunch train. To keep the emittance of the storage ring beam sufficiently low, approximately once a minute, a storage-ring bunch train will trade places with the accumulator-ring bunch train. Between swap-outs, the train in the accumulator will be topped off by the existing LINAC/booster injector. By swapping a storage-ring bunch train that has lost a portion of its current with the topped-off bunch train from the accumulator, the overall current in the storage ring will be maintained at a nominal 500 mA (LBNL 2018). This technique of electron bunch swap-out is shared among fourth generation ring synchrotrons. However, the Advanced Photon Source – Upgrade design concept is to perform a direct bunch swap into the storage ring. This swap-out design will share common pitfalls as well as advantages in any machine it is employed. This research provides a method to derive and quantify charge loss scenarios in different operational modes which could be used at other facilities. This was used to creates model that demonstrates the inverse-linear relationship of beam lifetime to dose equivalent rates and can be used to scale expected dose rates.

Gas bremsstrahlung (GB) will exist throughout the entire accelerator system as electrons collide with molecules of air located within the vacuum chamber. The amount of GB produced will vary linearly with the length of an accelerator straight, pressure, beam current, and electron energy. GB is often estimated to have a $1/k$ energy spectrum (with k denoted as the photon energy to distinguish it from the electron beam energy). Methods are demonstrated to calculate the GB produced and its effect on dose rates during early synchrotron operations. This is used for a comparison of Monte-Carlo technique efficacy against analytical calculations deriving the gas bremsstrahlung spectra. This research was not designed to be a validation experiment, however it does demonstrate numerical approximation characteristics against simulations to provide verification data as defined by (Roy, Oberkampf). Select results from this research on GB were published in Nuclear Inst. And Methods in Physics Research, A (Harvey 2020).

In any fourth-generation ring synchrotron, the temperature inside the storage-ring tunnel will need to be carefully controlled and the temporal variation limited in order for the MBA to meet its designed beam emittance. For existing facilities being retrofitted (ALS-U), this necessitates the redesign of the HVAC system supplying air flow in the storage-ring tunnel. As a result, several new HVAC penetrations will need to be made inside the inner storage-ring wall. Additional electrical penetrations will need to be added to the inner storage ring wall to support equipment inside the storage ring. This research addresses the reality of spatial limitations associated with existing facilities and the placement within of new accelerators that carry certain physical operational requirements. I provide techniques to simulate losses in the accelerator with associated dose rates through these HVAC and electrical penetrations with novel shielding designs that could be utilized at other facilities.

2 LITERATURE REVIEW

2.1 Particle Accelerators

The century long history of particle accelerators parallels the discovery of the atomic nucleus and natural radioactive decay. The demand for artificially created highly energetic particles has continuously grown. Breunlin provides a brief history of particle accelerators leading to generation four synchrotrons (Breunlin, 2016).

The earliest particle accelerators were electrostatic based machines in which a high electric potential difference was used to accelerate charged particles. The Cockcroft-Walton accelerator is the first accelerator circa 1932 credited with achieving a potential of 800 kV in which to accelerate protons (Cockcroft et. al, 1932).

A design variant beyond electrostatic machines are linear accelerators. This accelerator type is characterized by an accelerating electric field. A result of the single accelerator pass is that the maximum available accelerating potential is limited. This limitation was sidestepped with the development of repeated acceleration machines such as linear-staged accelerators, or circular design accelerators such as the cyclotron (Lawrence et. al, 1930). Cyclotrons are characterized by a magnetic dipole field that bends the particle trajectory into the shape of a spiral and a process that uses (alternating) potential voltage several times for acceleration. The energy gain achievable in a cyclotron particle accelerator is limited by this magnetic field (required to bend the beam), but also by desynchronization of the voltage input to the particle position, a problem experienced as particles exhibit relativistic effects.

Another design of the circular accelerator is the synchrotron. Synchrotrons are characterized by particles which follow a well-defined orbit instead of a decaying spiral. The time in which a particle is accelerated in a synchrotron is not limited by desynchronization or decaying orbit as in a cyclotron. To maintain a constant orbital radius, the magnetic field that bends the particle trajectory must be increased synchronously with rising particle energy. An early synchrotron design accelerated electrons up to 70MeV. The required magnetic steering of the particles produced the first observed synchrotron radiation (Elder et al., 1947). Synchrotron radiation is the electromagnetic radiation emitted when relativistic charged particles are subject to an acceleration perpendicular to their velocity. This first generation of synchrotrons produced this synchrotron as a by-product of magnetic steering of electrons, not as an objective of the acceleration.

Early synchrotrons required relatively large vacuum apertures and magnet geometries due to the particle beam size and large divergence. This limitation was due to the availability of only weak focusing magnetics. A milestone leading to development of the modern synchrotron was the discovery of strong focusing that could be produced by quadrupole magnets (Christofilos, 1950)(Courant et al., 1952). A quadrupole (four-pole) magnet provides a magnetic field configuration that produces a similar effect on a beam of charged particles as a lens does to a light beam. An important difference, as compared to a lens, is that a quadrupole magnet focuses in one vertical plane, but defocuses in the horizontal plane. Using a combination of focusing and defocusing quadrupoles, a net focusing effect may be used to achieve focusing in both planes. Strong focusing with quadrupoles exceeds weak focusing effects by multiple orders of magnitude, and therefore reduces the transverse beam dimensions. This effect allows for compact vacuum chambers and magnet geometries. Together with the longitudinal phase focusing, or shortening of the length of bunches, it became possible to construct synchrotrons capable of producing particle beams with high energies and intensities, but low emittances or spread. Combined with a stable radius orbit, the beams are able to circulate for hours in storage rings (Breunlin, 2016).

2.2 Synchrotrons

Synchrotron accelerators and their resulting synchrotron radiation have significant application in various research fields such as: chemistry, biology, crystallography, medicine and material science. Synchrotron radiation is useful as a beam diagnostic as it carries information about the transverse size and emittance of the electron beam as well. To accomplish this purpose, the visible and near-visible part of the radiation spectrum are focused by a lens in a diagnostic beamline, creating an image of the electron beam. Having a very low vertical emittance comes with an associated downside, such as: an increased loss rate of electrons from the beam or even an increased horizontal emittance. This is due to proximity of and the resulting interaction of electrons within the same bunch.

The first generation of synchrotrons used parasitic light sources, or synchrotron production from an accelerator in which synchrotron radiation generation is not the primary use.

This was followed by a second generation of accelerator with an associated synchrotron storage ring that was built exclusively for the production of synchrotron radiation from bending (dipole) magnets.

Third generation synchrotron light sources have been developed to further progress towards low electron beam emittance and are optimized for synchrotron radiation production in dedicated insertion devices. Insertion devices are magnetic structures inserted into straight sections of the storage ring for the purpose of synchrotron radiation production at high brightness. Insertion devices consist of a sequence of dipole magnets of opposite polarity causing no net deflection of the electron beam. The characteristic synchrotron radiation emitted from the insertion device depends largely on the design of the device. This design is often centered around the strength of the magnetic field and resulting physical gap between magnets which is tailored to the requirements of synchrotron radiation experiments, rather than by the dynamics of the stored electron beam (Breunlin, 2016).

Research facilities operating synchrotron radiation sources of the third generation exist worldwide. These operate at electron energies that are tailored to produce different synchrotron radiation energies. Operating at 1.9 GeV, the Advanced Light Source (ALS) produces soft x-rays, ultraviolet light, and infrared light in 40 different beamlines. Low-energy “soft” x-ray light is the ALS specialty, filling an important niche and complementing other Department of Energy light source facilities. These soft x-rays reveal the atomic and electronic structure of matter which is the first step toward designing new materials.

2.3 Fourth Generation Light Sources

Fourth generation light sources seek to further reduce the emittance in both the horizontal and vertical planes. The issue of large horizontal emittance seen in third generation light sources in the storage ring may be decreased by employing a larger number of bending magnets, each with a smaller beam deflection. The use of a multi-bend achromat (MBA) lattices to make multiple, relatively shallow bends and using strong quadrupole magnets for refocusing in between bends, allows for suppression of dispersion characteristics and lowers the net emittance. The net emittance of a MBA lattice can easily be one order of magnitude lower than in a comparable synchrotron light source of the third generation utilizing two (double-bend achromat) or three (triple-bend achromat) bending magnets per achromat, thus justifying the technological leap to naming a fourth generation storage ring light source (Hettel, 2014).

The MBA lattice, however, comes with design challenges for accelerator hardware and beam dynamics that needed to be solved prior to construction of a storage ring of this type. Namely, small apertures of the vacuum system require distributed pumping. Small vacuum chamber apertures, together with progresses in the field of magnet technology in terms of magnet performance and manufacturing precision (Johansson et al. 2014), make sufficiently high quadrupole and sextupole gradients feasible. These are a requirement of the MBA lattice.

The electron beam emittance is an important criterion in a synchrotron light source, since it has a significant influence on the brightness of the radiation produced. Brightness is the number of photons emitted per second, per mm^2, per $mrad^2$ and per 0.1% of the bandwidth of the radiation (Breunlin, 2016). As previously stated, the practical issue with lower beam emittance is significant beam losses due to instabilities of the electron bunches. These losses result in the generation of undesired secondary radiation due to bremsstrahlung radiation showers and drive the need for more frequent electron bunch top-off operations. At all energies, photons produced by bremsstrahlung dominate the unshielded radiation fields aside from the hazard of the direct beam itself. Additionally, as the electron beam and resulting bremsstrahlung photon energy increases, neutrons become a significant problem as the electromagnetic cascade produces photoneutrons.

2.4 Monte Carlo Methods in Radiation Transport

Monte Carlo methods and software such as Monte Carlo N-Particle 6 (MCNP6) use a calculation technique that is well suited for complicated problems such as electron beam losses and the resulting radiation showers. The principal concept of a Monte Carlo calculation is to follow the entire life cycle of a given particle from emission to death by absorption or escape from the simulated system boundary. The tally or outcome of the various interactions that may occur during the particle's life are randomly sampled and simulated according to the laws of particle physics. These methods are based upon random selection of alternate fates for each step of a particle's experience that is consistent with probability distributions for scattering angles, track lengths and distances between collisions. This is repeated for a large number of particles. A resulting simulation may sample $1x10^6$ to $1x10^9$ or more particle random walks. Making proper assumptions in Monte Carlo simulations are essential as a simulation will typically reflect only a fraction of the total number of particles in real systems. Without proper assumptions a detailed simulation of the transport process may result in a large cost of computing time (Chinaka, 2014).

2.5 Accumulator Ring

During operation of the upgraded ALS, the storage ring will contain about 11 bunch trains (each in turn containing about 26 electron bunches spaced 2 nanoseconds [nsec] apart), and the associated accumulator ring will contain one bunch train. The emittance of the beam in the accumulator will be approximately 2 nanometers (nm) rad (similar to the current ALS). Approximately once a minute, a storage-ring bunch train will trade places with the accumulator-ring bunch train. Fast kicker magnets will generate a pulse, sending a train from the storage ring to the accumulator. At the same time, the accumulator train will be moved to the storage ring (see Figure 2.1).

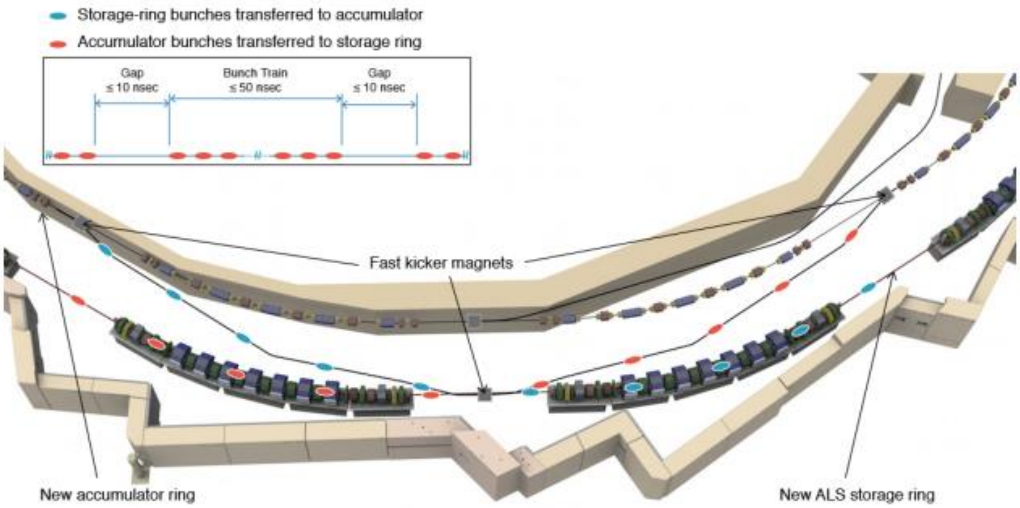

Figure 2.1. Illustration of bunch train swap-out between the storage and accumulator rings. A train of fresh bunches (red) is injected into the storage ring while simultaneously, a train of spent bunches (blue) is extracted. The "in" and "out" bunches will cross in the fast kicker structures installed on the storage ring (LBNL 2018).

Between swap-outs, the train in the accumulator will be topped-off by the existing LINAC/booster injector, similar to the current top-off injection into the storage ring. By swapping a storage-ring bunch train that has lost a portion of its current with the topped-off bunch train from the accumulator, the overall current in the storage ring will be maintained at 500 mA.

The accumulator ring has two main functions, as follows: to dampen the beam emittance before injection into the small storage-ring dynamic aperture, and to store the beam for top-off in between swap-outs (LBNL 2018).

The accumulation injection section is to be placed across from the current ALS injection section (corresponding to the ALS-U straight section with the swap-out fast kicker), aligning the layout phases of the two 12-fold periodic rings. The accumulator is planned to be anchored to the interior wall of the existing storage-ring tunnel, design emphasis is placed on attempting to minimize the magnet weight and ease the requirements on the support system.

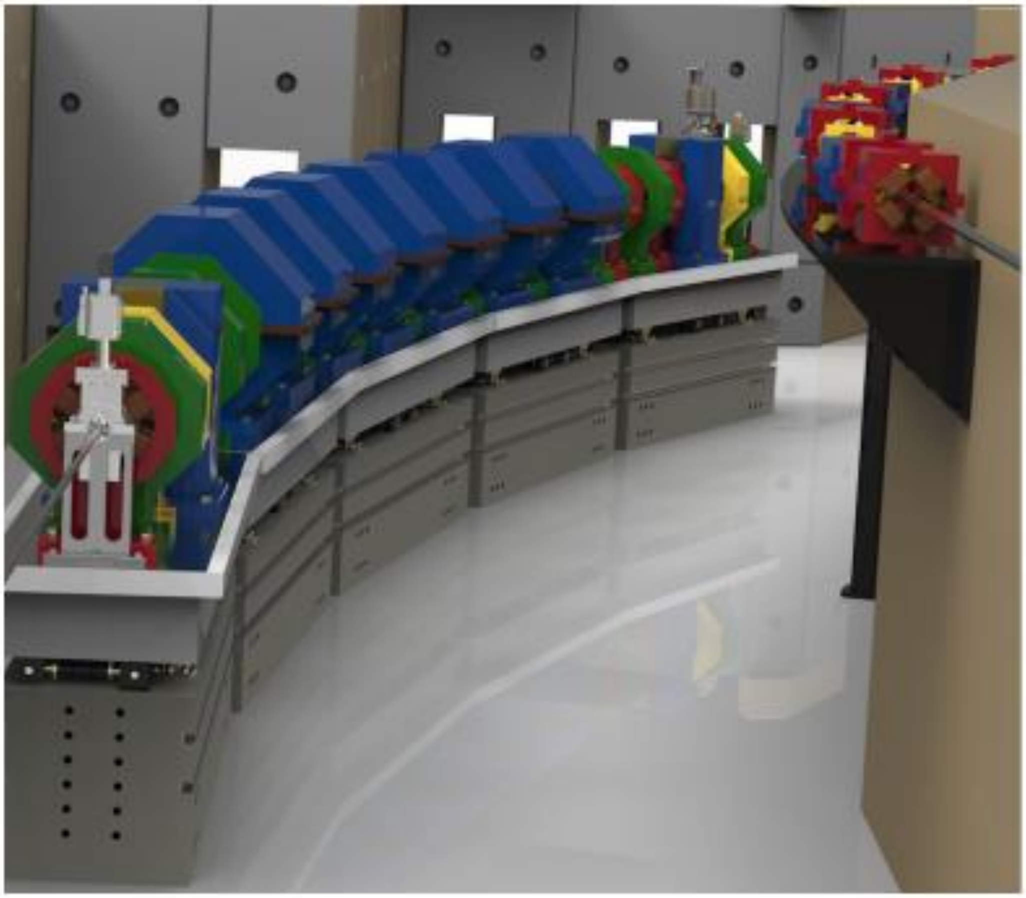

Figure 2.2. View from inside the tunnel showing a full arc of the storage ring and a portion of the accumulator ring anchored to the concrete wall (top right corner). Source: ALS-U Conceptual Design Report

2.6 Gas Bremsstrahlung

In high energy electron accelerators, electrons will interact with nuclei to produce photons by bremsstrahlung. When the produced high-energy photon interacts in the air, which consists of about 78% N and 21% O, it will do so mostly with the electric charge of the atomic nuclei to produce electron-positron pairs. After a given interaction step the two particles produced in the processes share equally the energy. In this way the overall number of particles in the shower is doubled at each interaction stage and their average energy is halved. The exponential growth in the number of secondaries continues until the typical energy per particle gets smaller than critical value E_c at 84 MeV, so that the interactions with atomic electrons becomes relevant and the overall energy of the shower starts to be dissipated (Mollerach 2017).

This gas bremsstrahlung (GB) will exist throughout the entire accumulator ring system as electrons collide with molecules of air located within the vacuum chamber. The amount of GB produced will vary linearly with the length of a straight, pressure, beam current, and electron energy.

The energy spectrum of the radiated photons ranges from zero to the energy of the incident electron and the number of photons in a given energy interval is approximately inversely proportional to the photon energy. The amount of energy radiated per energy interval is practically constant according to Fassò et al. (Fasso 1990). For thin targets of thickness x (where $x \ll X_o$), the spectrum of photons of energy k per energy interval dk (dN/dk), can be approximated by Equation 1. A typical straight length of vacuum chamber may be 7-meters, as opposed to the radiation length of air (X_o) 37 g/cm^2 at low vacuum pressures (5.3×10^{-10} atm). Thus, the length parameters become insignificant and drop out of the equation, $1/k$ remains (Cossairt 2011). The radiation length of a material is the mean length (in cm) to reduce the energy of an electron by the factor 1/e.

$$dN/dk \propto x / (X_o \cdot k) \qquad (1)$$

As derived above using thin target assumptions, GB is often estimated to have this $1/k$ energy spectrum (with k denoted as the photon energy to distinguish it from the electron beam energy). The spectrum extends essentially from zero to the kinetic energy of the stored electrons (Liu et, al 2001). The angular distribution is highly forward-peaked having a characteristic angle (i.e., a “1/e” angle) of 0.511/E in radians for electron beam energy E (MeV). The characteristic angle for ALS-U’s 2 GeV electron beam is 0.256 milliradians (SLAC 2017B).

2.7 HVAC and Electrical Penetrations

The temperature inside the storage-ring tunnel will need to be carefully controlled and the temporal variation limited in order for the ALS-U to meet its designed beam emittance. This necessitates the redesign of the HVAC system supplying air flow in the storage-ring tunnel. As a result, several new HVAC penetrations will need to be made inside the inner storage-ring wall. The exact location of these HVAC penetrations around the storage-ring inner wall has not yet been decided, but their dimensions are known. These penetrations will be placed at a height just below the accumulator ring and above the storage ring.

To support equipment inside the storage ring, additional electrical penetrations will need to be added to the inner storage ring wall. The new penetrations are anticipated to be 6-inches in diameter, which is wider than the current 4-inch diameter holes.

The most natural choice is to place the accumulation injection section across the current ALS injection section (corresponding to the ALS-U straight section with the swap-out fast kicker), aligning the layout phases of the two 12-fold periodic rings. The accumulator is planned to be anchored to the interior wall of the existing storage-ring tunnel (see Figure 2.2); design emphasis is placed on attempting to minimize the magnet weight and ease the requirements on the support system (LBNL 2018). This places a source of scatter radiation close to the planned HVAC penetrations.

2.8 Electron Bunch Swapping and Beam Lifetime

During operation of the upgraded ALS, the storage ring will contain about 11 bunch trains (each in turn containing about 26 bunches spaced 2 nanoseconds [nsec] apart), and the associated accumulator ring will contain one bunch train. To keep the emittance of the storage ring beam sufficiently low, approximately once a minute, a storage-ring bunch train will trade places with the accumulator-ring bunch train. Between swap-outs, the train in the accumulator will be topped off by the existing LINAC/booster injector. By swapping a storage-ring bunch train that has lost a portion of its current with the topped-off bunch train from the accumulator, the overall current in the storage ring will be maintained at a nominal 500 mA (LBNL 2018).

Having a lower beam emittance than ALS results in significantly more electron losses and hence lower beam lifetime. Beam lifetime is defined here as the time for the beam current to decrease to 1/e of its initial value due to continuous losses, with e being Euler's number. The two main processes contributing to the beam lifetime within a third-generation storage ring are the Touscheck scattering and gas scattering. However, fourth-generation synchrotrons utilize bunch swapping to help meet emittance requirements. Swapping the electron bunch trains between the storage-ring and the accumulator-ring result in additional loss modes not seen in third-generation synchrotrons. Estimates place the potential lifetime of ALS-U as low as 30 minutes but nominally near 60 minutes. Having a lower lifetime requires more frequent injection of electrons into the system to maintain current. Each injection of electrons from the booster ring, and each swap of the electron trains between the storage ring and accumulator ring has an associated efficiency. Losses that result from these injections and swaps lower beam lifetime.

Understanding the effect of beam lifetime and its relationship to bunch swapping is essential. This should also result in the ability to scale dose rates at specific locations as a function of beam lifetime.

3 Hypothesis Statements

3.1 Problem 1: Gas Bremsstrahlung

Gas bremsstrahlung (GB) will exist throughout the entire accumulator ring system as electrons collide with molecules of air located within the vacuum chamber. The amount of GB produced will vary linearly with the length of an accelerator straight, and with pressure, beam current, and electron energy. The radiation shielding considerations that account for gas bremsstrahlung production for the Advanced Light Source Upgrade's accumulator-ring, during early commissioning, need to be understood.

3.1.1 Hypothesis Statement 1

Null Hypothesis: Analytical expressions to derive gas bremsstrahlung fluence **can** approximate MCNP6 Monte-Carlo simulations and BBREM variance reduction biasing techniques within MCNP6 to 95% accuracy.

Alternate Hypothesis: Analytical expressions to derive gas bremsstrahlung fluence **cannot** approximate MCNP6 monte-carlo simulations and BBREM variance reduction biasing techniques within MCNP6 to 95% accuracy.

Decision Rule 1: the null hypothesis will be supported and the alternate rejected if the analytical expression and MCNP6 BBREM source terms are within a 95% average agreement over all energy bins up to the maximum energy of ALS-U (2 GeV).

3.2 Problem 2: HVAC and Electrical Penetrations

Constructing a new particle accelerator within the confines of the existing storage ring shielding presents a number of challenges. The ALS-U can meet its designed beam emittance if the temperature inside the storage-ring tunnel is carefully controlled and the temporal variation limited. This necessitates the redesign of the HVAC system supplying air flow in the storage-ring tunnel. As a result, several new HVAC penetrations will need to be made inside the inner storage-ring wall. The exact location of these HVAC penetrations around the storage-ring inner wall has not yet been decided, but their dimensions are known. Generally, these penetrations will be placed at a height just below the accumulator ring and above the storage ring. Due to ring symmetry, the exact location is unnecessary for analysis.

To support equipment inside the storage ring, additional electrical penetrations will need to be added to the inner storage ring wall. The new penetrations are anticipated to be 6 inches in diameter, which is wider than the current 4-inch-diameter holes. The radiation shielding considerations that account for bremsstrahlung radiation production from electron beam losses from the Advanced Light Source Upgrade need to be understood.

3.2.1 Hypothesis Statement 2

Null Hypothesis: Geometric factors in addition to the existing shield wall of the 3rd generation light source are sufficient to allow for the addition of an accumulator ring and its associated electron losses without supplemental shielding.

Alternate Hypothesis: Geometric factors in addition to the existing shield wall of the 3rd generation light source is not sufficient to allow for the addition of an accumulator ring and its associated electron losses without supplemental shielding.

Decision Rule 2: the null hypothesis will be supported and the alternate hypothesis will be rejected if dose equivalent rates at locations of interest are below the ALS shielding design criterion of 0.1 mrem/hr.

3.3 Problem 3: Electron Bunch Swapping

During operation of the upgraded ALS, the storage ring will contain about 11 bunch trains (each in turn containing about 26 bunches spaced 2 nanoseconds [nsec] apart), and the associated accumulator ring will contain one bunch train. To keep the emittance of the storage ring beam sufficiently low, approximately once a minute, a storage-ring bunch train will trade places with the accumulator-ring bunch train. Between such swap-outs, the train in the accumulator will be topped off with additional electrons by the existing LINAC/booster injector. By swapping a storage-ring bunch train that has lost a portion of its current with the topped-off bunch train from the accumulator, the overall current in the storage ring will be maintained at a nominal 500 mA ± 5 mA.

Having a lower beam emittance than ALS results in significantly more electron losses and hence lower beam lifetime. Estimates place the potential lifetime of ALS-U as low as 30 minutes but nominally near 60 minutes. Having a lower lifetime requires more frequent injection of electrons into the system to maintain current. Each injection of electrons from the booster ring, and each swap of the electron trains between the storage ring and accumulator has an associated efficiency loss. Efficiency losses that result from these injections and swaps lower beam lifetime.

The effect of beam lifetime and its relationship to bunch swapping need to be understood. Ultimately, given sufficient facility knowledge, dose rates at specific locations are going to be scalable with beam lifetime.

3.3.1 Hypothesis Statement 3

Null Hypothesis: The decrease of electron beam lifetime within ALS-U **will** have an inverse, linear relationship with dose rates resulting from electron losses.

Alternate Hypothesis: The decrease of electron beam lifetime within ALS-U **will not** have an inverse, linear relationship with dose rates resulting from electron losses.

Decision Rule 3: the alternate hypothesis will be rejected if dose equivalent rates at locations of interest do display an inverse, linear correlation with electron beam lifetimes. In that event, the null hypothesis will be supported.

4 METHODS & MATERIALS

4.1 MCNP6 Methods

The MCNP code automatically creates standard summary information that gives the user a better insight into the physics of the problem and the adequacy of the Monte Carlo simulation including: a complete accounting of the creation and loss of all tracks and their energy; the number of tracks entering and reentering a cell plus the track population in the cell; the number of collisions in a cell; the average weight, mean free path, and energy of tracks in a cell; the activity of each nuclide in a cell (that is, how particles interacted with each nuclide, not the radioactivity); and a complete weight balance for each cell (MCNP6). To quantify and gather sufficient statistics on results, MCNP6 offers a number of tallies and mesh options. The following tallies and mesh tallies were used in this work:

- F4 Track-Length Estimator: This estimator uses the fundamental definition of flux as the number of particle track lengths per unit volume. It collects particle of weight (W) and energy (E) makes a track-length (segment) (T) within a specified cell of volume (V). This segment makes a contribution W·T/V to the flux (fluence) in the cell. The sum of the contributions is reported as the F4 tally in the output (Shultis 2011).

- F5 Point Detector Next-Event Estimator: For each source particle and each collision event, a deterministic estimate is made of the fluence contribution at the detector point (or ring in an axisymmetric problem) This is done by tracing a pseudo-particle, without altering the original random walk path, from the collision site to the detector.

- FMESH: This card allows the user to define a mesh tally superimposed over the problem geometry. By default, the mesh tally calculates the track-length estimate of the particle flux averaged over a mesh cell in units of particles/cm^2 (MCNP6).

- TMESH: The mesh tally is a method of graphically displaying particle flux, dose, or other quantities on a rectangular, cylindrical, or spherical grid overlaid on top of the standard problem geometry. Particles are tracked through the independent mesh as part of the regular transport problem. The contents of each mesh cell can be plotted with the MCNP6 geometry plotter superimposed over a plot of the problem geometry. Four different mesh-tally types are provided by TMESH depending on the information the user wishes to view, but only type-1 track-averaged mesh tallies, which score track-averaged data such as flux, tracks, population and energy deposition, were used.

MCNP tallies also include the uncertainty, which is the estimated relative error defined to be one estimated standard deviation of the mean divided by the estimated mean. The uncertainty can be used to form confidence intervals about the estimated mean, allowing one to make a statement about what the true result of the Monte Carlo calculation itself and not to the accuracy of the result compared to the true physical value. This uncertainty may be interpreted as the following: 0.5 to 1.0 - not meaningful, 0.2 to 0.5 - factor of a few, 0.1 to 0.2 – questionable, < 0.1 - generally reliable (LANL).

For a well-behaved tally, the uncertainty will be proportional to 1 divided by the square root of the number of particle histories. To halve the uncertainty the total number of histories must be increased fourfold. The selection of the total number of particles ran for these simulations is based upon meeting sufficiently low uncertainty in the problem areas of interest, generally <0.1. Additionally, this selection is guided by available computing resources.

All materials specified in the simulations were sourced from *Compendium of Material Composition Data for Radiation Transport Modeling* (McConn et. al. 2011). Default values for cross-section sets were utilized as the simulations here primarily reviewed photon interactions with the exception of photo-neutron production. Specifically defined cross-section sets are more often used for neutron problems involving criticality and other nuclear interactions.

4.2 Benchmarking Strategy

As the ALS-U is not yet complete, there is currently no opportunity to obtain measured results to benchmark calculated and simulated values against. Each problem presented in this work is then benchmarked against available resources.

The problem of gas bremsstrahlung production is benchmarked against analytical derivations of the fraction of the electron beam power that is converted to photons combined with a conservative spectrum assumption of 1/*k*.

The problem of thick-target bremsstrahlung production of the electron beam colliding with a thick-target to produce radiation showers is benchmarked against the SHIELD11 analytical code to ensure dose equivalent rates can be reproduced.

The problem of beam lifetime due to charge loss and the derivation of charge lost in each area of interest is benchmarked against an ALS-U Beam Loss (LBNL 2021) document produced by the LBNL ALS-U Accelerator Physics group.

4.3 PROBLEM 1: GAS BREMSSTRAHLUNG

Gas bremsstrahlung (GB) will exist throughout the entire accumulator ring system as electrons collide with molecules of air located within the vacuum chamber. The amount of GB produced will vary linearly with the length of a straight, pressure, beam current, and electron energy.

4.3.1 MCNP6 Electron Interactions and Sampling

Electron interaction data tables are required both for problems in which electrons are actually transported, and for photon problems in which the thick-target bremsstrahlung model is used. Electron data tables are selected by default when the problem mode requires them. There are two electron interaction data libraries: el and el03. The electron libraries contain data on an element-by-element basis for atomic numbers from Z equal 1 to 94. The library data contain energies for tabulation, radiative stopping power parameters, bremsstrahlung production cross sections, bremsstrahlung energy distributions, K-edge energies, Auger electron production energies, parameters for the evaluation of the Goudsmit-Saunderson theory for angular deflections based on the Riley cross-section calculation, and Mott correction factors to the Rutherford cross sections also used in the Goudsmit-Saunderson theory (MCNP6). The default electron data tables were used for these simulations, which is the first electron data table listed in the xsdir file for the relevant element.

The MCNP code addresses the sampling of bremsstrahlung photons at each electron substep. The tables of production probabilities are used to determine whether a bremsstrahlung photon will be created. For data from the el03 library, the bremsstrahlung production is sampled according to a Poisson distribution along the step so that none, one or more photons could be produced; the el library allows for either none or one bremsstrahlung photon in a substep. If a photon is produced, the new photon energy is sampled from the energy distribution tables. By default, the angular deflection of the photon from the direction of the electron is also sampled from the tabular data. The direction of the electron is unaffected by the generation of the photon because the angular deflection of the electron is controlled by the multiple scattering theory. However, the energy of the electron at the end of the substep is reduced by the energy of the sampled photon because the treatment of electron energy loss, with or without straggling, is based only on non-radiative processes (MCNP6).

4.3.2 Gas Bremsstrahlung Spectra

Monte Carlo methods were used to reconstruct the $1/k$ assumption. MCNP6 was used to generate these alternate source terms. Two source terms were generated by MCNP6. The bremsstrahlung process generates many low-energy photons, but the higher-energy photons are often of more interest. The first source term is the standard MCNP6 physics database source that did not include use of variance reduction card BBREM. The second source term includes BBREM variance reduction.

BBREM biasing generates more high-energy photons by biasing each sampling of a bremsstrahlung photon toward a larger fraction of the available electron energy. The bias factors are normalized by the code in a manner that depends on both electron energy and material, so that although the ratios of the photon weight adjustments among the different groups are known, the actual number of photons produced in any group is not easily predictable. This biasing also increases the total number of bremsstrahlung photons produced because there will be more photon tracks generated at higher energies. The secondary electrons created by these photons will tend to have higher energies as well, and will therefore be able to create more bremsstrahlung tracks than they would at lower energies (MCNP6).

4.3.3 GB Source Term Input Parameters

The expected vacuum pressure within the accumulator ring system is expected to vary within sections of the accumulator ring, as well as to decrease with increasing runtime of the accelerator due to outgassing of materials. The expected vacuum pressure after 72 amp-hours of beam is conservatively estimated at 4.0×10^{-07} torr. After 1,000 amp-hours (LBNL 2019A), this is expected to drop approximately two orders of magnitude; this change is shown on Figure 4.1. The early operating time frame is the area of concern because during early phase operation, gas will be present in the highest concentrations and consequently bremsstrahlung radiation generation is anticipated to be highest.

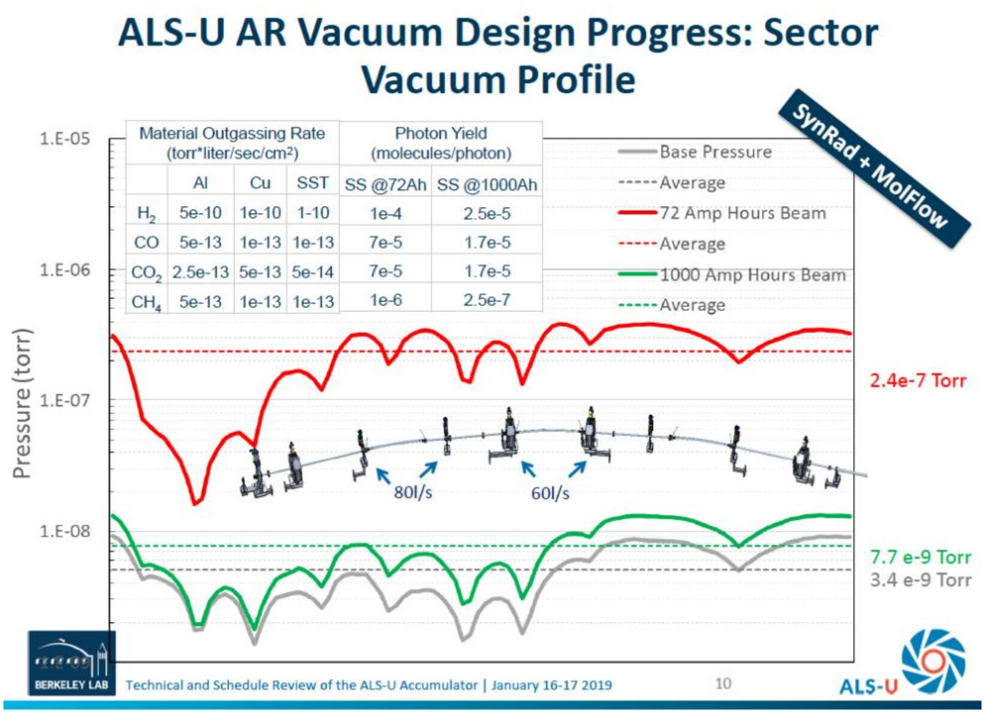

Figure 4.1. ALS-U accumulator-ring vacuum profiles from technical and schedule review of the ALS-U accumulator ring

The sections of accelerator beam directly following an accelerator straight are anticipated to produce the largest dose rates as the GB tangentially exits the system. The location of the highest dose rate will be the end of an accelerator straight that is composed of a 1.3-meter vacuum length section, a 4.5-meter length vacuum straight section, and a 1.3-meter-long vacuum straight all along the same axis before the electron beam is diverted by a dipole magnet (LBNL2019). This provides 7.1-meters of mass thickness of GB production material.

A fraction of the total electron beam power stored within a synchrotron ring is converted into GB power. That fraction's power is directly related to the mass thickness of the air in the arc section that the stored electrons pass through. Equation 2 (SLAC 2017A, 2017B) gives the fraction of bremsstrahlung power that is generated (Fbrem) for the accumulator ring straight, with the parameters provided in Table 4.1.

$$\text{Fbrem} = (L \times p \times P) / X_o = (716.8 \times 1.205\text{x}10^{-3} \text{ x } 5.26\text{x}10^{-10}) / 36.818 = 1.235\text{x}10^{-11} \qquad (2)$$

Table 4.1. Accumulator-Ring Electron Beam Parameters Used to Calculate GB

Parameter	**Value**	**Unit**
Electron energy, E	2	GeV
Beam average current, I	46	mA
Single-bunch current	1.76	mA
Vacuum pressure$_{72amp\text{-}hr,}$ P	$4.0\text{x}10^{-07}$	torr
Radiation length of air, X_o	36.818	g/cm^2
Effective length, L	716.8	cm
Air density, *p*	$1.205\text{x}10^{-03}$	$g/cm^3/atm$

The ALS-U accumulator ring is assumed to have a total stored beam power of 0.092 GW (46 mA × 2 GeV). Thus, the GB power is calculated in Equation 3 with the parameters provided in Table 4.1.

$$\textit{GB Power} = I \times E \times \text{Fbrem} = 46 \times 2 \times 1.235\text{x}10^{-11} = 1.136\text{x}10^{3}\ \mu\text{W} \qquad (3)$$

The total GB energy distribution of a 1/*k* fluence is provided by Figure 4.2. The total calculated output based upon the Table 4.1 parameters and the $1.136\text{x}10^3\ \mu W$ spectrum is $5.5\text{x}10^7$ photons per second with a mean photon energy by linear energy bin calculated to be 0.128 GeV.

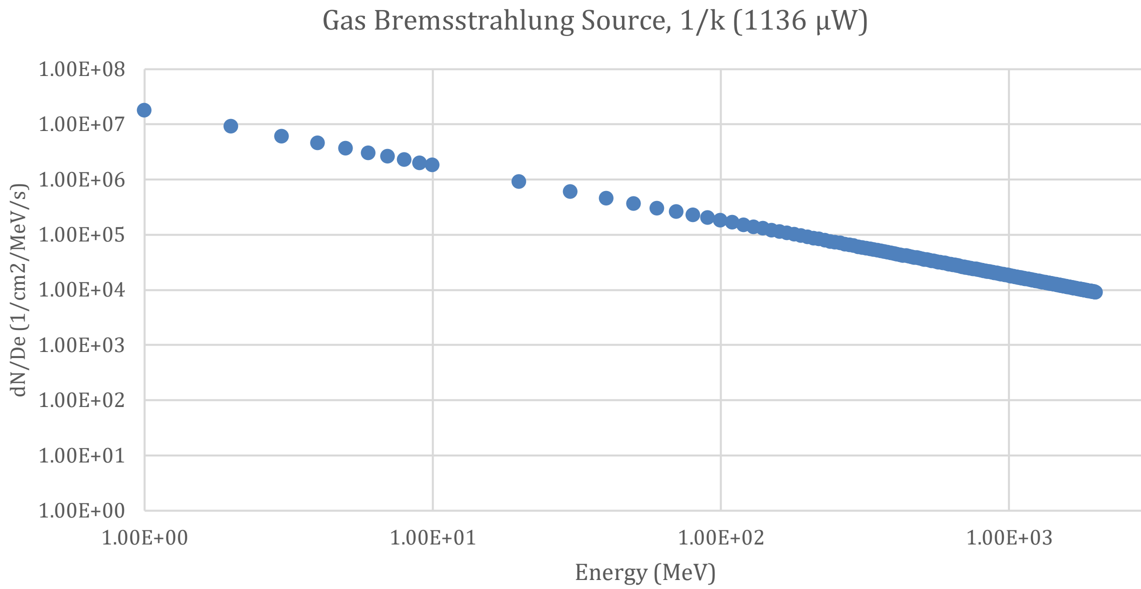

Figure 4.2. Total GB source fluence produced in the accumulator ring straight

Appendix I contains an example gas bremsstrahlung MCNP6 input deck. Variation in particle energy cutoff values from 0.1 MeV to 10 MeV and 0.1 MeV to 0.01 MeV for electrons and photons respectively were simulated to determine dose rates downstream of the GB interaction and outside of the shield wall. Increasing the particle energy cutoff value was found to change the results by <0.5%. To produce more efficient runtimes for the primary GB simulations, energy cutoff values for electrons and photons within MCNP6 were set at 0.1 MeV for both particle types.

4.4 PROBLEM 2: HVAC AND ELECTRICAL PENETRATION METHODS

4.4.1 Penetration Source Term

Bremsstrahlung will exist throughout the entire accumulator-ring and storage-ring system as electrons collide with molecules of air located within the vacuum chamber or scrape against stationary collimator components. The amount of gas bremsstrahlung produced will vary linearly with the length of an accelerator straight, and with pressure, beam current, and electron energy.

Gas bremsstrahlung is strongly forward scattering, and, at angles perpendicular to the rings, will not substantially contribute to dose rates through the proposed HVAC penetrations. The amount of bremsstrahlung produced through interactions with collimators will vary with the number of collimators and their location in the achromat. Appendix II contains an example HVAC and electrical penetration MCNP6 input deck.

4.4.2 Collimator Beam Loss Scenarios

Scattered particles reduce beam lifetime and increase energy deposition in the rings. Collimators are used to restrict beam losses to planned locations and protect the inner diameter of the accelerator vacuum tubes. The current expected lifetime of the ALS-U storage ring is approximately one hour. The placement of collimators is tied to special limitations and beam emittance characteristics, as such only a few collimator locations are feasible based upon performance-based design parameters (see Figure 4.3). While these chosen collimator locations will often be the location of losses, total beam loss could occur at nearly any point in the accelerator.

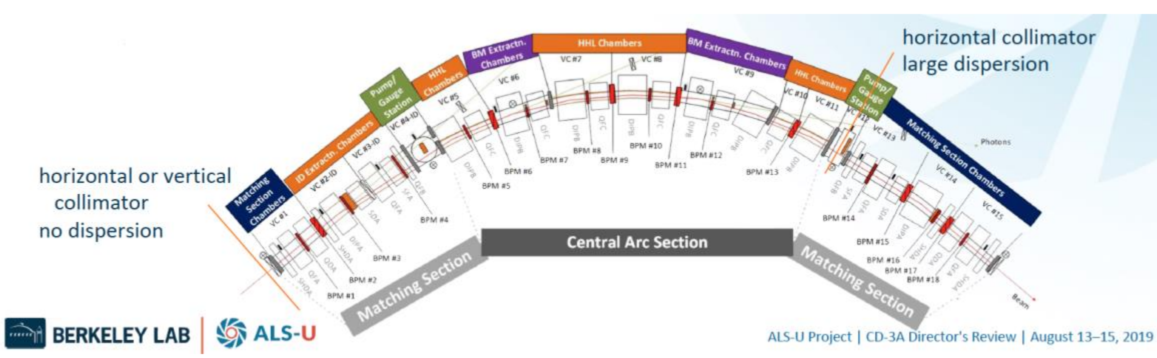

Figure 4.3. Potential available locations for collimators. Source: ALS-U Storage Ring: Particle Loss Studies and Ion Instabilities presentation

As shown on Figure 4.4, the effectiveness of the collimators is a trade-off of beam lifetime versus the ability of the collimator to reduce losses in the inner diameter.

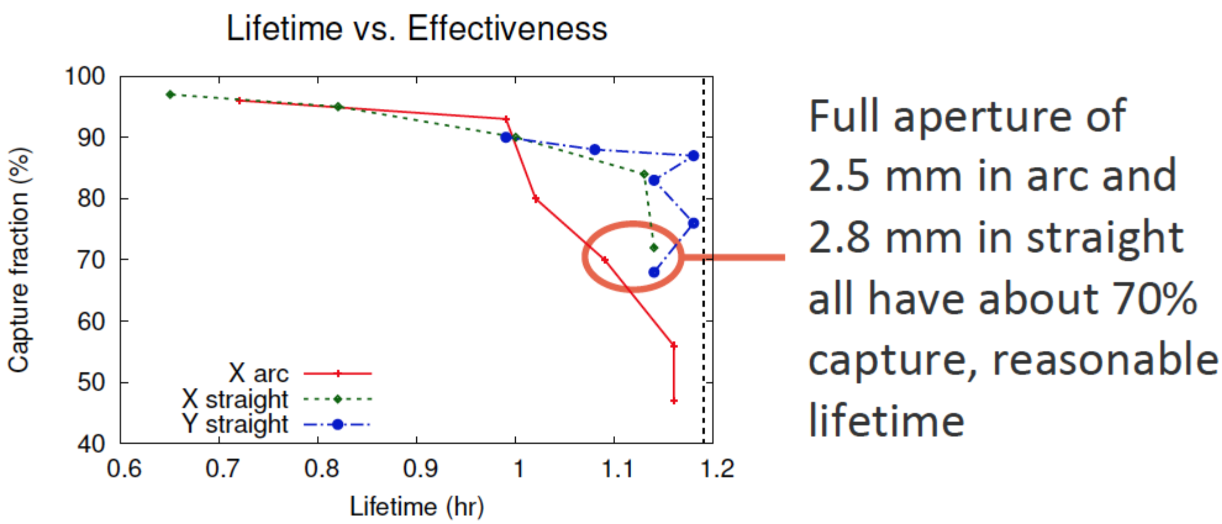

Figure 4.4. Trade-off of lifetime versus ability of collimator to reduce losses in inner diameters. Source: ALS-U Storage Ring: Particle Loss Studies and Ion Instabilities presentation

Based on the trade-offs of beam lifetime and capture fractions shown in Figure 4.4, the best location for the collimators is within the 2.5-mm full horizontal aperture in the arc and a 2.8-mm full vertical (Y) aperture in the accelerator straight. This provides a high capture percentage (~90%) while reducing beam lifetime by only 10%. This represents a projected worst-case beam loss to the inner diameter of 1.2% in 1-meter non-collimator sectors throughout the storage ring.

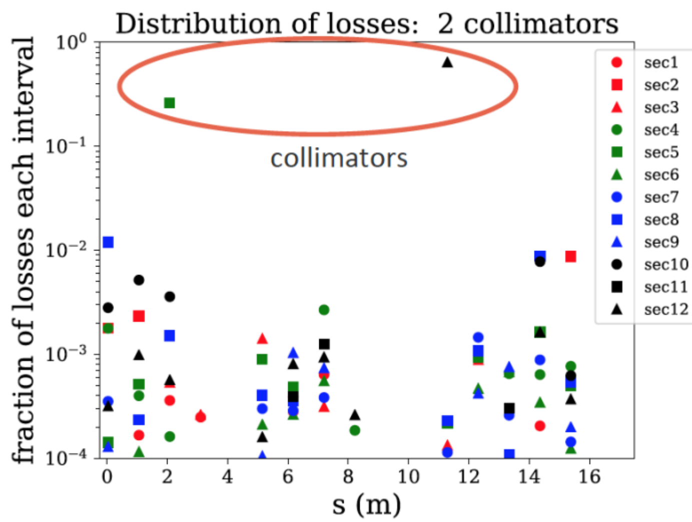

Figure 4.5. 90% capture using two collimators, resulting in 1.03-hour lifetime. Source: ALS-U Storage Ring: Particle Loss Studies and Ion Instabilities presentation

Reducing beam loss to the inner diameter in the majority of the sectors of the storage ring, the placement of these two collimators would result in the majority of the planned beam loss being confined to just two sectors, as shown in Figure 4.5. These would need to be shielded accordingly. The highest of the two collimator sectors could see ~75% of the anticipated beam loss (LBNL 2019B). This collimator information is for the storage ring, but accumulator ring collimators would follow similar engineering principles, as such it is assumed to be valid for the accumulator ring to estimate losses.

For the purpose of this research, two scenarios are simulated with respect to beam loss:

- Continuous loss: 5% beam loss, a conservative representation of the non-collimator sectors.

- A 100% beam dump: a conservative representation of the collimator sectors during a complete beam loss event.

4.4.2.1 Continuous Loss

During the ALS-U's top-off mode, the injection frequency can vary from a minimum of one injected shot every 12 seconds to one injected shot about every 30 seconds. This simulation assumes that the storage ring is being filled at one shot every 15 seconds. Filling at this rate requires an equal loss to maintain equilibrium. The number of electrons in both the storage-ring and accumulator-ring bunches was calculated using the parameters in Table 4.2 and Table 4.3 is shown in equation (4).

$$SR\ (nC/Bunch) = epb \times D \times (nC/C) = (7x10^{9})\ x\ (1.6x10^{-19})\ x\ (1x10^{9}) = 1.12\ nC/bunch \quad (4)$$

Table 4.2. Storage-Ring Electron Beam Parameters Used to Calculate Loss

ALS-U Storage-Ring Parameters	Value	Unit
Beam E	2	GeV
Injection E	2	GeV
Bunch Spacing	2	ns
Circumference	196.8	m
Beam Current (A)	500	mA
Electron Velocity (V)	$3x10^{8}$	m/s
Electrons per Bunch (EPB)	$7x10^{9}$	e-
Coulomb per Electron (D)	$1.6x10^{-19}$	-

It is assumed that the equivalent of 1.12 nC is lost every 15 seconds for the continuous loss scenario of the storage ring. This results in a charge loss of $2.69x10^{2}$ nC/hour, which is equivalent to $1.68x10^{12}$ electrons/hour. When considering 5% loss at the anticipated loss point, this implies a continuous loss of $8.4x10^{10}$ electrons per hour from the storage ring.

Table 4.3. Accumulator-Ring Electron Beam Parameters Used to Calculate Loss

Accumulator Ring Parameters	Value	Unit
Beam E	2	GeV
Injection E	2	GeV
Bunch Spacing	2	ns
Circumference	185*	m
Beam Current (A)	50	mA
Electron Velocity (V)	$3x10^8$	m/s
Electrons per Bunch (EPB)	$7x10^8$	e-
Coulomb per Electron (D)	$1.6x10^{-19}$	–
*Assumed		

The bunches in the accumulator ring are anticipated to be similar to the storage ring at 1.12 nC because that is the requirement for the storage-ring swap-out. The current of the accumulator ring is one-tenth of the storage ring, and the same fraction of loss as the storage ring is assumed, resulting in the loss of 0.112 nC every 15 seconds. This results in $2.69x10^1$ nC/hour, which is equivalent to $1.68x10^{11}$ electrons/hour. Given the assumed 5% loss point, this results in the continuous loss of $8.4x10^9$ electrons per hour from the accumulator ring.

4.4.2.2 100% Beam Dump

ALS/ALS-U's 500 mA current is equal to 0.5 coulomb/s, or $3.13x10^{18}$ electrons circling the storage ring per second at $1.6x10^{-19}$ coulomb/electron. With a circumference of 196.8 meters (m), and velocity of $3x10^8$ meters/second (m/s), it takes $2.05x10^{12}$ electrons present in the storage ring to result in 500 mA. Therefore, it can be anticipated that if a 100% beam dump occurs, 2.05×10^{12} electrons will be dumped.

A conservative beam current of 50 mA (0.05 coulomb/s) was assumed during accumulator ring modeling. The beam current is equivalent to 3.13×10^{17} electrons circling the accumulator ring per second. With a circumference of 185 m, and velocity of 3×10^{8} m/s, it takes 1.93×10^{11} electrons present in the accumulator ring to produce a 50-mA beam current. This is the assumed number of particles for the accumulator ring in the 100% loss, beam dump scenario.

4.5 PROBLEM 3: ELECTRON BUNCH SWAPPING

4.5.1 Beam Lifetime

Beam lifetime is defined here as the time for the beam current to decrease to 1/e of its initial value due to continuous losses, with e being Euler's number. The beam lifetime in an electron storage ring is mainly determined by the two effects, Touschek scattering and electron gas bremsstrahlung scattering. However, fourth-generation synchrotrons utilize bunch swapping to help meet emittance requirements. Swapping the electron bunch trains between the storage-ring and the accumulator-ring result in additional loss modes not seen in third-generation synchrotrons. Losses that result from these injections and swaps are instabilities that affect the beam lifetime. Third-generation synchrotrons are affected by a similar aperture limitation for longitudinal planes of electron bunches but this effect is negligible for most electron storage rings.

When defining total beam lifetime, one must define partial lifetimes of the primary loss modes, Touschek lifetime and (elastic and inelastic) beam-gas scattering lifetime. One may define the three partial lifetimes as shown in Equation (5) (Lee, 2005):

$$1/\tau = 1/\tau_t + 1/\tau_v\,, \qquad (5)$$

where τ is the total beam lifetime, τ_t is the Touschek lifetime, and τ_v collectively denotes the elastic and inelastic beam-gas scattering lifetimes. However, in real measurements, they are combined. As such, it is not easy to identify the separate components.

To include charge losses due to electron bunch swapping, one may approach the problem from a perspective of conservation of charge to maintain steady state current. For nominal conditions, the total injected charge will be: storage ring lifetime loss + accumulator lifetime losses + storage ring injection losses + storage ring swap-out extraction losses + accumulator swap-out injection losses + ATS losses + STA losses. The following subsections detail the derivation of charge losses at each transfer line per fill cycle and steady-state current top-off, correlating them with the associated beam lifetime.

4.5.2 Transfer Line Source Terms

Bremsstrahlung may exist throughout the entire volume of the accumulator and storage rings. Bremsstrahlung production varies based upon the number of collimators and their location in the achromat. Scattered particles reduce beam lifetime and increase energy deposition in the rings. Collimators are used to restrict beam losses to planned locations and protect the inner diameter of the accelerator vacuum tubes. ALS-U shielding design goals are set at 30-minutes lifetime and a capture percentage of 95% for both the accumulator ring and storage ring. While the chosen collimator locations will often be the location of the majority of losses, total beam loss could occur at nearly any point in the accelerator.

Each transfer line has its own extraction efficiency established in the ALS-U Accelerator Physics document (LBNL 2021). The assumed extraction efficiencies for this simulation are:

- BTA – 0.96
- ATS – 0.998
- STA – 0.998

Although BTA losses are assumed 4% to provide a buffer for effects not included in simulations, 2% is predicted.

Two scenarios for each transfer line are simulated: the routine losses during SR filling (‘Fill’), and the routine losses during SR top-off (‘Top-Off’). One additional scenario is simulated for the BTA, the loss of an electron train during fill.

The fill cycle refers to the filling of the SR to its full charge capacity. The electron train is formed in the AR via injection through the BTA. Once a single electron train (26 bunches) is filled to 20% charge capacity, it is sent to the SR via the ATS. This is repeated for all 11 trains.

As each electron train contains 5.98 nC of charge a scenario in which the entire train equivalent of charge is lost during injection from the booster to the accumulator ring was simulated. In the event of a loss of a train during injection from the booster to the accumulator, the BTA is estimated to lose 5.98 nC (3.7×10^{10} electrons).

Once all SR trains are at 20% charge capacity, a single train is sent back to the AR via the STA. This train is then filled to 40% charge capacity. Once that charge is reached, the train is sent back to the SR via the ATS and another train is sent to the AR via the STA. This is repeated for all 11 trains. This cycle is then repeated until all trains reach 60% charge capacity, then 80%, and finally 100%. At this point the fill cycle is complete. The fill cycle to reach 500 mA in the ALS-U SR is expected to take approximately 15 minutes, or 180 second for each of the 5 cycles.

Table 4.4 shows an abbreviated charge transfer chart detailing the expected losses for each transfer line over a fill cycle. Each line in the table is repeated for all 11 trains before moving into the next train. During the 15-minute fill cycle: the BTA is estimated to lose 13.2 nC (8.2×10^{10} electrons), the ATS 2.0 nC (1.2×10^{10} electrons), and the STA 1.3 nC (8.2×10^{9} electrons).

Table 4.4. ALS-U Fill cycle transfer line charge losses (nC/cycle)

FILL

SR Capacity	Description	Charge Moved (nC)	Extraction Efficiency	BTA Charge Lost	ATS Charge Lost	STA Charge Lost
0.2	BTA fill of 1 train (26 bunches) to 0.2	5.98	0.96	0.2392	-	-
	ATS swap of 1 train	5.98	0.998	-	0.01196	-
0.4	STA swap of 1 train (26 bunches)	5.98	0.998	-	-	0.01196
	BTA fill of 1 train (26 bunches) to 0.40	5.98	0.96	0.2392	-	-
	ATS swap of 1 train	11.96	0.998	-	0.02392	-
0.6	STA swap of 1 train (26 bunches)	11.96	0.998	-	-	0.02392
	BTA fill of 1 train (26 bunches) to 0.6	5.98	0.96	0.2392	-	-
	ATS swap of 1 train	17.94	0.998	-	0.03588	-
0.8	STA swap of 1 train (26 bunches)	17.94	0.998	-	-	0.03588
	BTA fill of 1 train (26 bunches) to 0.8	5.98	0.96	0.2392	-	-
	ATS swap of 1 train	23.92	0.998	-	0.04784	-
1	STA swap of 1 train (26 bunches)	23.92	0.998	-	-	0.04784
	BTA fill of 1 train (26 bunches) to 1.0	5.98	0.96	0.2392	-	-
	ATS swap of 1 train	29.9	0.998	-	0.0598	-
			Total Charge loss per Fill cycle (nC)	**13.156**	**1.9734**	**1.3156**
				BTA	**ATS**	**STA**

The purpose of the top-off cycle is to maintain the SR current at 500 mA and achieve 1% current stability. This process is similar to the fill cycle. During routine operations in top-off, gas and Touschek scattering, or simply particle loss within a bunch due to single particle-particle collisions, result in relatively consistent loss rates at relatively predictable locations. These losses establish the beam lifetime. Table 4.5 details the charge losses per hour during top-off under different beam lifetime scenarios. As stated, shielding design goals are based upon a 30-minute beam lifetime in the SR. The SR is assumed to have 500 mA stored current at 2.0 GeV, representing a charge of 328 nC. Within the AR, the 45-mA current corresponds to a charge of 30 nC, or 1.71×10^{11} electrons present in the accumulator ring, distributed throughout the circumference of 182 meters. During top-off with an assumed beam lifetime of 30-minutes: the BTA is estimated to lose 26 nC/hr (0.008 nC/s), the ATS 12 nC/hr (0.002 nC/s), and the STA 11 nC/hr (0.002 nC/s) (LBNL 2021).

Appendices III-V contain example electron bunch swapping MCNP6 decks for the Booster-to-Accumulator, Accumulator-to-Storage, Storage-to-Accumulator transfer lines respectively.

Table 4.5. ALS-U Top-off transfer line charge losses per cycle (nC/cycle)

TOP-OFF

Train	Step	Description	Charge Moved (nC)	Extraction Efficiency	BTA Charge Lost	ATS Charge Lost	STA Charge Lost
1	1	ATS swap of 1 fresh train	29.9	0.998	-	0.0598	-
	2	STA swap of 1 spent train	26.7375	0.998	-	-	0.053475
	3	BTA top-off of 1 spent train	3.1625	0.96	0.1265	-	-
2	4	ATS swap of 1 fresh train	29.9	0.998	-	0.0598	-
	5	STA swap of 1 spent train	26.7375	0.998	-	-	0.053475

	6	BTA top-off of 1 spent train	3.1625	0.96	0.1265	-	-
	7	ATS swap of 1 fresh train	29.9	0.998	-	0.0598	-
3	8	STA swap of 1 spent train	26.7375	0.998	-	-	0.053475
	9	BTA top-off of 1 spent train	3.1625	0.96	0.1265	-	-
	10	ATS swap of 1 fresh train	29.9	0.998	-	0.0598	-
4	11	STA swap of 1 spent train	26.7375	0.998	-	-	0.053475
	12	BTA top-off of 1 spent train	3.1625	0.96	0.1265	-	-
	13	ATS swap of 1 fresh train	29.9	0.998	-	0.0598	-
5	14	STA swap of 1 spent train	26.7375	0.998	-	-	0.053475
	15	BTA top-off of 1 spent train	3.1625	0.96	0.1265	-	-
	16	ATS swap of 1 fresh train	29.9	0.998	-	0.0598	-
6	17	STA swap of 1 spent train	26.7375	0.998	-	-	0.053475
	18	BTA top-off of 1 spent train	3.1625	0.96	0.1265	-	-
	19	ATS swap of 1 fresh train	29.9	0.998	-	0.0598	-
7	20	STA swap of 1 spent train	26.7375	0.998	-	-	0.053475
	21	BTA top-off of 1 spent train	3.1625	0.96	0.1265	-	-
	22	ATS swap of 1 fresh train	29.9	0.998	-	0.0598	-
8	23	STA swap of 1 spent train	26.7375	0.998	-	-	0.053475
	24	BTA top-off of 1 spent train	3.1625	0.96	0.1265	-	-
	25	ATS swap of 1 fresh train	29.9	0.998	-	0.0598	-
9	26	STA swap of 1 spent train	26.7375	0.998	-	-	0.053475
	27	BTA top-off of 1 spent train	3.1625	0.96	0.1265	-	-
	28	ATS swap of 1 fresh train	29.9	0.998	-	0.0598	-
10	29	STA swap of 1 spent train	26.7375	0.998	-	-	0.053475
	30	BTA top-off of 1 spent train	3.1625	0.96	0.1265	-	-

	31	ATS swap of 1 fresh train	29.9	0.998	-	0.0598	-
11	32	STA swap of 1 spent train	26.7375	0.998	-	-	0.053475
	33	BTA top-off of 1 spent train	3.1625	0.96	0.1265	-	-
				Charge loss per top-off cycle (nC)	**1.3915**	**0.6578**	**0.588225**
					BTA	ATS	STA

Table 4.6. ALS-U Top-off transfer line charge losses per hour by beam lifetime (nC/hr)

Top-Off Lifetime Scaling

Lifetime (hr) at 500 mA (achieves 1% current stability)	Injection rate required for lifetime (nC/s)	Injection rate (nC/hr)	Top-off cycles/hr	Top-off Injection Frequency (s)	BTA Charge Lost (nC/hr)	ATS Charge Lost (nC/hr)	STA Charge Lost (nC/hr)
0.1	0.9	3240	93.14	3.51	129.6	61.27	54.79
0.2	0.45	1620	46.57	7.03	64.8	30.63	27.39
0.3	0.3	1080	31.05	10.54	43.2	20.42	18.26
0.4	0.23	810	23.28	14.06	32.4	15.32	13.7
0.5*	0.18	648	18.63	17.57	25.92	12.25	10.96
0.6	0.15	540	15.52	21.08	21.6	10.21	9.13
0.7	0.13	462.86	13.31	24.6	18.51	8.75	7.83
0.8	0.11	405	11.64	28.11	16.2	7.66	6.85
0.9	0.1	360	10.35	31.63	14.4	6.81	6.09
1	0.09	324	9.31	35.14	12.96	6.13	5.48
1.1	0.08	294.55	8.47	38.65	11.78	5.57	4.98
1.2	0.08	270	7.76	42.17	10.8	5.11	4.57
1.3	0.07	249.23	7.16	45.68	9.97	4.71	4.21

1.4	0.06	231.43	6.65	49.19	9.26	4.38	3.91
1.5	0.06	216	6.21	52.71	8.64	4.08	3.65
1.6	0.06	202.5	5.82	56.22	8.1	3.83	3.42
1.7	0.05	190.59	5.48	59.74	7.62	3.6	3.22
1.8	0.05	180	5.17	63.25	7.2	3.4	3.04
1.9	0.05	170.53	4.9	66.76	6.82	3.22	2.88
2	0.05	162	4.66	70.28	6.48	3.06	2.74

* Shielding design basis

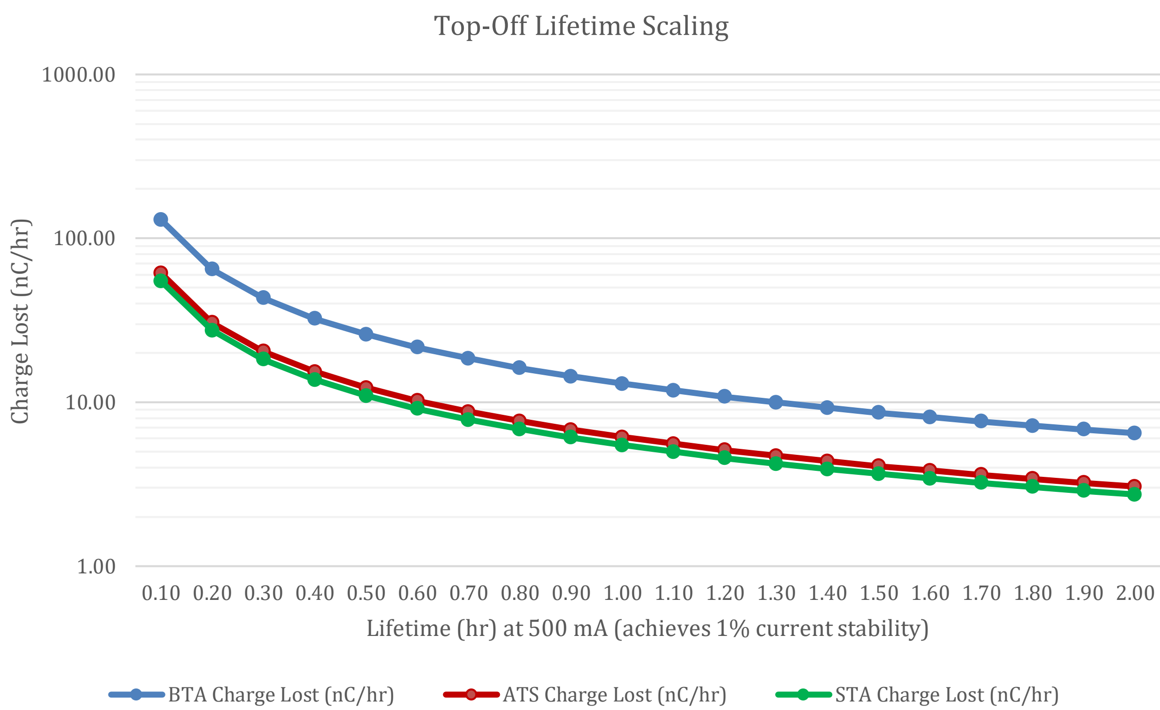

Figure 4.6. ALS-U Top-off transfer line charge losses per hour by beam lifetime (nC/hr)

4.5.3 Benchmark of Anticipated Electron Bunch Swapping Source Term

In 2021, the ALS accelerator physics group released a draft of their *ALS-U Beam Loss* document (LBNL 2021) in which charge losses for ALS-U operations were calculated. Results from the derivations in Section 4.4.2, Transfer Line Source Terms, are compared here against the document. The ALS-U document includes more sophisticated accelerator physics simulations that incorporate Touschek lifetimes and electron beam gas-scattering lifetimes.

Per LBNL 2021, A nominal injection involves <= 1 nC and is expected to happen every 30 seconds. For nominal conditions, the total injected charge will be equal to storage ring lifetime loss + accumulator lifetime losses + storage ring injection losses + storage ring swap-out extraction losses + accumulator swap-out injection losses + ATS losses + STA losses. This will be dominated by the first two contributions, so the total expected injection rate for top-off with a beam lifetime of 0.5-hr is 0.2 nC/s. For a fill cycle to the storage ring from zero current, an injection of about 6 nC over 15-s, repeated for a total of 15 minutes (nominal case) is expected.

During this injection into the accumulator ring via the BTA transfer line, it is expected that 98% of the injected beam is captured. To provide a buffer for effects not included in these simulations (like collective instabilities in the booster) a more conservative estimate for the BTA losses is 4%. With the injection rate above, this would correspond to losses of 0.2 nC/s·4% = 0.008 nC/s in top-off/swap-out and 6 nC/15 s · 4% = 0.016 nC/s when filling from zero (LBNL 2021).

The ATS transfer line is designed to enable transfer with zero losses and tracking simulations including realistic errors indicate that the design accomplishes this. The apertures throughout the beamline are designed to provide at least 6-sigma + 1 mm of clearance for the electron beam. The only places where the apertures are tighter than this are the extraction septa of the AR and the injection septa of the SR. Based on realistic tracking the losses at those places are expected to be smaller than 0.2%. During swap-out, the losses in these septa would therefore be similar to the injection losses in the storage ring, i.e., 30nC/30s · 0.2% = 0.002 nC/s (LBNL 2021).

The STA transfer line layout is a mirror symmetric copy of the ATS line. The emittance of the beam transferred through it is slightly larger, but the apertures for both lines are design to not have any losses in the central part of the transfer line. Losses again would be concentrated in the septa at either ends. Based on realistic tracking the losses at those places are expected to again be smaller than 0.2%. During swap-out, the losses in these septa would therefore be similar to the injection losses in the storage ring, i.e., 30nC/30s · 0.2% = 0.002 nC/s (LBNL 2021).

Table 4.7. Benchmark of Charge Loss Derivation to ALS-U Beam Loss Simulation

Transfer Line	Mode	Derivation	ALS-U Beam Loss	Unit	Derivation : ALS-U Beam Loss
BTA	Fill	0.015	0.016	nC/s	0.91
	Top-Off (0.5hr lifetime)	0.007	0.008	nC/s	0.90
ATS	Top-Off (0.5hr lifetime)	0.003	0.002	nC/s	1.70
STA	Top-Off (0.5hr lifetime)	0.003	0.002	nC/s	1.52
	TOTAL	0.0283	0.0280	nC/s	1.01

Table 4.7 compares the derived charge loss from Section 4.4.2 (converted to nC/s) against the listed charge loss rates provided by LBNL 2021. For the BTA, both the fill and top-off values are ≤ 10% different, and are slightly less conservative. For the ATS and STA, the derived top-off values are 42% and 34% higher than those provided by LBNL 2021, and are more conservative. Initially, this sounds like the models do not demonstrate good fit but the LBNL 2021 document

only reported to 1-significant figure and the level of charge being compared is quite small on the pC level. Thus, the better comparison is that of the overall sum of charge losses derived against the sum of those provided by LBNL 2021 which is nearly the same at 1% difference. While, some differences exist due to more sophisticated accelerator physics simulations being used for LBNL 2021, the charge derivation model provided does benchmark the overall loss of charge in the system well.

5 RESULTS AND DISCUSSION; Gas Bremsstrahlung

5.1 Benchmark of MCNP6 GB Source Term Against 1/*k*

To benchmark the production of MCNP6 GB energy and flux, the two MCNP6 source terms were compared against the analytically derived spectra consisting of the 1/*k* GB energy spectra combined with analytical expressions to calculate the fraction of energy converted from the incident electron into photons. The produced GB flux by energy bin is compared here.

As shown on Figure 5.1, the 1/*k* source term (analytical expression) produces the largest high-energy fraction of bremsstrahlung photons of the three options described in section 4.1.1. The larger fraction of high-energy photons results in higher effective dose rates and more penetrating radiation that is more difficult to shield. Additionally, the MCNP6 source terms represent a 0-degree sample downstream of the accelerator straight. While the bremsstrahlung radiation from 1-keV electrons is spread over 140 degrees, and even has a significant backward component, the photons produced by 10-MeV electrons are broadcast in a 2.8-degree FWHM beam (Marshall et. al.). As such, a 0-degree sample will be composed of higher-energy, forward-scattered radiation. It is noted that the use of MCNP6 BBREM variance reduction nearly approximated the 1/*k* spectrum at larger energies of interest and reduced sampling error associated with the simulation at high energies; see Figure 5.2.

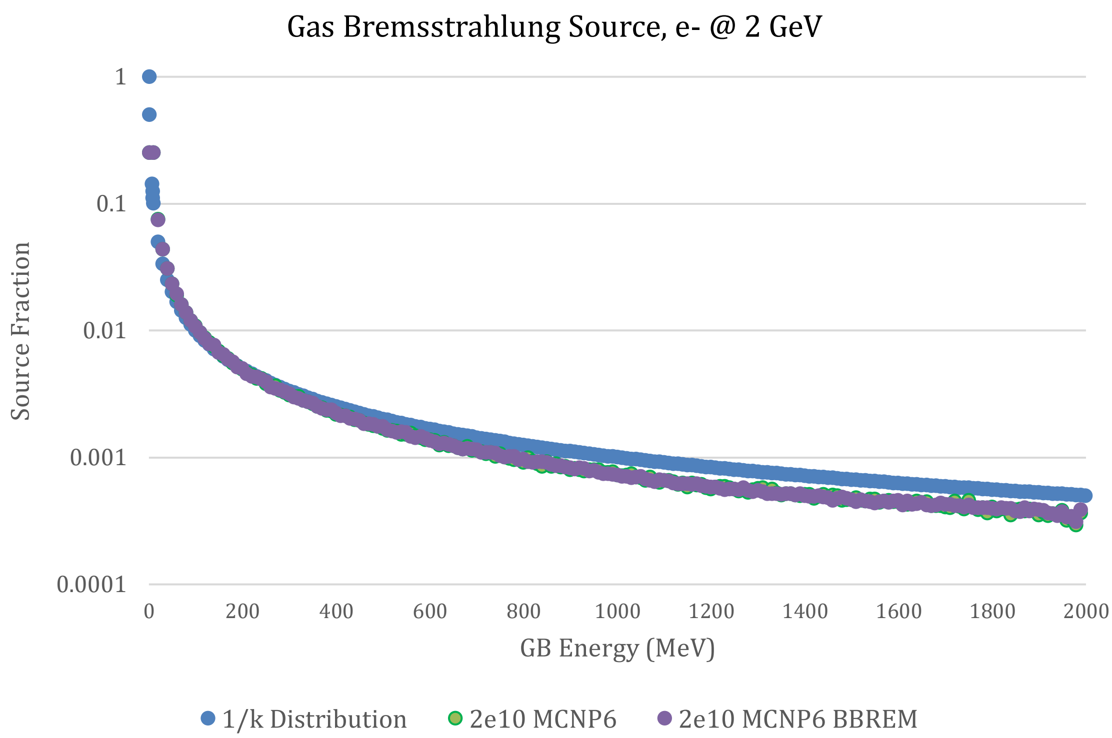

Figure 5.1. MCNP6 gas bremsstrahlung source fraction by energy

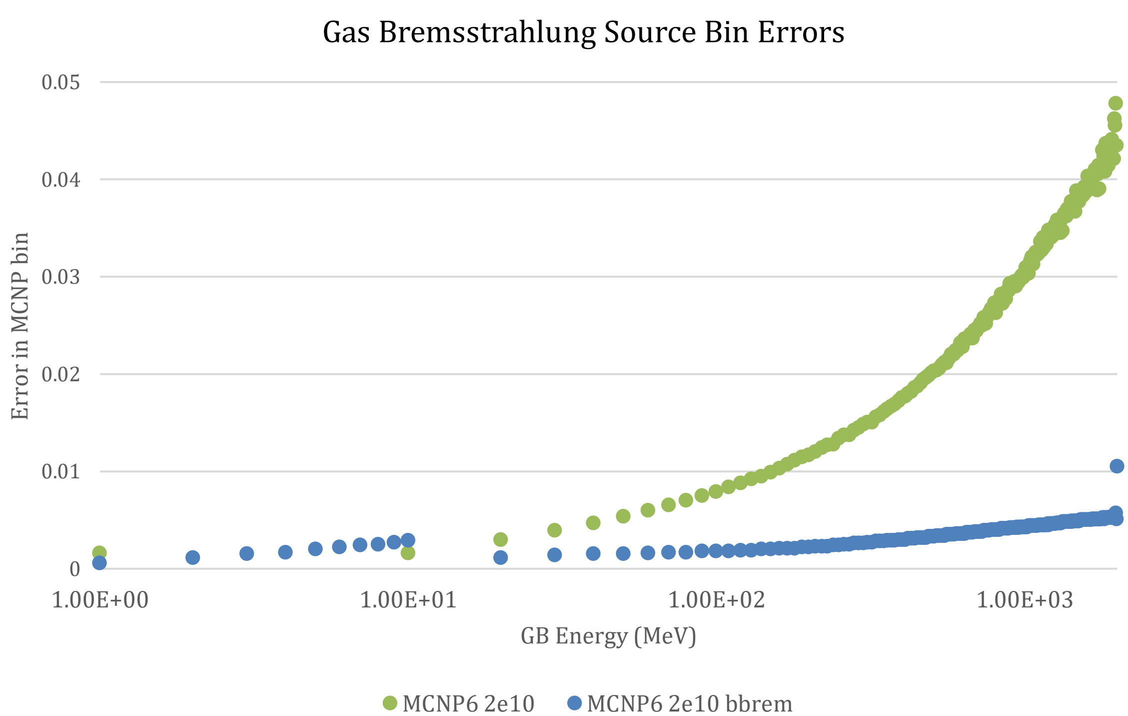

Figure 5.2. MCNP6 gas bremsstrahlung binning errors by energy

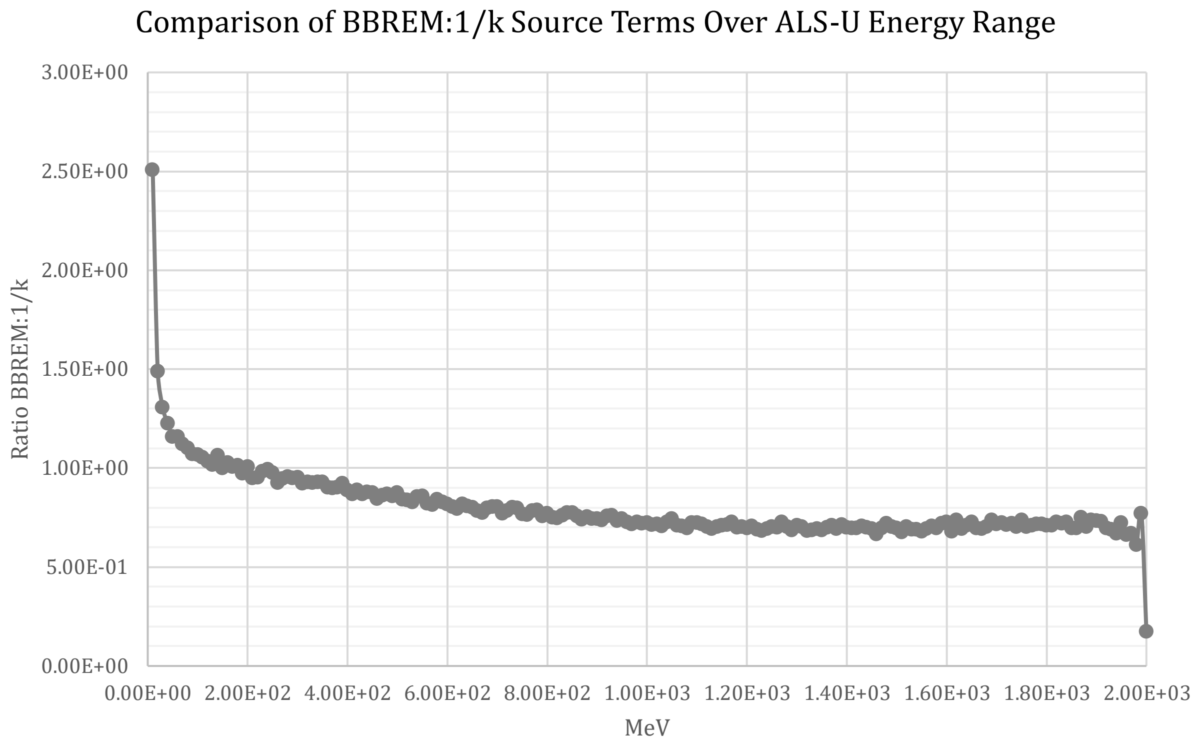

Figure 5.3. Source Term Comparison of MCNP6 BBREM to 1/k Analytical Expression

A BBREM:1/*k* source spectra comparison of energy, flux, and error indicated the analytical expression approximated the Monte-Carlo simulation, but the analytical expression predicts a large source term than the Monte-Carlo simulation. The Monte-Carlo simulation was only about 80% of the magnitude of the average bin value over the energy increments of the analytical expression. The use of the 1/*k* spectrum is more conservative as the angular distribution of GB with the direct generation method is broader due to multiple scattering, resulting in bremsstrahlung with wider polar angles and lower flux on target at long distances, such as between the accumulator ring source and the storage-ring shield wall. The 1/*k* source was arbitrarily selected for the remainder of this topic project to provide additional conservatism over the immediate alternatives when calculating dose. The 1/*k* approach is commonly described in literature (Liu et, al 2001).

5.2 MCNP Environment and Results

To characterize the dose rate resulting from GB, a model was developed in MCNP6. The transport model was based on available schematic and technical data for ALS-U. The geometry and placement of components is subject to change. The accumulator-ring components were broken down into individual connecting cells in an MCNP6 environment for radiation transport modeling purposes.

5.2.1 Dose Rates Exiting the Vacuum Chamber

To characterize the GB dose rates expected upon exiting the vacuum chamber wall (0.8 mm), a simple 1 cm^3 F4 tally cell was placed on axis with the accelerator straight. No collision with the H-gradient dipole magnet is assumed. ICRP 21 photon flux-to-dose rate conversion factors were used as identified by the MCNP manual and the publication *Fluence to Dose Equivalent Conversion Factors Calculated with EGS3 for Electrons from 100 keV to 20 GeV and Photons from 11 keV to 20 GeV*.

Photon Dose Rate Exiting the Vacuum Chamber = 546.3 rem/hr $\pm$ 0.05 rem/hr

5.2.2 Dose Rates Following Collisions with Accumulator Ring Components

Following production of GB, the photons will tangentially exit the accumulator ring system through the vacuum chamber wall and outward beyond the H-gradient dipole magnet (LBNL2018). Depending on beam positioning, these photons will collide with a downstream SD-sextupole magnet, a downstream quadrupole magnet, or both; see Figure 5.4. However, this simulation assumes no contact by the photons with the small ion pump that follows the SD-sextupole magnet. The electrons will be steered by the dipole magnet and remain within the vacuum chamber.

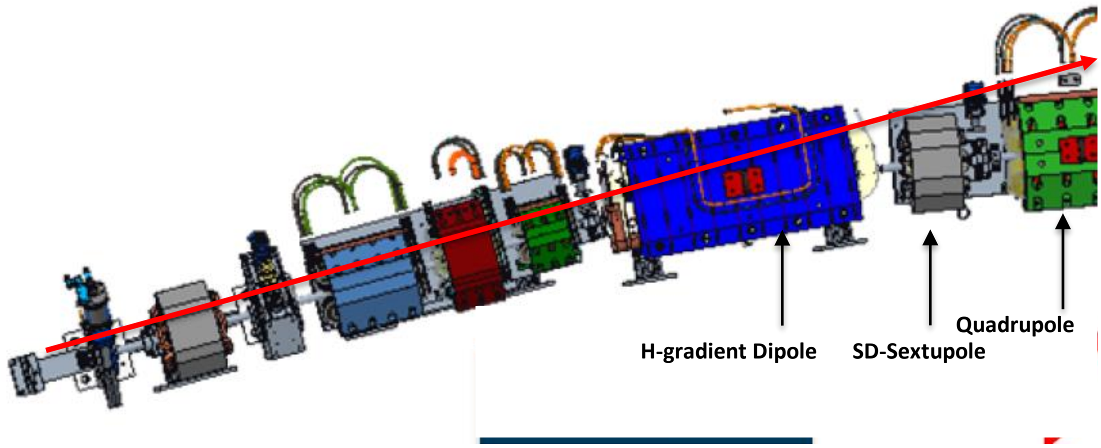

Figure 5.4. GB production will tangentially exit the accumulator ring (red arrow) through an H-gradient dipole magnet while the accelerator electrons are steered away.

Assuming the beam position is limited to the lower- diameter aperture following the straight (circled on Figure 5.5), the beam will collide with either the SD-sextupole magnet or the quadrupole magnet in the achromat.

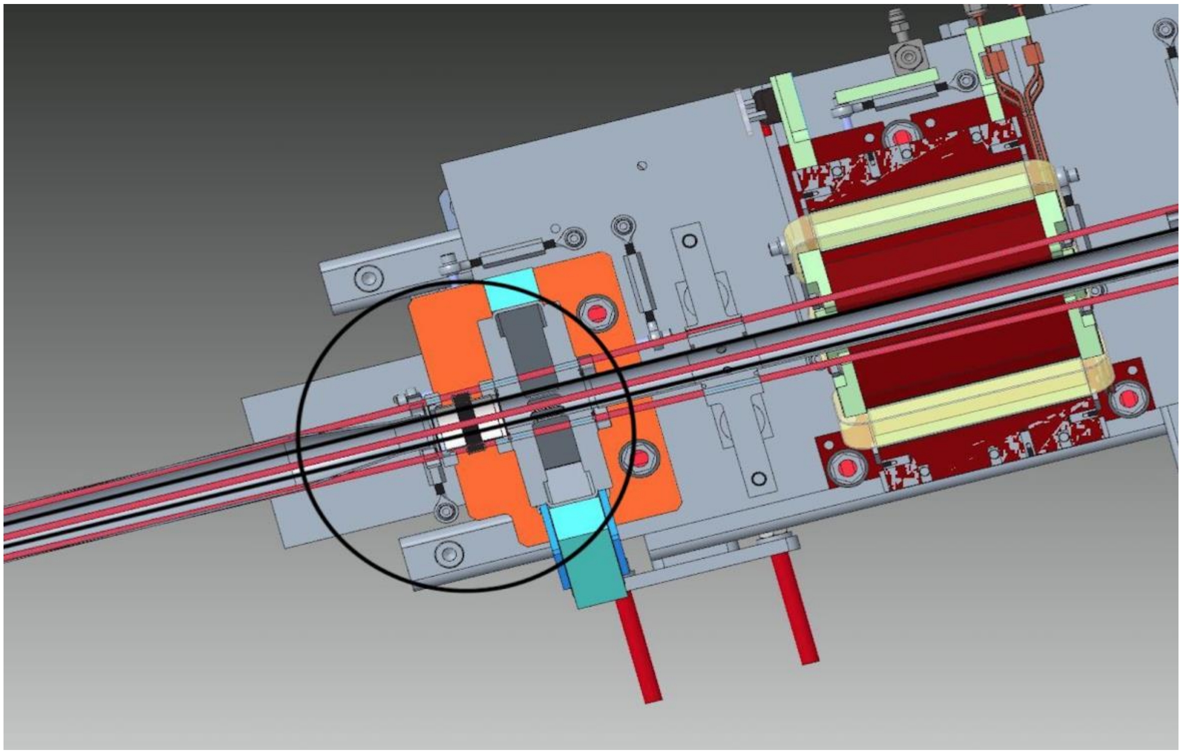

Figure 5.5. GB ray trace defining a limiting aperture in black lines

Figure 5.6 shows that if the beam is limited to the aperture defined on Figure 5.5, the beam position will reduce to the lines shown as 2, 3, or 4. These beam paths will result in differing amounts of interaction with the beamline components.

The most conservative position (#2) results in 18.86 cm of the SD-sextupole magnet colliding with the GB, with the quadrupole missing the interaction pathway. The least conservative position (#4) results in no collisions with the SD-sextupole magnet, but 32.57 cm of interaction pathway with the quadrupole magnet.

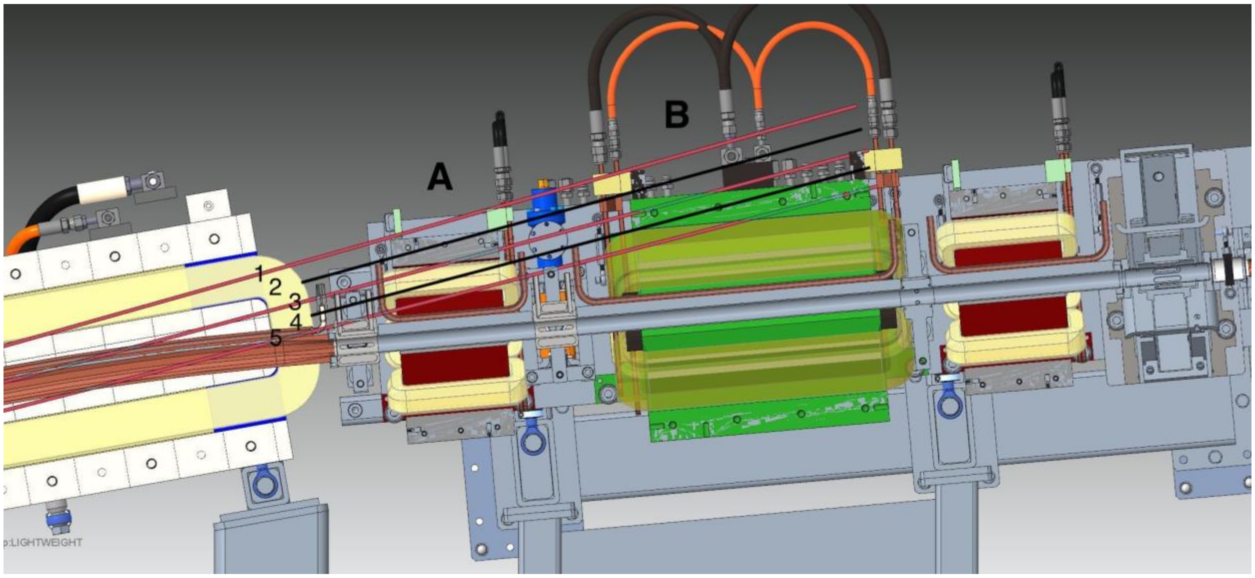

Figure 5.6. GB interaction pathways by beam position

The magnets are modeled as a cylinder of varying length composed as solid iron. These lengths are defined based on measurements taken on Figure 5.6.

Figure 5.7 on the next page shows the simulated affected dose rates due to accumulator-ring GB colliding with the SD-sextupole magnet in rem/hr. Figure 5.8 shows the relative error of the simulation by location in a mesh tally within the storage ring shielding.

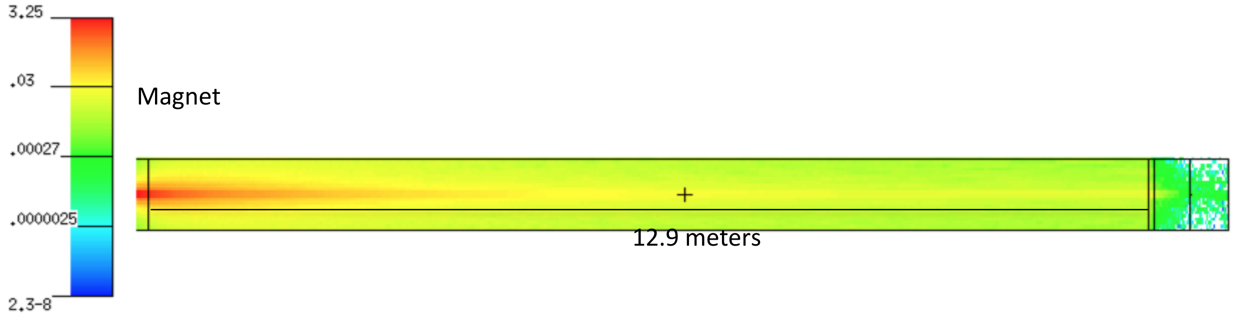

Figure 5.7. Effective dose rates in rem/hr for the simulated collision of the ALS-U accumulator-ring GB with a magnet

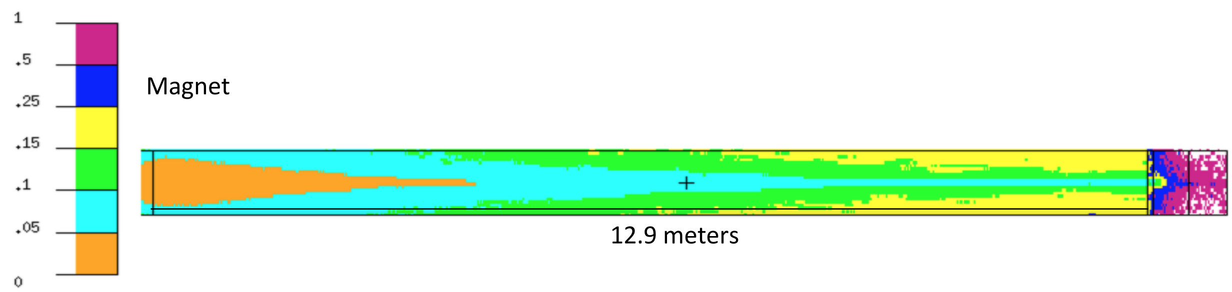

Figure 5.8. Relative error of the effective dose rate simulation shown on Figure 5.7

5.2.3 Dose Rates at the Storage-Ring Shield Wall

The ALS radiation shielding enclosures are constructed using both cast-in-place concrete structures and precast (removable) roof panels and wall blocks. Linac-vault walls are a minimum of 4 feet thick, as is the vault roof. Booster-synchrotron shielding is cast in place; the tunnel walls are a minimum of 2.5 feet thick, as is the tunnel roof. Removable roof blocks are provided in three locations around the booster for access to equipment and for maintenance.

The storage ring has a fixed (cast-in-place) inner wall and a removable (precast) outer wall section and roof section around its entire circumference to facilitate beamline egress from the tunnel. The storage-ring tunnel walls are nominally 1.5 feet thick; the roof of the storage ring is 1 foot thick. In some locations, the storage-ring shield wall and roof thicknesses differ from the nominal values, and in some locations lead shielding is added. This lead shielding is present at the ratchet walls at thicknesses between 3 and 4 inches (LBNL 2016).

This simulation assumes the GB has direct incidence upon a 3-inch-thick (7.62 cm) lead shield, immediately followed by a 1.5-foot-thick (45.72 cm) concrete shield wall, located 12.9 meters down the X-axis from the rear of the SD-sextupole magnet. This represents a worst-case scenario given the additional shielding located at some portions of the storage ring.

Due to the long distance to the shield wall following GB interactions with the SD-sextupole magnet, a number of variance reduction techniques were used to decrease the estimated tally uncertainties for the simulation and the amount of time to conduct the simulation.

Source Writing/Reading. To decrease the computer runtime for the shield wall simulation, the system was performed in two stages. A surface source write tally was created at the end of the SD-sextupole magnet, and a long run was performed to simulate the scatter within the magnet in the first stage. The simulation starts from that surface source, thus greatly reducing the computing time necessary for a simulation in the second stage.

Void Cells. A cell representing the direct path toward the shield wall from the SD-sextupole magnet was constructed encompassed by a zero importance (void) cell. If a particle enters the void cell, it is unlikely to exit that cell and contribute to the simulation; therefore, it is eliminated.

Particle Splitting. To help simulate particles scattering through the shield wall, the shield wall and F4 tally box were assigned increasing importance. A particle that makes it to the next segment in the +X direction is split into multiple particles with reduced weight so that any fraction that enters the detector cell may contribute to the simulation tally. This helps to guide the simulation in the direction of interest. In general, if used the splitting factors of 10X were assigned two different times in locations of high interaction downstream in the model. This may be done twice within a shieldwall downstream of the initial problem in front of the area of interest, 10X in the first half-thickness and another 10X in the second half-thickness for a total split of 100X.

5.2.3.1 No SD-Sextupole or Quadrupole Magnet Collisions, Beam Path #1

Assuming the electron beam path is not restricted to the aperture shown on Figure 5.5, the GB beam path could be limited to Beam Path #1 as shown on Figure 5.6. On this axis, the GB would not collide with either the SD-sextupole or the quadrupole magnets. Without the collisions, the only shielding media for the beam is the 3 inches of lead and the 1.5 feet of shield wall. A F4 tally cell was placed tangential to the GB exit from the vacuum chamber, indicating the following result.

Photon Effective Dose Rate After Exiting the Shield Wall = $3.45x10^{-01}$ rem/hr $\pm$ $4.6x10^{-2}$ rem/hr

Additionally, a Y-Z axis mesh tally was placed on the outside of the shield wall in order to show the variation between areas not tangential to the GB exit from the vacuum chamber; see Figure 5.9. The highest dose rate areas are localized and tens of centimeters wide at this distance downstream.

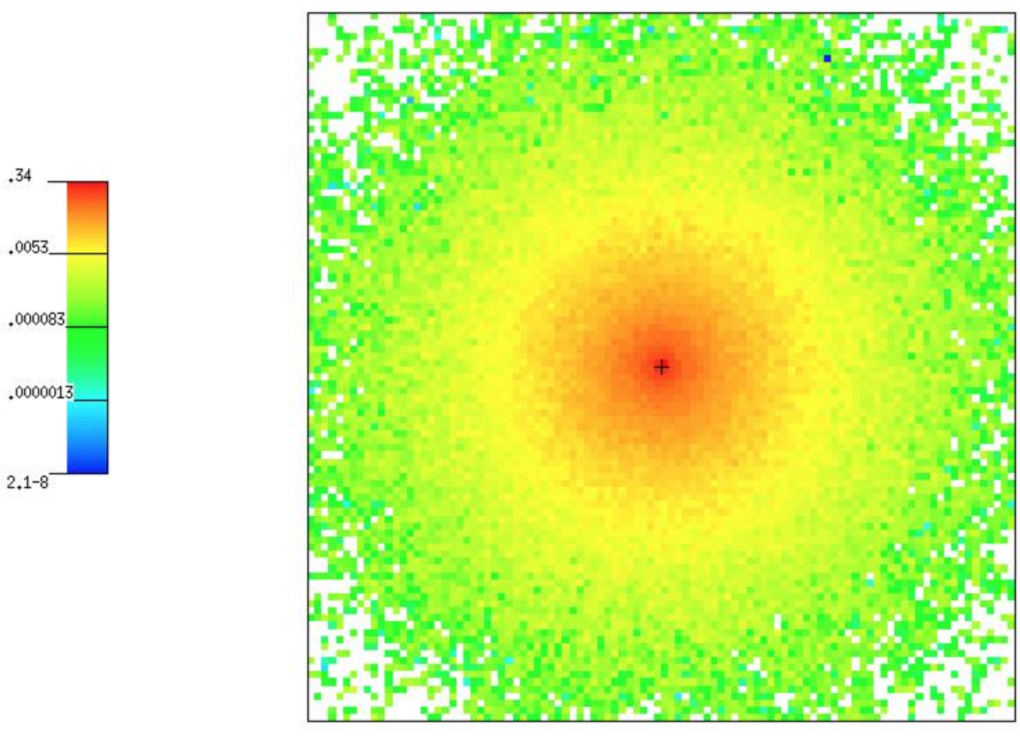

Figure 5.9. Beam Path #1 Y-Z axis photon effective dose rates (rem/hr) following collision with the shield wall

5.2.3.2 Beam Path #2

Assuming the electron beam path is restricted to the aperture shown on Figure 5.5, the GB beam path could be limited to Beam Path #2 as shown on Figure 5.6. On this axis, the GB would collide with 18.86 cm of the SD-sextupole magnet. Additionally, the GB would collide with the 3 inches of lead shielding and the 1.5 feet of shield wall. Based upon review of the proposed layouts, this is the most conservative scenario if the electron beam path is restricted to the aperture shown on Figure 5.5.

After traversing the shield wall, the effective dose is reduced to below Radiation Area posting requirements (5 mrem/hr). A F4 tally cell was placed tangential to the GB exit from the vacuum chamber, indicating the following result.

Photon Effective Dose Rate Exiting the Shield Wall = 1.15×10^{-3} rem/hr $\pm$ 3.34×10^{-4} rem/hr

Additionally, a Y-Z axis mesh tally was placed on the outside of the shield wall in order to show the variation between areas not tangential to the GB exit from the vacuum chamber; Figure 5.10.

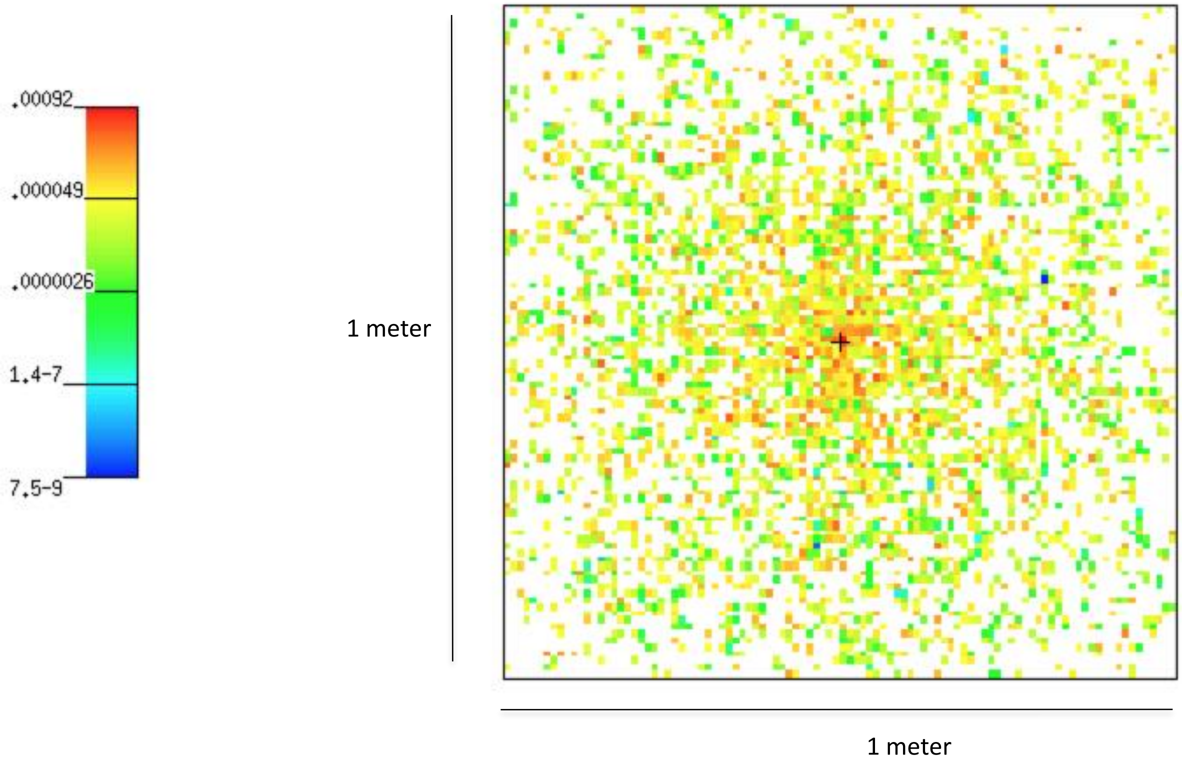

Figure 5.10. Beam Path #2 Y-Z axis photon effective dose rates (rem/hr) following collision with the shield wall.

These dose rates appear to be in an acceptable range for health and safety of workers nearby as the dose rates are below the posting level for Radiation Areas. The uncertainty associated with the simulation for beam path #2 is quite high, varying from approximately a factor of 0.25 up to 1; see Figure 5.11. As such, the result is considered relatively unreliable but may be within a factor of a few from the true value.

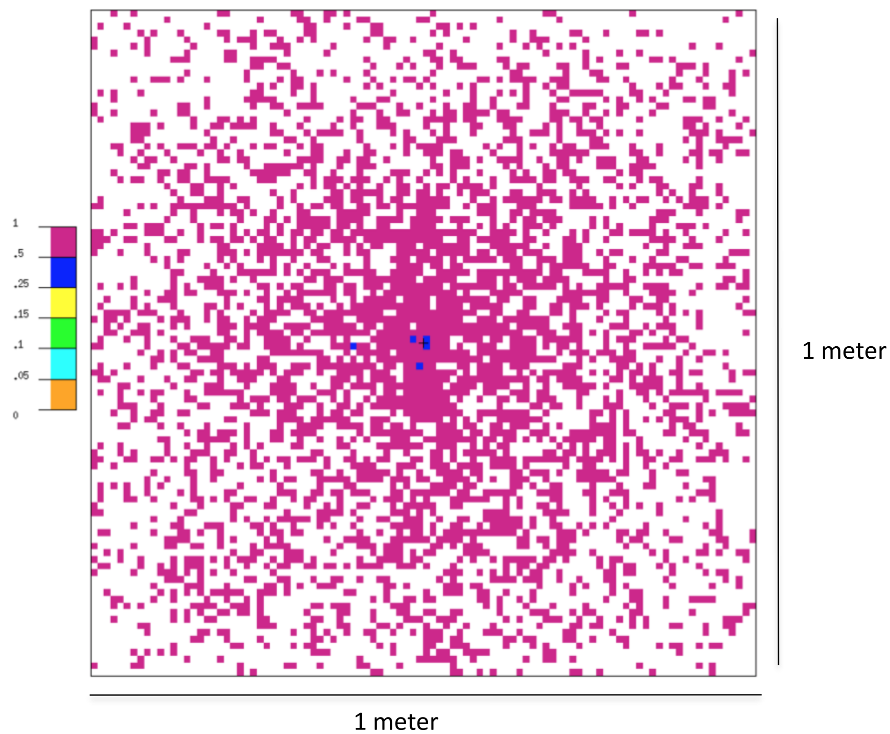

Figure 5.11. Beam Path #2 Y-Z axis relative error

5.2.3.3 Beam Path #4

Assuming the electron beam path is restricted to the aperture shown on Figure 5.5, the GB beam path could be limited to Beam Path #4 as shown on Figure 5.6. On this axis, the GB would collide with 32.57 cm of the quadrupole magnet. Additionally, the GB would collide with the 3 inches of lead shielding and the 1.5 feet of shield wall. This is the least conservative scenario if the electron beam path is restricted to the aperture shown on Figure 5.5.

After traversing the shield wall, the effective dose is reduced to below Radiation Area posting requirements (5 mrem/hr). A F4 tally cell was placed tangential to the GB exit from the vacuum chamber, indicating the following dose rate.

Photon Effective Dose Rate After Exiting the Shield Wall = $3.2\text{x}10^{-5}$ rem/hr $\pm$ $8.0\text{x}10^{-6}$ rem/hr

Additionally, a Y-Z axis mesh tally was placed on the outside of the shield wall in order to show the variation between areas not tangential to the GB exit from the vacuum chamber; see Figure 5.12**.** This confirms that the highest dose rate areas are highly localized.

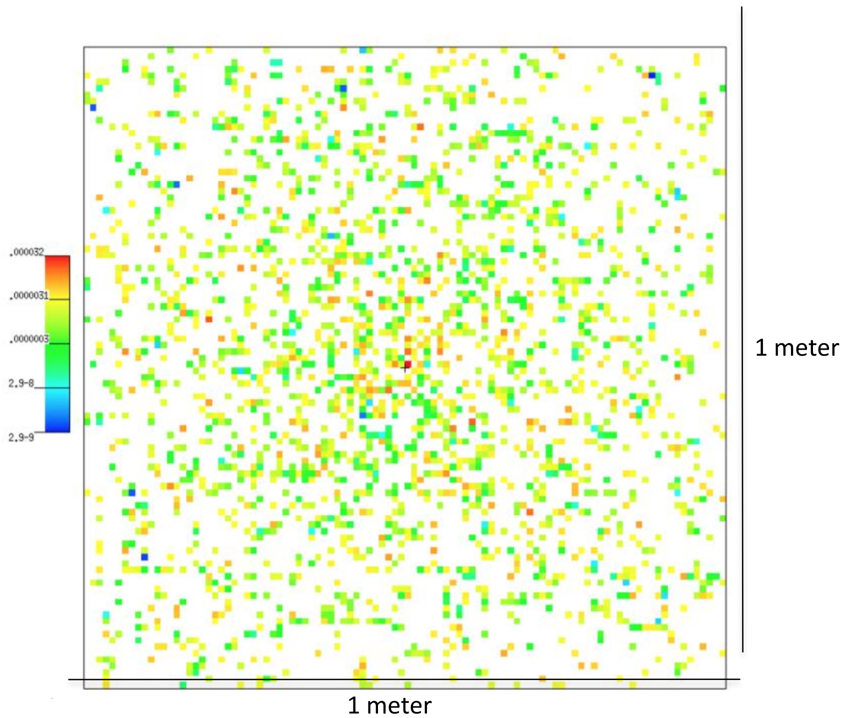

Figure 5.12. Beam Path #4 Y-Z axis photon effective dose rates (rem/hr) following collision with the shield wall.

These dose rates appear to be in an acceptable range for health and safety of workers nearby as the dose rates are below the posting level for Radiation Areas. However, the error associated with the simulation is extremely high at a factor of 0.5 up to 1 and should not be considered as valid; see Figure 5.13.

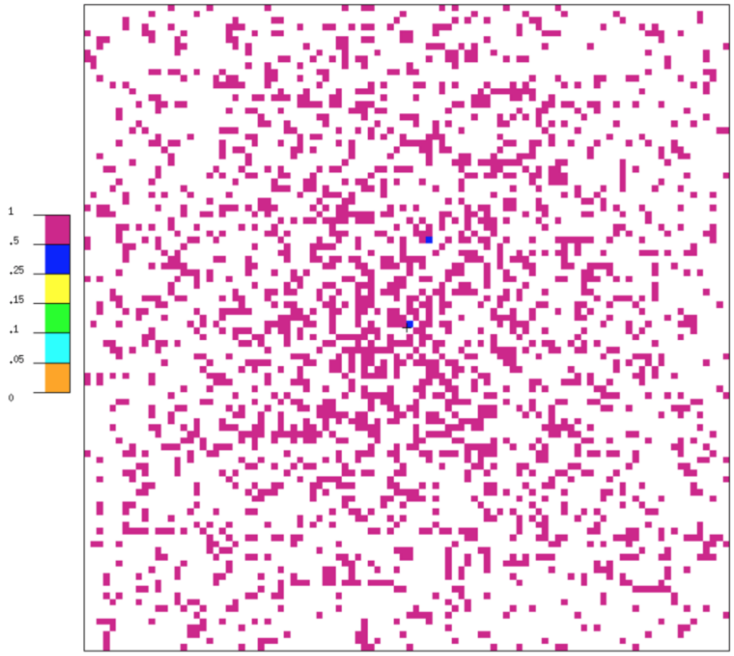

Figure 5.13. Beam Path #4 Y-Z axis relative error

6 RESULTS AND DISCUSSION; HVAC & ELECTRICAL PENETRATIONS

6.1 Source Term Generation Techniques

To generate bremsstrahlung for this simulation of the ALS-U's 2-GeV, 500 mA storage-ring electron beam the technique of a thick-target glancing collision was used to minimize self-absorption of the radiation and maximize dose rates at 90º.The 2-GeV accumulator-ring beam were collided against the side of a copper block (10cm x 10cm x 40cm). at an angle of 10 milliradians (mrad). This copper block represents a conservative approximation of collimator sources that could occur at ALS-U. This simulates a conservative beam loss scenario in which the highest dose rates are anticipated to be at approximately 90° and little self-shielding is present. This configuration is shown in Figure 6.1.

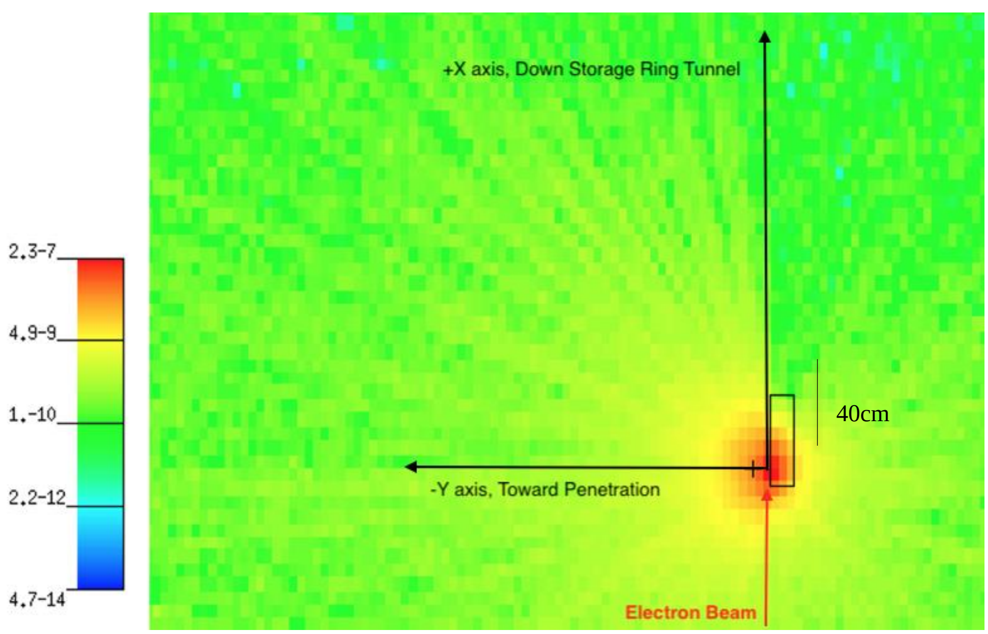

Figure 6.1. MCNP6 source term generation environment (ICRP21 (rem/hr)/(p/cm2-s))

6.1.1 Photon and Neutron Source Spectra

To collect the spectra of photons and neutrons reaching the penetration produced by the collision of the electron beam with the collimator, a F4 energy tally cell was placed a 30 cm in the –*y* direction perpendicular to the collimator blocks.

An additional F4 energy tally cell was placed at 1 foot outside the HVAC penetration to represent the particle energies that pass through the HVAC penetration. These two spectra and their relative error are shown on Figures 6.2 through 6.5. Figure 6.2 shows that the lateral photon spectra is largely composed of lower energies with significant contribution from isotropic 511 keV annihilation photons due to pair production. Figure 6.3 shows significant uncertainty at photon energies above ~2 MeV. This is due to poor contribution from higher energy photons which are largely forward scattered.

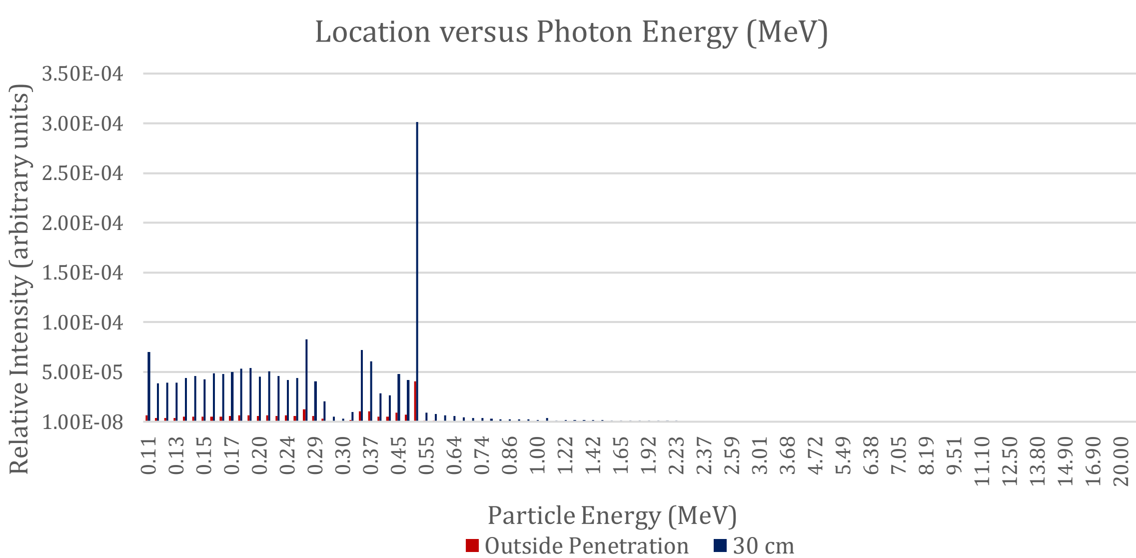

Figure 6.2. Photon energy spectrum (MeV) at two locations: outside of the penetration and at 30cm -Y

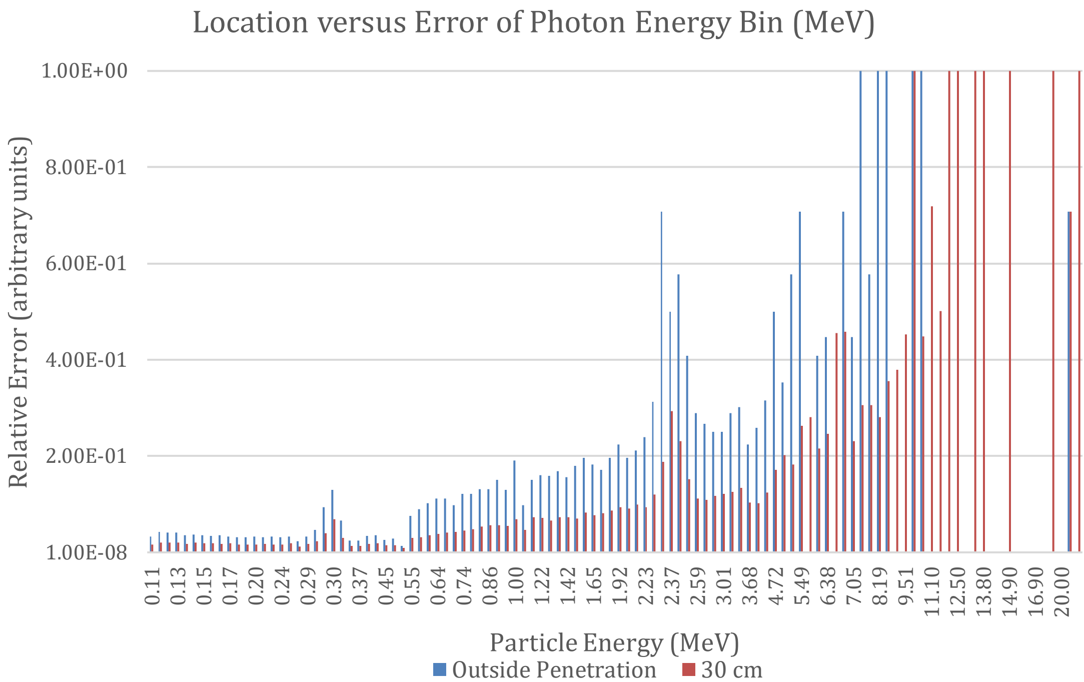

Figure 6.3. Photon energy bin error at two locations: outside of the penetration and at 30cm -Y

Figure 6.4 shows that the lateral neutron spectra is composed of mixed energies with relatively high uncertainty throughout the spectrum shown in Figure 6.5.

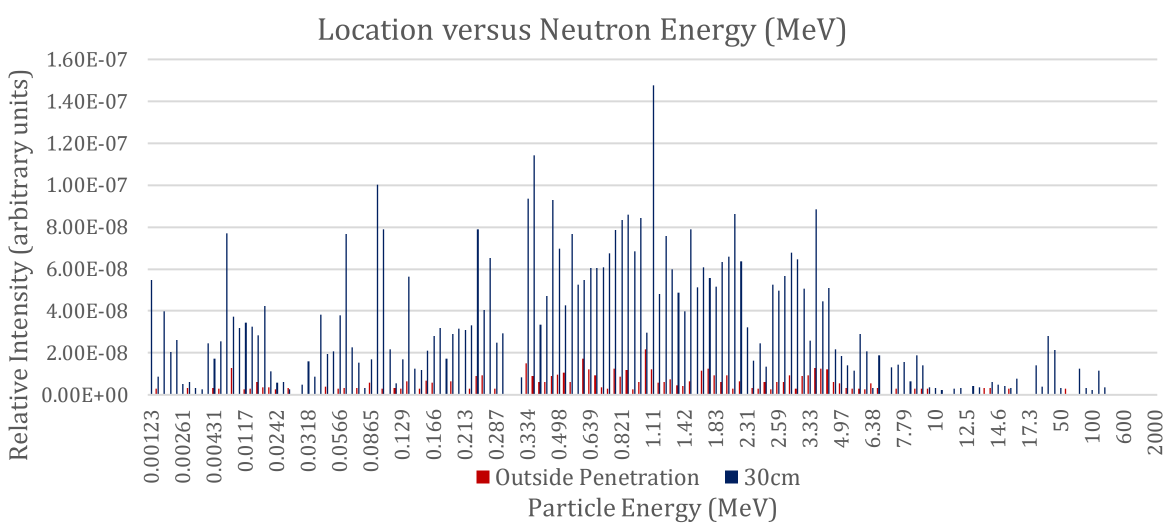

Figure 6.4. Neutron energy spectrum (MeV) at two locations: outside of the penetration and at 30cm -Y

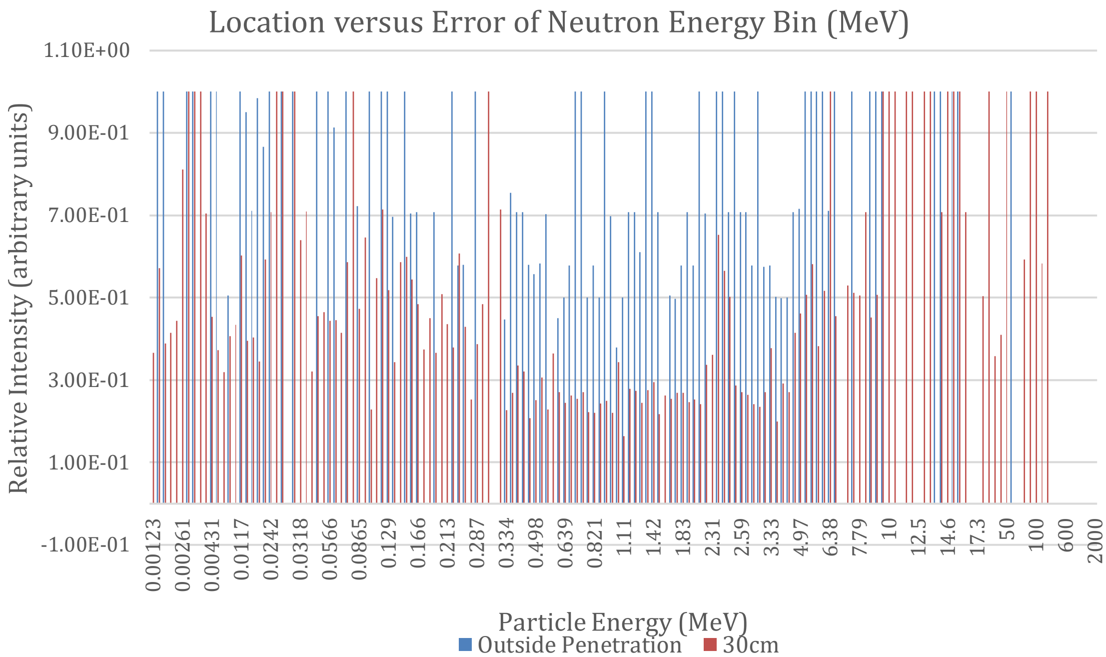

Figure 6.5. Neutron energy bin error at two locations: outside of the penetration and at 30cm -Y

6.2 MCNP Environment and Results

To characterize the dose rate resulting from the beam losses, a model was developed using the MCNP6 software. The transport model was based on available schematic and technical data for ALS-U.

The storage-ring and accumulator-ring collimators are simulated as being located perpendicular to each other, adjacent to the HVAC and electrical penetrations. This represents an additional measure of conservatism as the two collimators would not likely be placed immediately next to each other.

The storage ring has a fixed (cast-in-place) inner wall and a removable (precast) outer wall section and roof section around its entire circumference to facilitate beamline egress from the tunnel. However, the storage-ring tunnel walls are nominally 45-cm (1.5-feet) thick; the roof of the storage ring is 30-cm (1-foot) thick. The storage-ring shield wall and roof thicknesses in some locations differ from the nominal values, and lead shielding is present at the ratchet walls at thicknesses between 7.6-cm (3-in) and 10.2-cm (4-in) in some locations. This simulation assumes a 45-cm-thick (1.5-foot) concrete shield wall, located adjacent to the accumulator ring and storage ring along the *y*-axis. The current estimated dimensions of the HVAC duct to be installed are 40.6-cm (16-in) tall by 45.7-cm (18-in) deep and approximately 15.2-cm wide (6-in) (see Figure 6.6).

Due to the distance to the shield wall following bremsstrahlung interaction with the collimator, a number of variance reduction techniques were used to decrease the estimated tally uncertainties for the simulation and the amount of cpu time to conduct the simulation.

Particle Splitting. To help simulate particles scattering through the shield wall, the HVAC penetration, air in front of the F4 tally box, and the F4 tally box were assigned increasing importance. A particle that makes it to the next segment in the –*y* direction using this technique is split into multiple particles with reduced weight so that any fraction that enters the detector cell may contribute to the simulation tally. This helps to guide the simulation in the direction of interest.

A few items to note:

The variation in particle energy cutoff values from 0.1 MeV to 10 MeV and 0.1 MeV to 0.01 MeV for electrons and photons, respectively, were simulated with dose rates on the downstream side of the shield wall. The dose rates varied by <0.5% of the domains of the cutoff values investigated. To produce more efficient runtimes, energy cutoffs for electrons and photons within MCNP6 were set at 0.1 MeV for both particle types. Doing so, based on the observation of insignificant variance, it has no decernible input on the outcomes of the modeled system.

ICRP 21 photon flux-to-dose rate conversion factors were used as identified by the MCNP manual and the publication Rodgers 1984, *Fluence to Dose Equivalent Conversion Factors Calculated with EGS3 for Electrons from 100 keV to 20 GeV and Photons from 11 keV to 20 GeV*.

NCRP 38 (NCRP) neutron flux-to-dose rate conversion factors were used as identified by the MCNP manual and the publication *Neutron dose per fluence and weighting factors for use at high energy accelerators.* For energies above those listed in NCRP38, Cossairt and Vaziri 2008, *Neutron Dose per Fluence and Weighting Factors for Use at High Energy Accelerators*, were used.

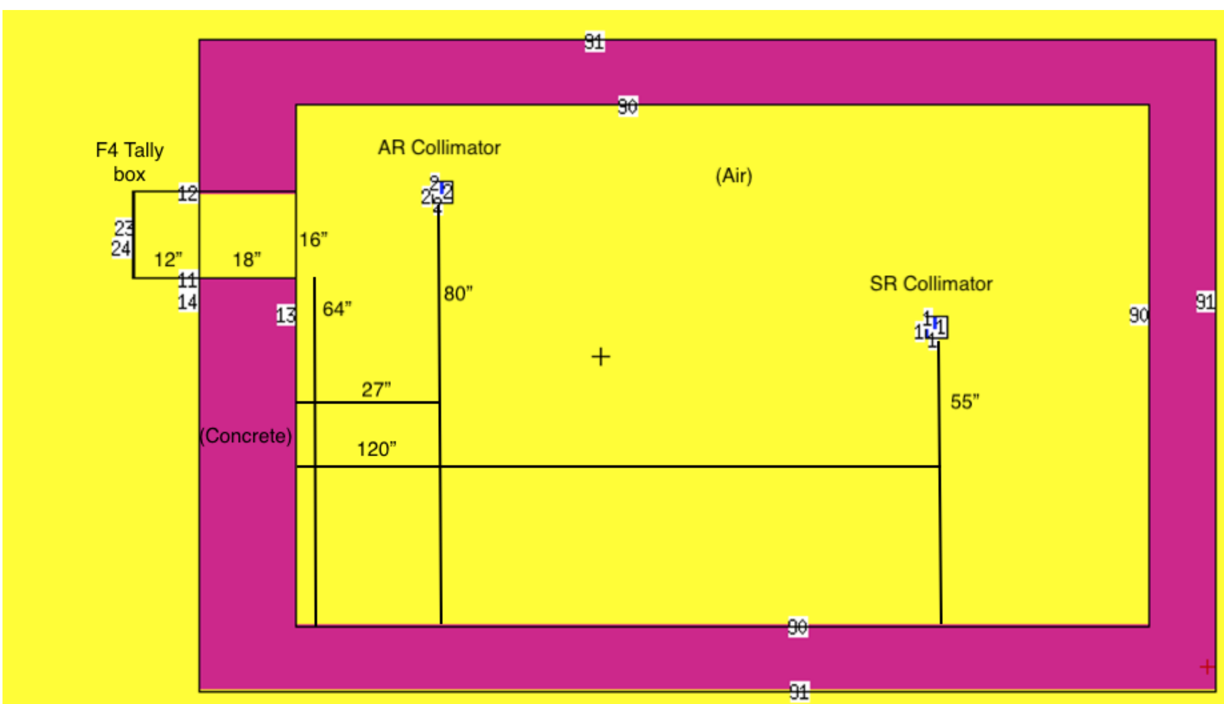

Figure 6.6. MCNP6 environment and dimensions of AR and SR to HVAC Penetration

6.2.1 Dose Rates Exiting the HVAC Penetration

To characterize the dose rates expected upon exiting the HVAC penetration from both the accumulator ring and storage ring, a F4 tally cell with the same area of the penetration was placed 30-cm beyond the exit of the penetration on axis with the penetration. The average photon and neutron cell tally results corresponding to dose rates of the F4 cell at this location outside the penetration are presented below and in Figures 6.7 through 6.10 along with their relative uncertainty.

Scenario 1: 5% Continuous Loss

Photon Dose Rate at 30-cm outside of HVAC Penetration = 3.41 mrem/hr ± 0.008

Neutron Dose Rate at 30-cm outside of HVAC Penetration = 1.44 mrem/hr ± 0.083

Combined Dose Rate at 30-cm outside of HVAC Penetration = 4.85 mrem/hr

Scenario 2: 100% Beam Dump

Photon Dose at 30-cm outside of HVAC Penetration = 82.8 mrem ± 0.008

Neutron Dose at 30-cm outside of HVAC Penetration = 35.1 mrem ± 0.083

Combined Dose at 30-cm outside of HVAC Penetration = 117.9 mrem

Note: If a 100% beam dump is experienced, the numbers provided above represent a dose to the F4 tally cell from a nearly instantaneous event, not a dose rate.

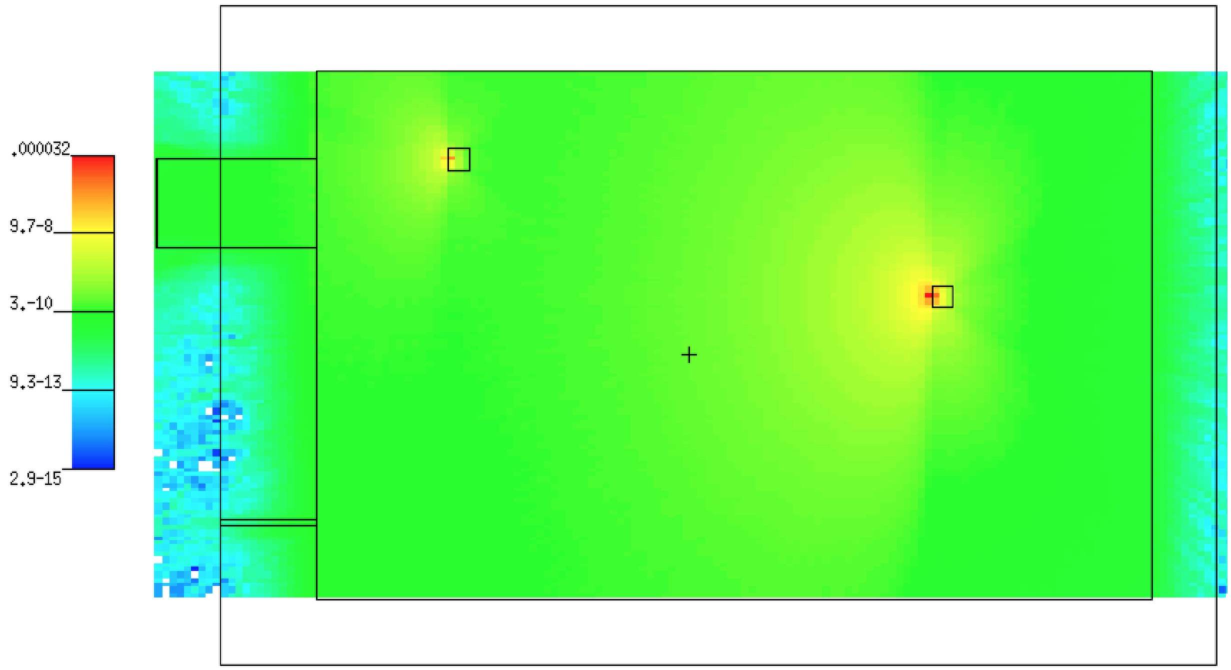

Figure 6.7. Photon dose rate tally result (ICRP21 (rem/hr)/(p/cm2-s)) of AR and SR tunnel cross section

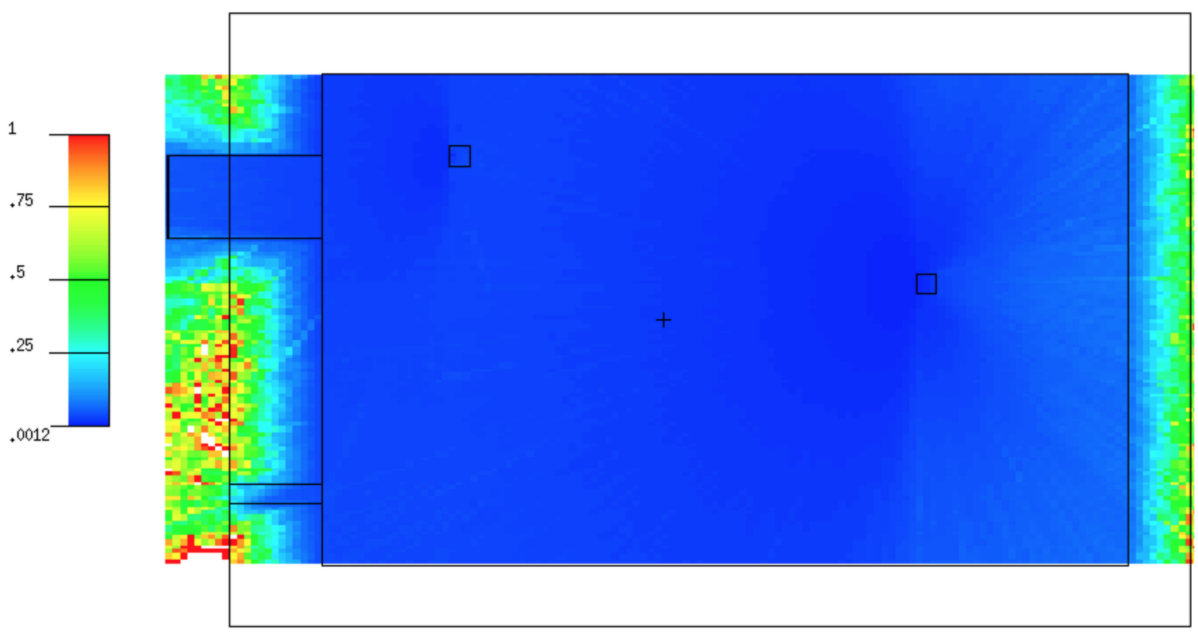

Figure 6.8. Photon dose rate relative error of AR and SR tunnel cross section

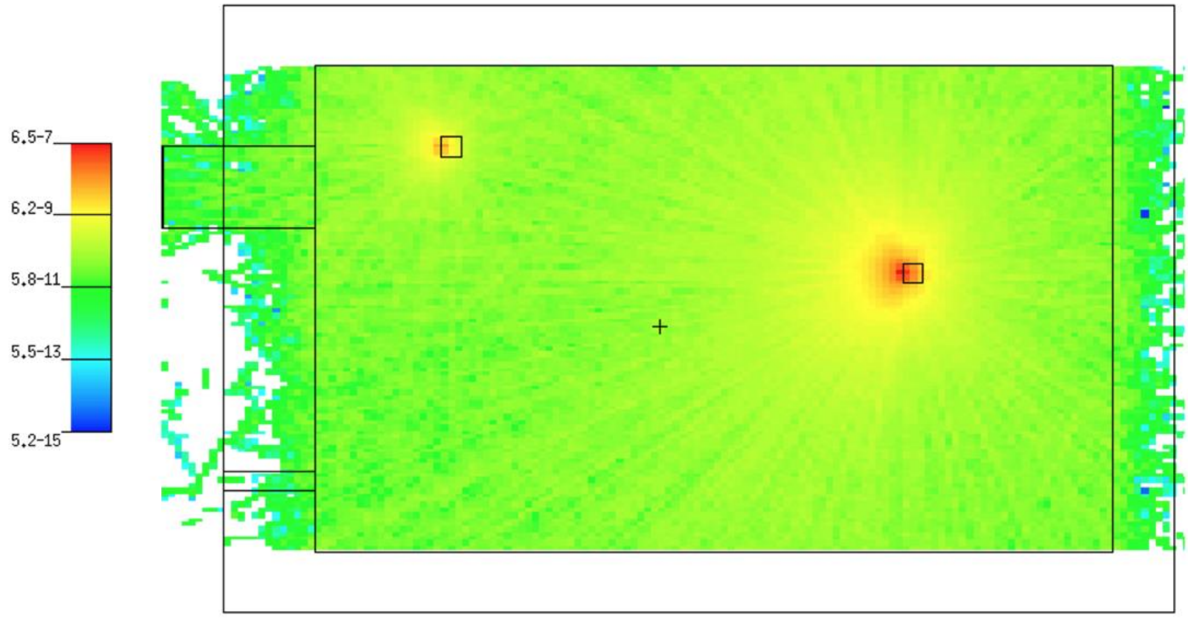

Figure 6.9. Neutron dose rate tally result (ICRP21 (rem/hr)/(p/cm2-s)) of AR and SR tunnel cross section

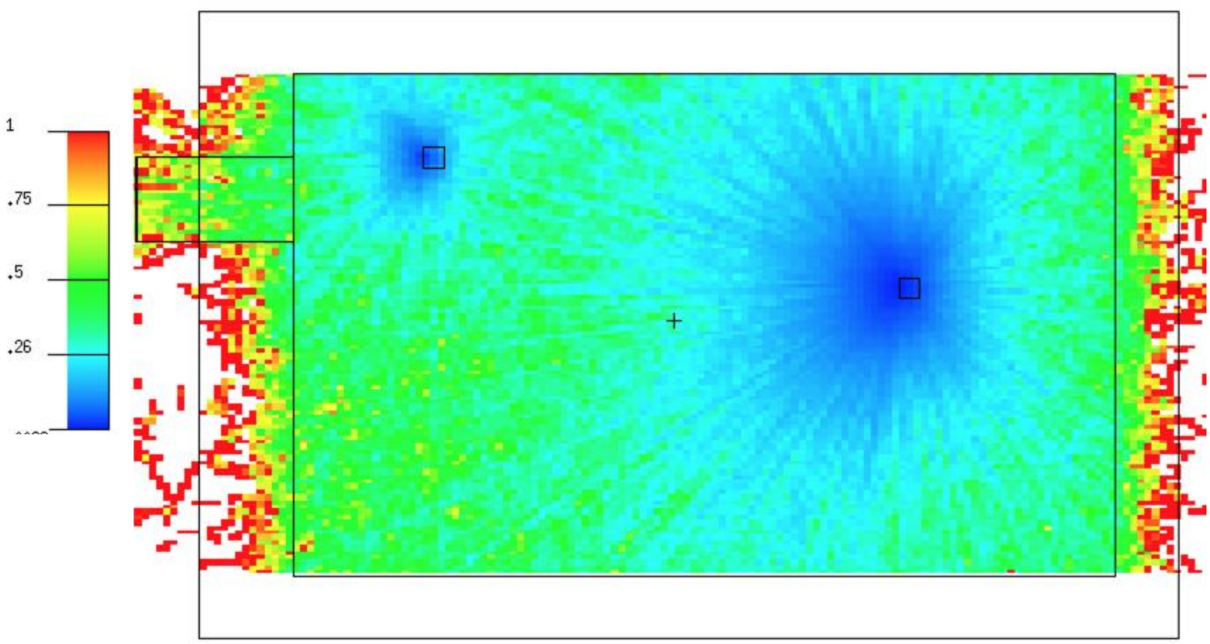

Figure 6.10. Neutron dose rate relative error of AR and SR tunnel cross section

6.2.2 Other Characteristics of the Radiation Exiting the HVAC Penetration

During the course of the simulation, a number of other characteristics of the HVAC penetration radiation fluence were noted.

Although the accumulator ring is assumed to run at one-tenth of the current of the storage ring, it contributes approximately 44% of the photon dose and 33% of the neutron dose to the F4 tally cell outside the penetration. This is largely due to geometric factors associated with their different heights, as well as distances from the F4 tally cell.

If the HVAC penetration were to be moved to a higher *z*-coordinate, as an example if it was flush with the roof block, the photon dose rate decreases to 2.67 mrem/hr from 3.41 mrem/hr. At this location the accumulator ring contributes approximately 58% of the photon dose rate. This is due to the decreased line of sight with the storage ring. However, this decrease is not substantial enough to avoid the additional shielding requirements necessary at the original location.

Simulations with and without the forward and rear walls of the storage ring were performed in order to determine the influence of scatter off the concrete walls to the dose and dose rate at the F4 tally cell. The difference observed in dose rate at the tally cell between runs with walls and without was <2%. This indicates that line of sight provides a critical contribution to the tally cell outside the shield wall.

6.3 Shielding Design of HVAC Penetration

The dose and dose rates for both scenarios were simulated using varying thicknesses of different types of shielding. It was determined that the limiting scenario for shield requirements is the Scenario 1: 5% continuous loss. This would have the shielding requirement of 0.1 mrem/hr radiation field. By meeting this design goal, Scenario 2's requirement, 5 mrem/event, will be met as well.

6.3.1 Shielding Requirements by Material for Scenario 1 (5% Continuous Loss)

To ensure that the desired institutional dose rate requirement of 0.1 mrem/hr is met in the 5% loss non-collimator sectors, the photon and neutron dose rates should each be limited to 0.05 mrem/hr. This limitation is conservative as a photon-shielding material will also provide some amount of shielding for neutrons, and vice versa. The photon and neutron values for concrete may be added together to determine compliance with the 0.1 mrem/hr limit.

A number of different shielding materials were simulated. All shielding simulations were run to an uncertainty of <0.05. As shown in Table 6.1 and on Figure 6.11, the following options will meet the required shielding criteria of 0.1 mrem/hr:

- 15-in of concrete
- 5-in of stainless steel and 9-in of polyethylene
- 3-in of lead and 9-in of polyethylene

Table 6.1. Dose rates (mrem/hr) versus inches of shielding for 5% continuous loss

Shielding Thickness (in)	Photon Dose (mrem/hr)			Neutron Dose (mrem/hr)	
	Concrete	Steel	Lead	Concrete	Polyethylene
0	3.41	3.41	3.41	1.44	1.44
1	2.5	1.08	0.19	1.2	0.92
3	1.32	0.14	0.01	0.7	0.35
5	0.62	0.02	-	0.48	0.15
7	0.35	-	-	0.31	0.09
9	0.2	-	-	0.23	0.04
11	0.12	-	-	0.15	-
13	0.07	-	-	0.12	-
15	0.04*	-	-	0.04*	-

* Projected

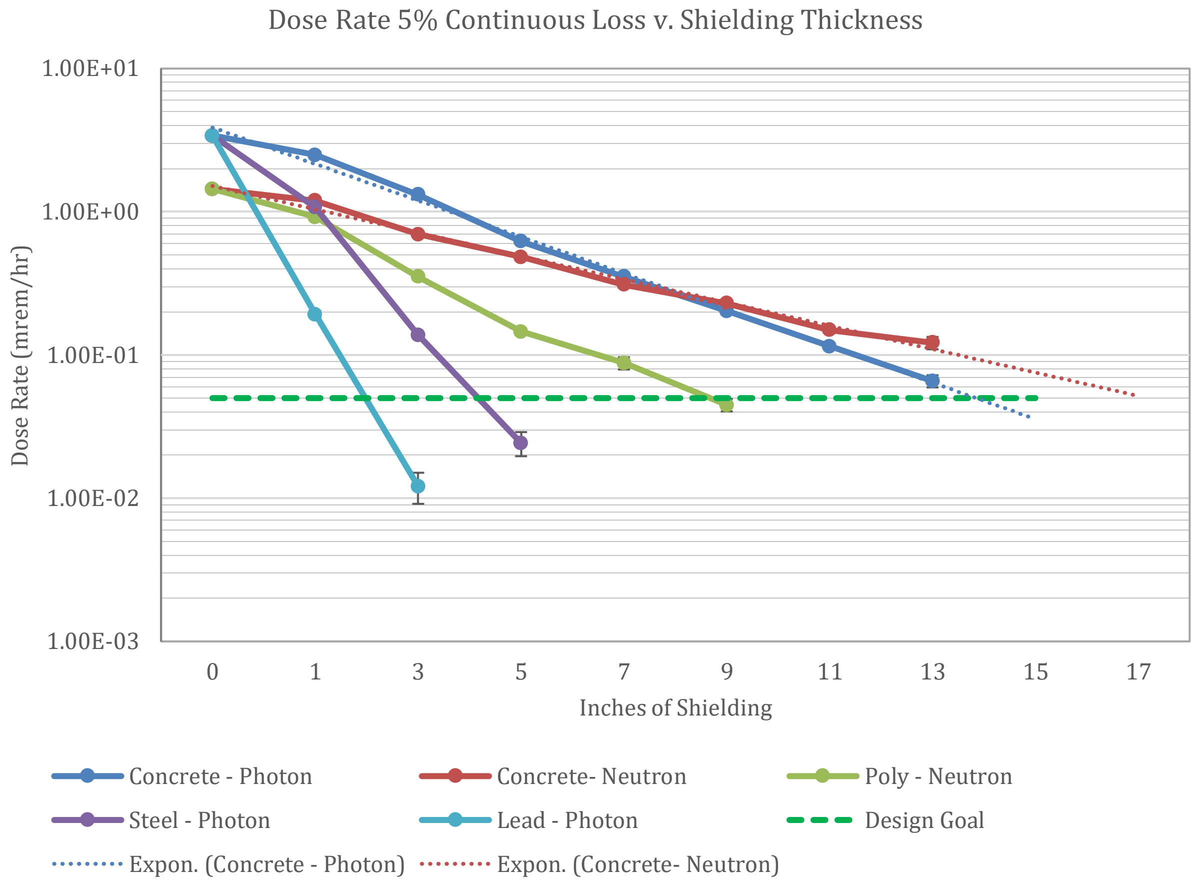

Figure 6.11. Dose rates (mrem/hr) versus inches of shielding for 5% continuous loss

6.3.2 Shielding Requirements by Material for Scenario 2 (100% Beam Dump)

The worst-case scenario dose for an abnormal event, such as 100% beam dump in a single area, is <5 mrem per event at any accessible location. Similar worst-case scenario dose logic is currently employed at the designated beam loss area called the Jackson Hole scrapers in Sector 8 of the storage ring. The roof blocks of the storage ring are nominally 12 inches of concrete and represent the highest accessible dose rates outside the storage ring.

A number of different shielding materials were simulated. All shielding simulations were run to an uncertainty of <0.05. Figure 6.12 and Table 6.2 present options that satisfy Scenario 2 shielding requirements.

This research has determined that the shielding required to meet the desired institutional dose rate requirement for the 5% continuous loss scenario (0.1 mrem/hr) is sufficient to bring the combined photon and neutron dose to <1.7 mrem per abnormal event. This meets the worst-case scenario dose of 5 mrem per event and is within the range of currently observed doses current doses seen per abnormal event at the Jackson Hole scrapers.

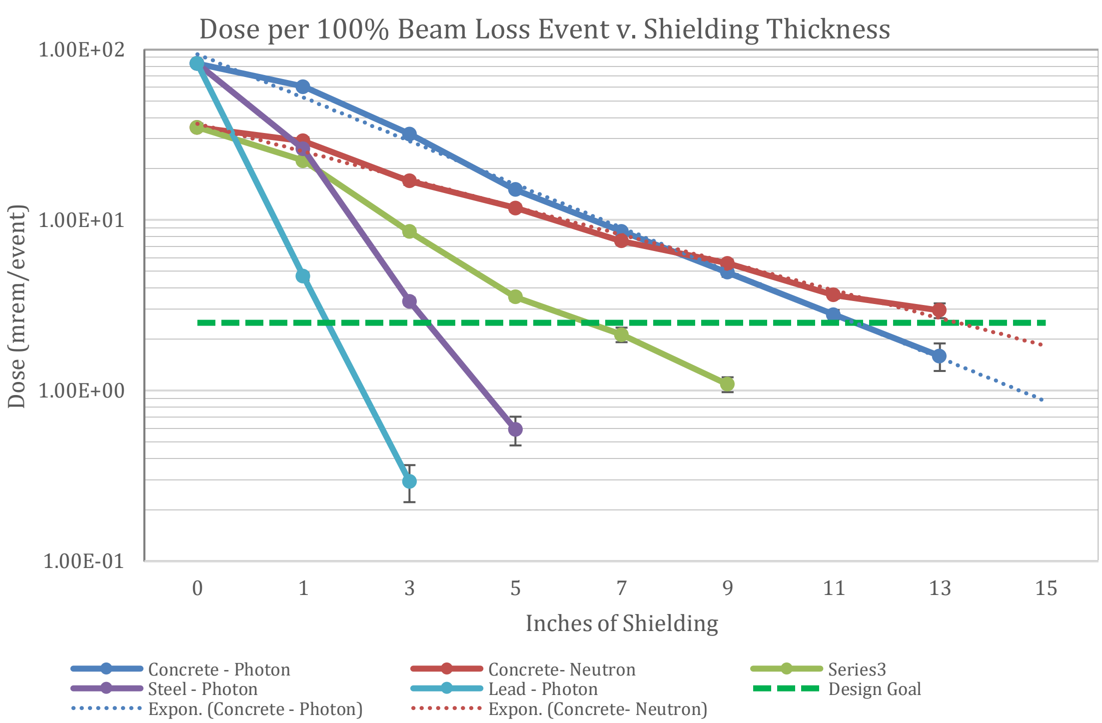

Figure 6.12. Dose (mrem) versus inches of shielding for 100% beam dump event

Table 6.2. Dose (mrem) versus inches of shielding for 100% beam dump event

Shielding Thickness (in)	Photon Dose (mrem/event)			Neutron Dose (mrem/event)	
	Concrete	Steel	Lead	Concrete	Polyethylene
0	82.78	82.78	82.78	35.05	35.05
1	60.63	26.12	4.68	29.12	22.36
3	32.04	3.34	0.29	16.94	8.54
5	15.12	0.59	-	11.77	3.54
7	8.58	-	-	7.54	2.13
9	4.93	-	-	5.59	1.09
11	2.79	-	-	3.64	-
13	1.6	-	-	2.96	-
15	0.9*	-	-	1.8*	-

* Projected

6.3.3 Novel Shielding Designs

Labyrinth Design

Shielding guidance shown in Tables 6.1 through 6.2 above were included in the MCNP environment in order to test their validity in traditional labyrinth designs that may be implemented within the HVAC penetration. As discussed in Section 6.3.1, it was determined that 3 inches of non-labyrinth design stainless steel should reduce the photon dose rate from 3.41 mrem/hr at the F4 tally cell to approximately 0.138 mrem/hr. Although streaming through the labyrinth is present, overlapping barriers result in more overall shielding than expected using the traditional thickness, as discussed below.

An overlapping two-barrier high-Z material (steel or lead) and low-Z material (polyethylene) labyrinth was added to the HVAC penetration as shown on Figure 6.13. Although not an ideal absorber of neutrons, steel or lead will interact with fast neutrons via inelastic scatter as long as the energies are above the first excited state of the nucleus, typically several hundred kiloelectron volts (keV). At energies below this first excited state, inelastic scattering becomes energetically impossible, and only elastic scattering is left as the removal process aside from nuclear reactions. Elastic scattering is an inefficient mechanism for energy transfer from neutrons scattering off a much more massive nucleus such as iron or lead.

The first excited state of Fe-56 is 847 keV. Neutrons having kinetic energies above 847 keV in a given spectrum will be slowed in inelastic scattering to approximately that energy. At this point, neutrons will have a low probability of interacting in any remaining iron medium and will pass through to the polyethylene where they will be thermalized and absorbed. Thus, it is important that the iron or lead shielding be backed or capped by the low-Z polyethylene shield.

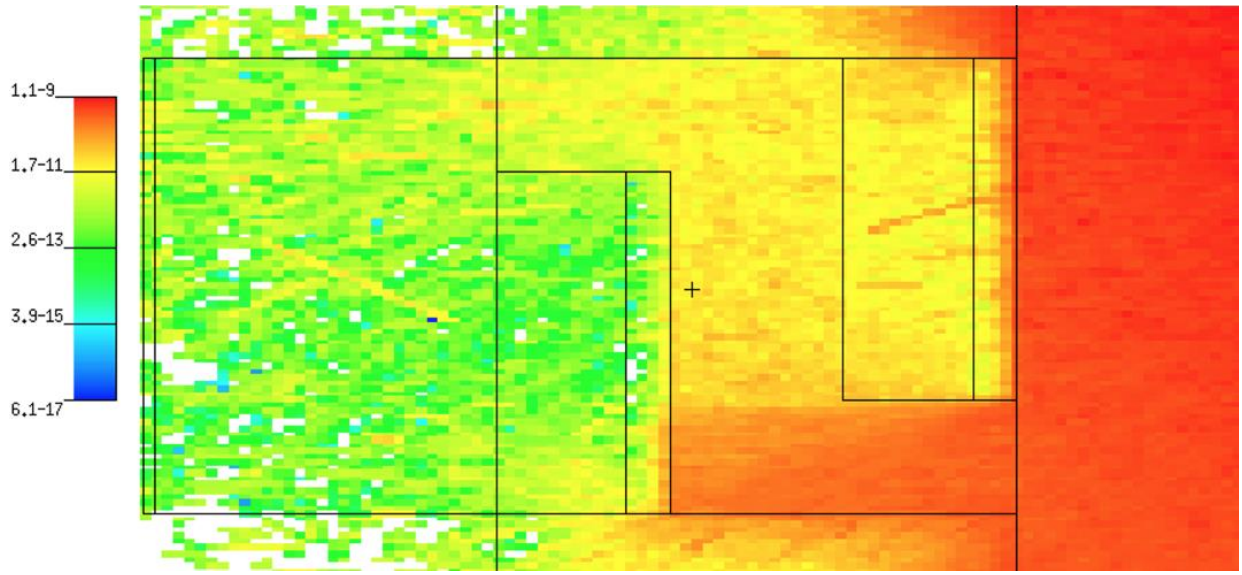

Figure 6.13. Two-barrier labyrinth HVAC shield design dose rate tally result viewed from above (ICRP21 (rem/hr)/(p/cm2-s))

Different geometries with varying amounts of stainless steel or lead and varying amounts of polyethylene of labyrinth shielding were simulated. The dose and dose rates are shown below in Tables 6.3 and 6.4.

Scenario 1: 5% Continuous Loss

Table 6.3. Dose rate (mrem/hr) versus inches of shielding for 5% continuous loss

Inches of Shielding		**Dose Rate (mrem/hr)**		
Stainless Steel	**Polyethylene**	**Photon**	**Neutron**	**Combined**
4	8	$9.72\text{x}10^{-02} \pm 0.025$	$1.02\text{x}10^{-01} \pm 0.198$	$1.99\text{x}10^{-01}$
5	9	$6.5\text{x}10^{-02} + 0.034$	$8.12\text{x}10^{-02} + 0.21$	$1.47\text{x}10^{-01}$
Lead	**Polyethylene**	**Photon**	**Neutron**	**Combined**
3	9	$5.81\text{x}10^{-02} \pm 0.035$	$9.46\text{x}10^{-02} \pm 0.18$	$1.53\text{x}10^{-01}$
3	11	$4.21\text{x}10^{-02} \pm 0.06$	$7.85\text{x}10^{-02} \pm 0.21$	$1.21\text{x}10^{-01}$

Scenario 2: 100% Beam Dump

Table 6.4. Dose (mrem/event) versus inches of shielding for 100% beam dump

Inches of Shielding		Dose (mrem/event)		
Stainless Steel	Polyethylene	Photon	Neutron	Combined
4	8	2.36 + 0.025	2.48 + 0.198	4.84
5	9	1.59 + 0.034	1.97 + 0.21	3.56
Lead	Polyethylene	Photon	Neutron	Combined
3	9	1.41 + 0.035	2.30 + 0.18	3.71
3	11	1.02 + 0.06	1.91 + 0.21	2.93

While the Scenario 2 design goal of less than 5 mrem/event is met with all proposed combinations, Scenario 1's design goal of less than 0.1 mrem/hr is not. With a total available depth of 18-inches in which to place shielding, it is assumed that exceeding 12-inches combined would negatively impact the functionality of the HVAC system. Thus, the best combination of shielding materials is 3-inches of lead and 9-inches of polyethylene. This is calculated to result in a dose rate of 0.15 mrem/hr in the 5% continuous loss scenario and is considered to be consistent with the ALARA philosophy although the design goal was not met as the design is too expensive and complex to be installed in a confined area.

This simulation used a number of conservative assumptions such that the dose rates present outside of the HVAC penetrations is likely below 0.1 mrem/hr design goal.

Traditional Shielding Design

If a non-labyrinth style shield block design is used, 12-inches of concrete placed on the outside of the penetration would be sufficient to reduce dose rates and total dose per event to acceptable levels. This is considered equivalent to the existing shieldwall thickness.

6.4 Shielding Requirements of Electrical Penetration

Dose rates adjacent to the electrical penetration are dominated by the storage ring. This is because dose rates outside the storage-ring walls are closely tied to line-of-sight paths with the two rings. The accumulator-ring’s position with respect to the penetration does not provide line of sight pathways or easy entry into the electrical penetration for scattering.

The electrical penetration’s line-of-sight from the storage ring will be maximized at heights equal to that of the storage ring on the shield wall. As the height and/or radius of the electrical penetration decreases, less radiation will have line of sight or the ability to efficiently scatter through the penetration. Therefore, the limiting factor for the height and radius of a cylindrical electrical penetration is the line of sight with the storage ring.

Facility experience has determined that synchrotron radiation emerging through the electrical penetrations is easily shielded by a shield design of a few millimeters of steel positioned either on the inside or outside shield wall for each electrical penetration.

6.4.1 Limiting Dimensions for the Electrical Penetration

The ALS-U Project has expressed interest in using 6-inch-diameter holes for the electrical penetration. This simulation uses only 6-inch holes for the simulations and seeks to set a maximum centerline height at which the holes may be placed on the storage-ring wall in areas other than directly downstream of the large achromat accelerator straights on the ratchet walls. Holes less than 6 inches may also be used.

The dose and dose rates for both scenarios were simulated by varying the height of penetration. It was determined that the limiting scenario for shield requirements is the Scenario 1, 5% continuous loss, 0.1 mrem/hr requirement. By meeting this design goal, Scenario 2's requirement, 5 mrem/event, will be met as well.

The combined photon and neutron dose rates are plotted on Figure 6.14. This shows that at approximately 21 inches above the floor the dose rate due to bremsstrahlung radiation exceeds the design goal of 0.1 mrem/hr. Thus, the height limit of the centerline of the 6-inch-diameter electrical penetration is set at 20 inches above the floor.

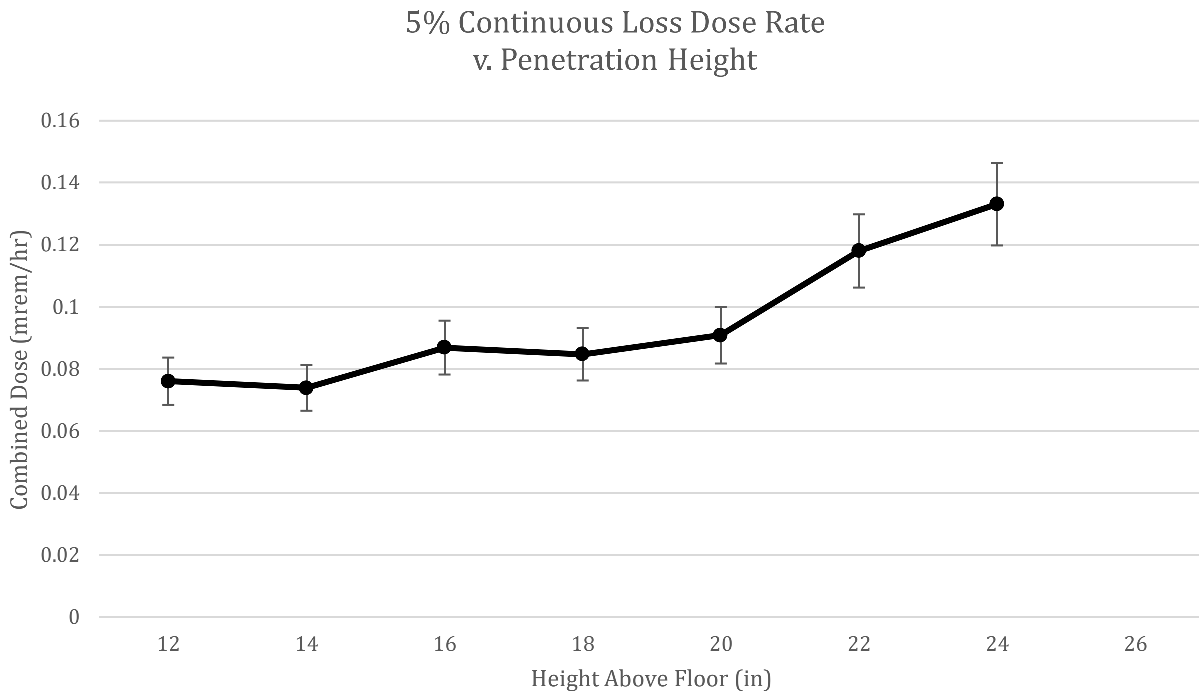

Figure 6.14. Combined photon and neutron dose rates in the electrical penetrations versus height above the floor

6.5 Benchmarks of MCNP6 Simulation

As the ALS-U is not yet constructed these simulations do not have a measured baseline, in response two benchmarks were created:

- Comparison against ALS measured data for a 100% beam loss event above a scraper
- Comparison against a similar geometry and charge loss model in SHIELD11 in order to provide thick-target bremsstrahlung baseline numbers to which the MCNP6 results could be compared.

6.5.1 ALS Measured Data

In order to compare the Monte-Carlo MCNP6 code in a comparable simulation to that of ALS-U against measured data, a simulation was created to reproduce a 100% beam loss event at the current 1.9-GeV ALS. During an unplanned beam loss event from 500 mA at the ALS on February 09, 2023, the SR025 Roof Neutron and Gamma monitors recorded an integrated dose of 2.76 mrem and 4.62 mR, respectively. The summed integrated dose from this event was 7.4 mrem. This location is above one of the two Jackson Hole scrapers resting on the concrete roof block of thickness 30-cm. The scraper location height for the ALS within the storage ring tunnel remains 55-inches off of the storage ring tunnel floor as shown in Figure 6.6. For the purposes of comparison against the simulation, both the measured data and simulated data represent a scraper location of 50% beam-intercepting efficiency of 95% of the total beam current. The other 50% of the beam-interception being lost at the other scraper location, and the other 5% of the total beam current being spread around the storage ring. Figure 6.15 shows the beam loss event in the telemetry program RPix with the integrated dose, shown in the top right corner of the figure, of the 2-minute loss event summing to 7.4 mrem.

Measurement error may be caused by random effects and systematic effects in the measurement process. Measurement errors may also be spurious errors, such as those caused by human blunders and instrument malfunctions. However, these spurious errors are not taken into account in the statistical evaluation of measurement uncertainty. The error of a measurement is unknowable, because one cannot know the error without knowing the true value of the quantity being measured. However, the uncertainty of a measurement may be to characterize the dispersion of the values that could reasonably be attributed to the actual value. The uncertainty of a measured value thus gives a bound for the likely size of the measurement error (MARLAP 2004).

To quantify this measurement uncertainty, the factors contributing to the measurement should be considered. In this case, the location of the detectors themselves as well as the location of their sensitive volume will contribute to the value. Although the detectors were resting on the floor, the measurements from the sensitive volume of the detectors are going to be approximately 10- and 15-cm above the surface for photon and neutron respectively. An additional error related to the location could be poor placement of the detectors not in the highest radiation field location. This may be considered a spurious error and is not considered further. The primary uncertainty with this measurement is the source assumption of a 50/50 split of the 95% of the beam current between the two scrapers. This could be conservatively bounded at a 60/40 split. As such if this was not the maximum source the true value could be 10/50 or 0.2 higher. If this was the maximum source, the value could be 0.2 lower at another location. This 20% measurement uncertainty should be considered bounding for this system. As such, the measured value should be considered bounded at 7.4 mrem $\pm$ 1.5 mrem.

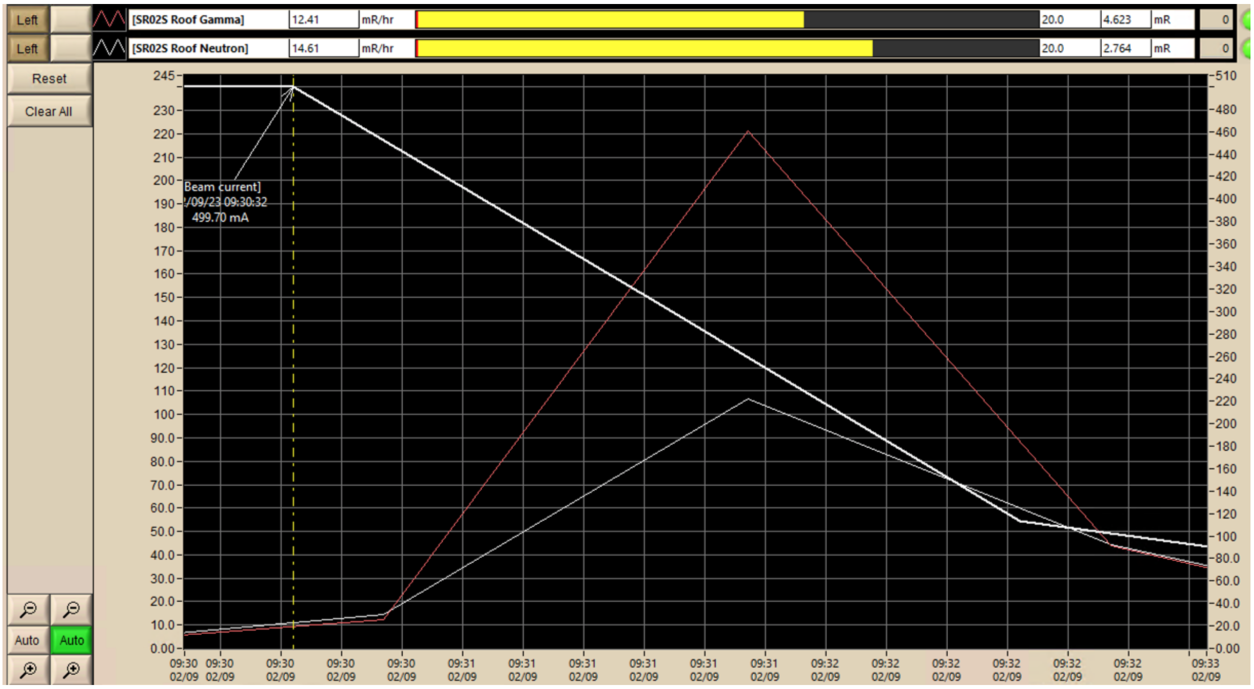

Figure 6.15 RPix Depiction of ALS 500 mA Beam Loss Event

The MCNP6 simulation attempted to reproduce these measurements by colliding the ALS's 500 mA, 1.9-GeV electrons into a copper block at a 10-mrad glancing angle. The concrete roof thickness at this location is 30-cm. The F5 photon and neutron tallies are located 30-cm above the surface of the roof as opposed to the measurement location's 10- and 15-cm. The photon and neutron F5 tallies recorded 2.1 mrem and 4.0 mrem per 100% beam loss event, respectively. Both tallies had uncertainties of <0.01.

The simulated ALS summed dose of 6.1 mrem/event compares well against that of the 7.4 mrem/event measured data or 82.4% of the measured values. This slight underprediction of the measured value can partially be attributed to the additional 15 or more cm to the simulated location. Additionally, the assumed 50/50 split of scraper efficiency in the simulation may also not reflect the exact split of the as-found equipment. The simulated value of 6.1 mrem/ event is within the bounding measurement uncertainty of 7.4 mrem ± 1.5 mrem. This comparison serves as a baseline of simulated to measured data in a comparable system. As such, this application may be extended to modeling ALS-U and its systems with the understanding that it represents an estimate of losses at a new accelerator not verified data or models. The 1.9-GeV ALS and 2.0-GeV ALS-U will share many similarities regarding geometry and loss mechanisms in a simple case such as this, but there will need to be many new measurements taken at the completed ALS-U in order to verify the results of this larger work.

A discussion of potential bias to be added to simulations from this work is addressed in the conclusion.

6.5.2 Analytical Code SHIELD11

SHIELD11 is a computer code for performing shielding analyses around a high energy electron accelerator. It makes use of simple analytic expressions for the production and attenuation of photons and neutrons resulting from electron beams striking thick targets, such as dumps, stoppers, collimators, and other beam devices. The formulae in SHIELD11 are based on the extrapolation of experimental data using simple physics ideas. These scaling methods have been tested against a limited set of conditions: 1-15 GeV electrons striking 10-20 radiation lengths of iron (Nelson, 2005).

The SHIELD11 model used for benchmarking was a 1kW beam of 10 GeV electrons striking a standard-target arrangement—namely, a 12-inch long cylinder of iron, having a radius of 2-inches. The primary shield is a 5-ft thick concrete wall, the inside surface of which runs parallel to the beam line at a distance of 4-ft. The dose rate at 90º on the exterior of the wall is examined.

A similar MCNP6 simulation under these conditions were performed. The source assumed direct incidence on a 10x10x40cm iron block located 4-ft away from a 5-ft thick concrete wall running parallel to the beam.

The MCNP6 simulated a combined dose equivalent rate of $1.52 \times 10^{-1} \pm 4.57 \times 10^{-2}$ rem/hr, while the SHIELD11 code produced a combined dose equivalent rate of 4.69×10^{-1} rem/hr. This indicates values of MCNP6 to be a factor of 0.324 that of SHIELD11. In a similar comparison of radiological simulation codes for the electron accelerator NSLS-II, MCNP6 produced values that were a factor of 0.625 that of SHIELD11 (Xia 2018). While comparison of Monte Carlo simulation values such as these against an analytical code like SHIELD11 has limited value, it does show that the bremsstrahlung source term generation and corresponding secondary radiation does produce dose equivalent rate values that are reproduceable in other (measurement-based) analytical software prior to modeling a complex geometry.

7 RESULTS AND DISCUSSION; ELECTRON BUNCH SWAPPING

7.1 Booster-To-Accumulator (BTA)

7.1.1 BTA Source Term Generation

To generate the bremsstrahlung for the simulation associated with the Booster-to-accumulator swap, ALS-U's 2-GeV was collided directly into a thick target copper block (10cm x 10cm x 40cm). This copper block being representative of a collision with a magnet following a beam loss. This simulates a conservative beam loss scenario.

The amount of charge lost in the BTA will vary depending on the state of fill of the bunch train and the mode in which the accelerator is operating, whether top-off or fill. Tables 4.5 and 4.6 detail the charge loss per fill cycle and charge loss during top-off operations.

7.1.2 BTA Geometry

As shown in Figures 7.1 and 7.2 below, the BTA follows a path from the booster into the accumulator ring at the BTA septum. This path is outlined in red in the figure. To reach this point, the BTA takes a 10-degree upward angle that is a 14-degree incidence with the inner storage ring wall that is 1-meter thick. These assumptions are built into the source term of the Monte Carlo model.

Figure 7.1. Booster-to-Accumulator path

Figure 7.2. Booster-to-Accumulator Injection Septum

The SR and AR have a fixed (cast-in-place) inner wall and a removable (precast) outer wall section and roof section around its entire circumference to facilitate beamline egress from the tunnel. The tunnel walls in Sector 1 are nominally 1-meter thick; while the roof in Sector 1 is 0.45-meters thick and steps down to 0.3-meters in the roof block that follows. The penetration located above the BTA septum is 0.3-meters in diameter.

Table 7.1. Penetration Locations and Distance to Points of Interest

Points of Interest	Sector #	Roof block #	Roof block thickness (in)	Distance from SR (cm)	Distance from AR (cm)	Distance from BTA (cm)
AR collimators in Straight 1, BTA septum	1	82	18	188.83	48.84	27.79
	2	7	12	187.81	43.34	-
SR Y-collimator	3	13	12	182.44	45.61	-
	4	20	12	187.13	41.89	-
	5	27	12	189.19	46.08	-
	6	34	12	191.52	43.09	-
	7	41	12	189.02	40.09	-
	8	48	12	177.85	43.38	-
	9	55	12	194.17	49.16	-
	10	62	12	193.75	44.03	-
SR X-collimator	11	69	18	183.88	46.62	-
SR X-collimator, BTA	12	75	18	264.28	31.46	88.09

all distances (cm) are estimations from penetration center to nearest AR/SR point

7.1.3 BTA MCNP6 Environment

To characterize the dose rate resulting from the beam losses, a simple model was developed using the MCNP6 software. The transport model was based on available schematic and technical data for ALS-U. This environment is shown in Figures 7.3 and 7.4.

ALS-U's 2-GeV bunch train is collided directly into a thick target copper block (10cm x 10cm x 40cm). This copper block is representative of a collision with a magnet following a routine efficiency-related or complete beam loss from the BTA. The e- train is assumed to collide directly under each penetration although in Sector 1 there is approximately a 28-cm distance to the center of the penetration. Other sectors contain similar penetrations but the closest distance to a loss point is in Sector 1 and hence this represents the most conservative system to model. Moving in the +Z direction, there is 40-cm of air before reaching the penetration passing through the 30-cm roof block.

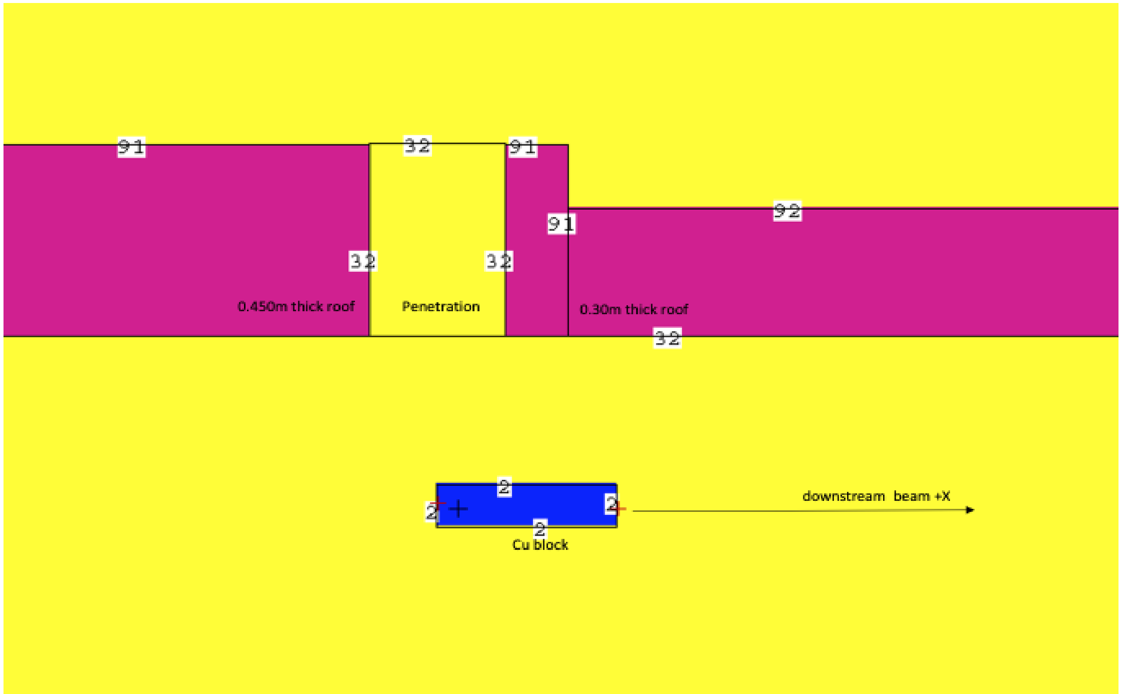

Figure 7.3. BTA MCNP6 Environment showing the copper block in relation to the shield roof penetration; X-Z

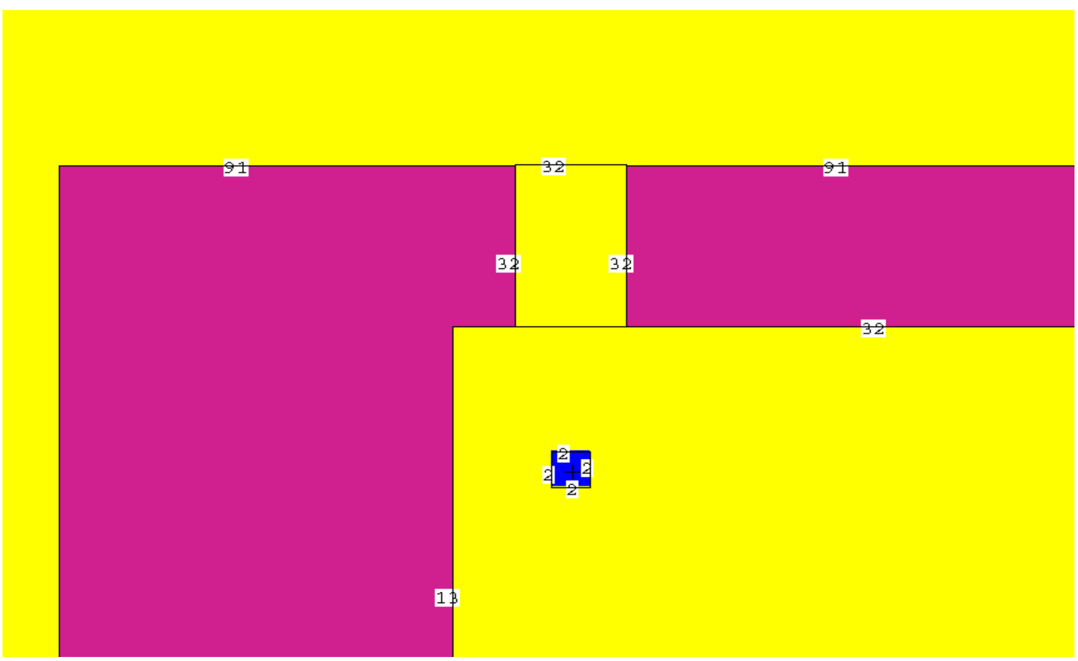

Figure 7.4. BTA MCNP6 Environment showing the copper block in relation to the shield roof penetration; X-Y

7.1.4 BTA Simulation Results

Due to the distance through the roof block following bremsstrahlung generation within the Cu block, a number of variance reduction techniques were used to decrease the estimated tally uncertainties for the simulation and the amount of cpu time to conduct the simulation. These included lower electron energy cutoffs (as noted below) and particle splitting/biasing by a factor of 10 in three separate locations moving through the roof block.

The impact of variation in electron energy cutoff values from 0.5-MeV to 0.1-MeV was simulated. It was observed that regardless of this variation dose rates above the roof block varied by <1% as a result. As the results of this simulation were insensitive to the domain of 0.1 to 0.5-MeV, energy cutoffs for electrons within MCNP6 were set at 0.5-MeV in the Cu block and 0.1-MeV for the rest of the geometry during the simulation.

The locations of interest that are anticipated to experience the highest dose rates are defined below:

- LOC1: Dose/dose rate 30-cm above the exit of the roof block penetration
- LOC2: Dose/dose rate 30-cm above the 30-cm thick roof block downstream
- LOC3: Dose/dose rate 30-cm outside of the lateral 1-m thick interior wall

Figure 7.5 below shows a MCNP6 photon T-mesh of the BTA electron train collision. Associated doses and dose rates at both locations outside of the roof listed in Table 7.2 for various beam loss scenarios and associated charge losses. The values provided in the table were generated by use of MCNP6 F5 next-event estimator tallies and carried an associated simulation uncertainty of <0.05.

Dose rates associated with loss of the electron trains in the BTA produce a combination of photon and neutron fields. Neutron fields at location 1 are noted to be the highest and most comparable to the photons fields (photon:neutron approximately 2:1) while those at location 2 are approximately 20:1.

Photon and neutron dose rates outside of the inner 1-m wall at LOC3 were found to be negligible compared to those on the roof platform.

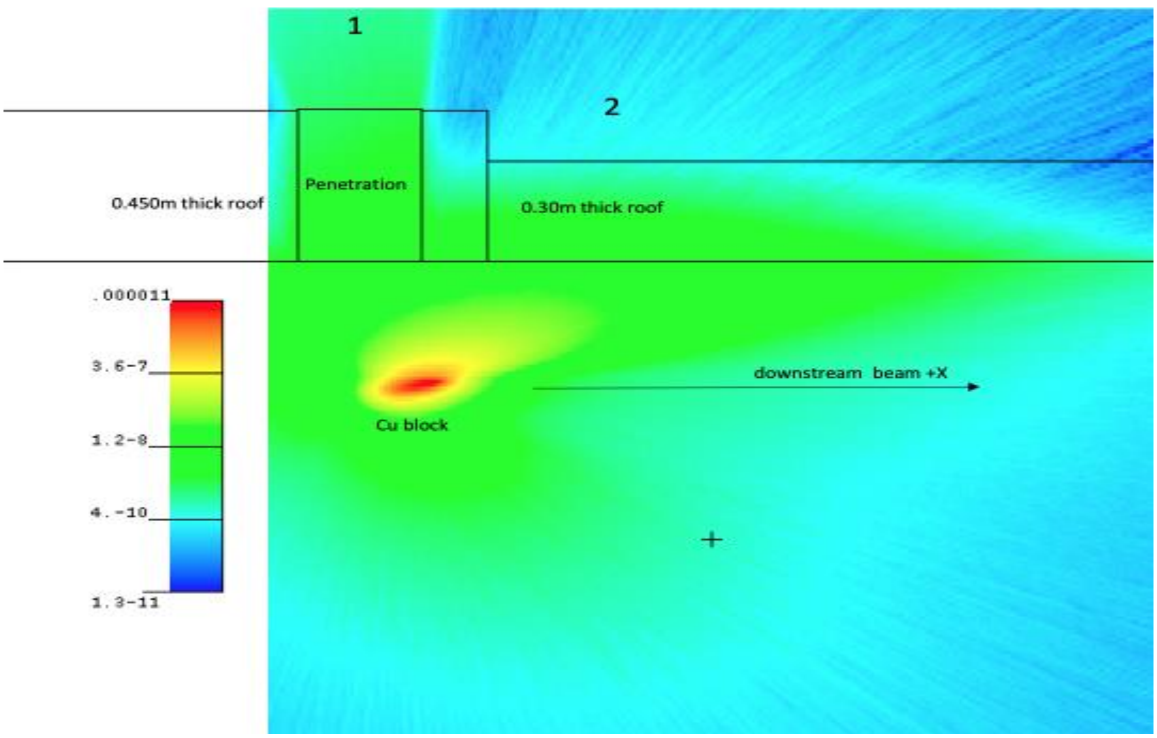

Figure 7.5. Photon dose rate tally result (ICRP21 (rem/hr)/(p/cm2-s)) of BTA collision

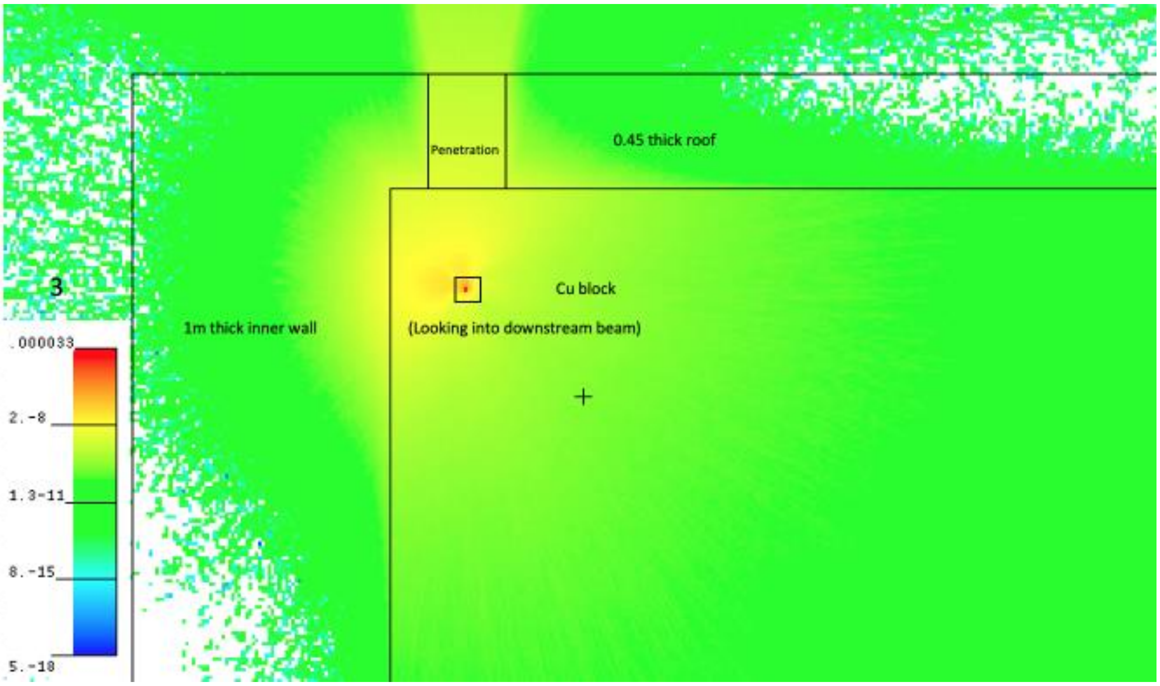

Figure 7.6. Photon dose rate tally result (ICRP21 (rem/hr)/(p/cm2-s)) of BTA collision

Table 7.2. BTA Doses and Dose Rates by Loss Scenario and Top-Off Lifetime

Scenario		BTA nC lost	LOC1			LOC2			Unit
			Photon	Neutron	*Total y+n*	Photon	Neutron	*Total y+n*	
BTA inj. Loss event		5.98	10.36	5.11	15.48	3.02	0.17	3.19	*mrem/event*
SR fill cycle, lasts 0.25 hr		13.16	22.8	11.25	34.05	6.63	0.38	7.01	*mrem/event*
Top-off by lifetime (hr) at 500 mA (achieves 1% current stability)	0.1	129.6	224.58	110.8	335.38	65.35	3.7	69.05	*mrem/hr*
	0.2	64.8	112.29	55.4	167.69	32.68	1.85	34.52	
	0.3	43.2	74.86	36.93	111.79	21.78	1.23	23.02	
	0.4	32.4	56.14	27.7	83.85	16.34	0.92	17.26	
	0.5*	25.92	44.92	22.16	67.08	13.07	0.74	13.81	
	0.6	21.6	37.43	18.47	55.9	10.89	0.62	11.51	
	0.7	18.51	32.08	15.83	47.91	9.34	0.53	9.86	
	0.8	16.2	28.07	13.85	41.92	8.17	0.46	8.63	
	0.9	14.4	24.95	12.31	37.26	7.26	0.41	7.67	
	1	12.96	22.46	11.08	33.54	6.54	0.37	6.9	
	1.1	11.78	20.42	10.07	30.49	5.94	0.34	6.28	
	1.2	10.8	18.71	9.23	27.95	5.45	0.31	5.75	
	1.3	9.97	17.28	8.52	25.8	5.03	0.28	5.31	
	1.4	9.26	16.04	7.91	23.96	4.67	0.26	4.93	
	1.5	8.64	14.97	7.39	22.36	4.36	0.25	4.6	
	1.6	8.1	14.04	6.93	20.96	4.08	0.23	4.32	
	1.7	7.62	13.21	6.52	19.73	3.84	0.22	4.06	
	1.8	7.2	12.48	6.16	18.63	3.63	0.21	3.84	
	1.9	6.82	11.82	5.83	17.65	3.44	0.19	3.63	
	2	6.48	11.23	5.54	16.77	3.27	0.18	3.45	

* Shielding design basis

If electron train injection loss events are localized to the septum underneath of the penetration, the loss may produce doses from 3 to 15 mrem. Thus, a radiation area is created in the event of loss of a train during injection.

During the fill cycle, routine losses are assumed to be localized to the septum underneath the penetration. Given this assumption, a dose of 34 mrem/event could be anticipated above the penetration and 7 mrem/event above the roof blocks; producing radiation areas greater than 5 mrem in any one hour during fill.

During top-off operations, routine losses with an assumed beam lifetime of 0.5 hours may result in consistent dose rates of 67 mrem/hr above the penetration and 14 mrem/hr on the roof. However, beam lifetimes are expected to be closer to 1 hour. This would produce dose rates closer to 34 mrem/hr above the penetration and 7 mrem/hr on the roof. A radiation area above the BTA septum is still produced in either scenario.

7.1.5 Need for Potential Supplemental Shielding

The design objective for controlling personnel exposure from external sources of radiation in areas of continuous occupancy (2,000 hours per year) shall be to maintain exposure levels below an average of 0.5 millirem (mrem) per hour and as far below this average as is reasonably achievable. The current ALS's shielding design criteria is <0.1 mrem/hour and < 5 mrem/event where workers could be considered to be in continuous occupancy.

The design objectives for exposure rates for potential exposure to a radiological worker in areas where occupancy differs from the continuous 2,000 hours per year shall be as low as reasonably achievable (ALARA) and shall not exceed 20 percent of the applicable standards in the

Code of Federal Regulations, Title 10, Section 835.202 (Occupational dose limits for general employees).

The sector 1 roof area is not an area of continuous occupancy, at less than 0.05 occupancy factor. However, dose rates must still be controlled in a manner consistent with ALARA principles. Supplemental shielding above the penetration should be pursed consistent with dose rates measured during operations following input of required equipment into the penetration.

7.2 Accumulator-to-Storage (ATS)

7.2.1 ATS Geometry

The accumulator-to-storage (ATS) transfer line swaps a filled train in the accumulator ring to the storage ring where it replaces a depleted train that has been swapped out via the storage-to-accumulator (STA). The ATS transfer line is shown highlighted in red in Figure 7.7.

Figure 7.7. The Accumulator-to-Storage transfer line (highlighted in red)

Once the filled train has reached the end of the ATS, it is injected into the storage ring via the ATS septum, shown in Figure 7.8. The assumed efficiency factor of this injection process is 0.998.

Figure 7.8. Accumulator-to-Storage Injection Septum

The roof block over the top of the ATS injection septum is the final 45-cm thick block prior to transitioning to 30-cm thick blocks in subsequent sections. The outer storage ring wall adjacent to the ATS injection septum transitions down to as low as approximately 60-cm thick.

7.2.2 ATS Source Term Generation

To generate the bremsstrahlung for the simulation, ALS-U's 2-GeV bunch train is collided directly into a target copper block (10cm x 10cm x 5cm) representative of a collision with a magnet following injection due to a routine efficiency-related or complete beam loss from the ATS.

Prior to entering the injection septum, the ATS is angled 10 degrees off from the storage ring. This angle is assumed for the simulation collision, resulting in the 0-degree downstream radiation colliding directly into the outer storage ring wall several meters down the tunnel.

The amount of charge lost in the ATS will vary depending on the state of fill of the bunch train and the mode in which the accelerator is operating, whether top-off or fill. Tables 4.5 and 4.6 detail the charge loss per fill cycle and charge loss during top-off operations.

During fill operations, the ATS is estimated to lose 1.97 nC of charge over the 0.25-hour long fill. The amount of charge lost varies with the amount of charge being transferred from the AR to the SR as the increased charge resulting in increased inefficiency of the transfer. The filling of the final 20% of the SR capacity has the highest charge loss rate at 0.0598 nC/train over the course of 3 minutes. During fill operations, the ATS loses 1.97 nC of charge during the 15-minute fill period. This is equivalent to 1.23×10^{10} electrons lost during the fill.

During top-off operations, the ATS loses approximately 12.25 nC/hr of charge at an assumed beam lifetime of 0.5 hours. This is equivalent to 2.12×10^{7} electrons/s of continuous loss.

7.2.3 ATS MCNP6 Environment

To characterize the dose rate resulting from the beam losses, a model was developed using the MCNP6 software. The transport model was based on available schematic and technical data for ALS-U. The geometry and placement of components is subject to change.

The ATS injection septum is simulated as a 1-cm thick-walled stainless steel rectangular box under vacuum with the 10cm x 10cm x 5cm-target copper block inside. The roof block over the top of the ATS injection septum is modeled as 45-cm thick concrete prior to transitioning to a 30-cm thick block. The outer storage ring wall adjacent to the ATS injection septum transitions is modeled as a consistent 30-cm thick concrete wall. This geometry is shown in Figures 7.9 and 7.10 below.

No penetrations with direct line-of-sight to the assumed ATS injection loss point exist in the storage ring tunnel.

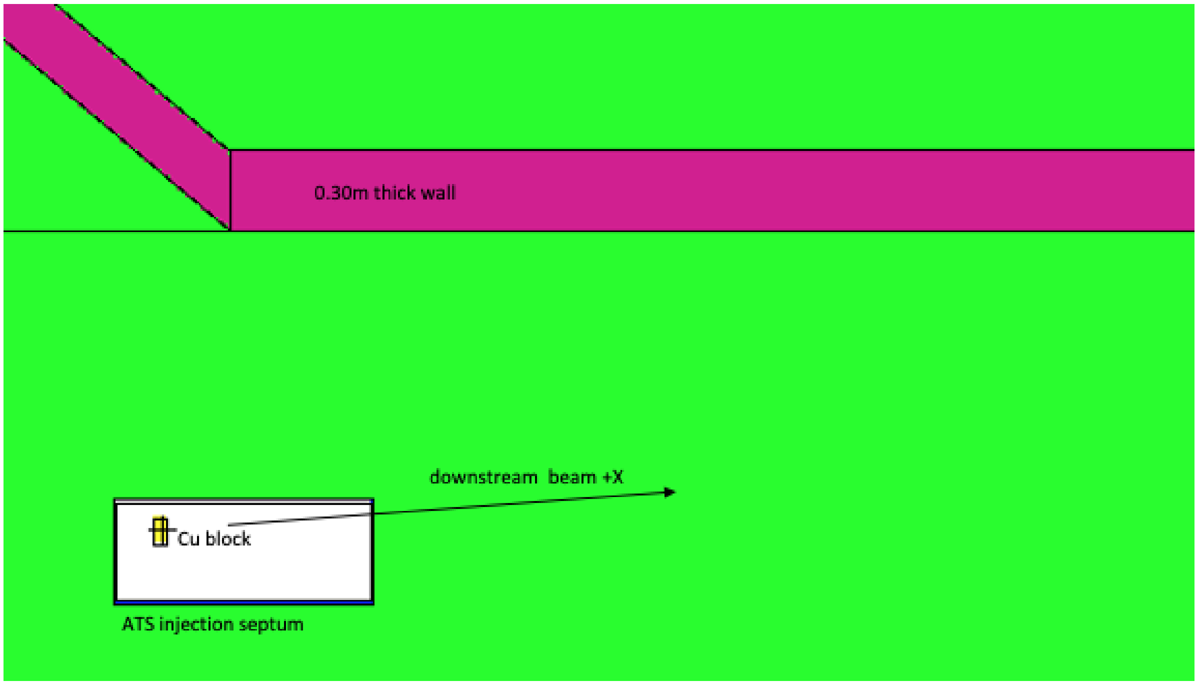

Figure 7.9. ATS MCNP6 Environment showing the injection septum in relation to the shield wall X-Y

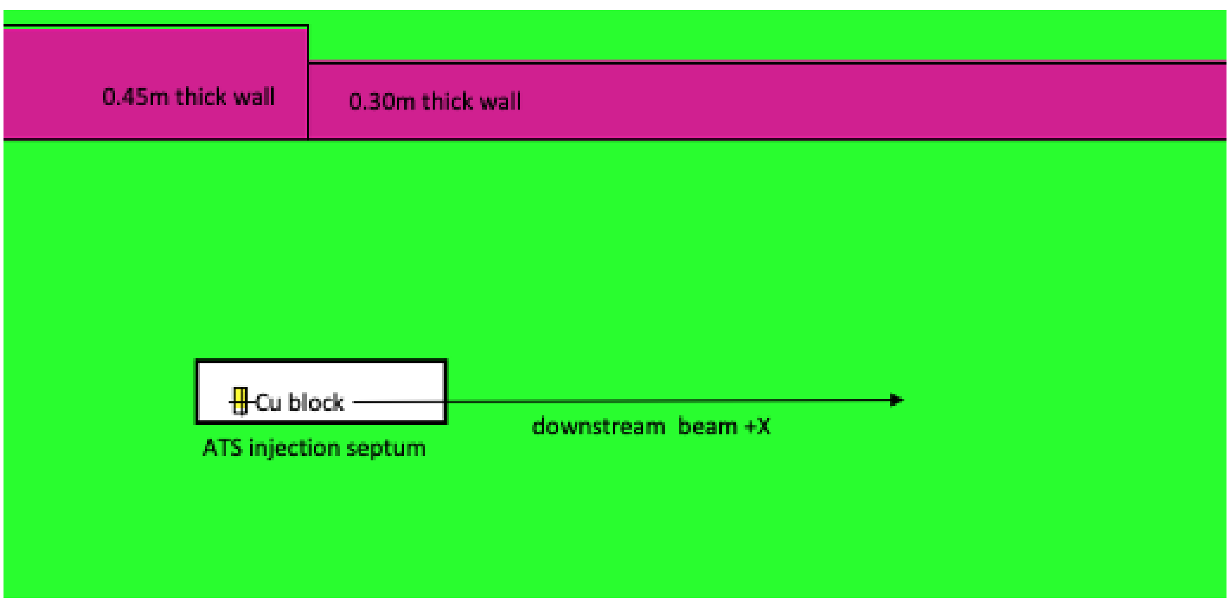

Figure 7.10. ATS MCNP6 Environment showing the injection septum in relation to the shield roof thickness X-Z

7.2.4 ATS Simulation Results

Due to the distance downstream through the storage ring tunnel, following bremsstrahlung interaction with the Cu block, a number of variance reduction techniques were used to decrease the estimated tally uncertainties for this simulation and the amount of cpu time to conduct the simulation. To produce more efficient runtimes while using MCNP6, energy cutoffs for electrons were set at 0.01 MeV. The energy cutoffs for photon runs and neutron runs were set at 0.1 MeV.

In the following section, the locations of interest are defined as:

- LOC1: Dose/dose rate 30-cm above the roof at the inside of the outer storage ring wall at 4.1-meters downstream of the Cu block collision

- LOC2: Dose/dose rate 30-cm outside of the lateral 1m thick interior wall at 8.6-meters downstream of the Cu block collision

Figure 7.11 below shows the MCNP6 photon t-mesh of the ATS electron train collision. Associated doses and dose rates by length downstream of the collision are shown in Figure 7.12 for both locations outside of the roof and outside of the outer storage ring wall.

Dose rates associated with loss of the electron trains in the ATS produce a combination of photon and neutron fields. The neutron fields peak adjacent to major collision areas such as the target Cu block and collision of remaining high-energy photons within the concrete wall.

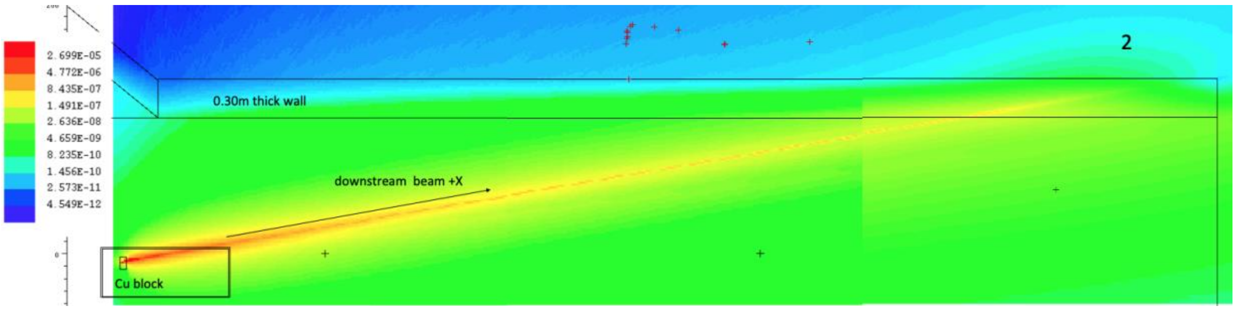

Figure 7.11. Photon dose rate tally result (ICRP21 (rem/hr)/(p/cm2-s)) of ATS collision; X-Y

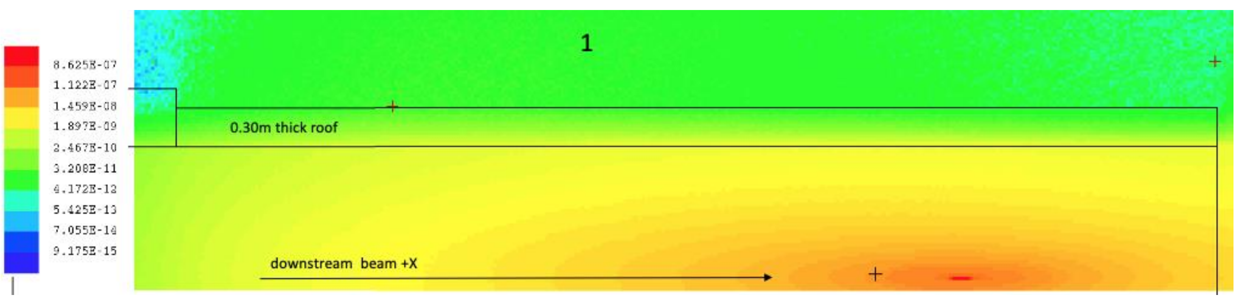

Figure 7.12. Photon dose rate tally result (ICRP21 (rem/hr)/(p/cm2-s)) of ATS collision; X-Z

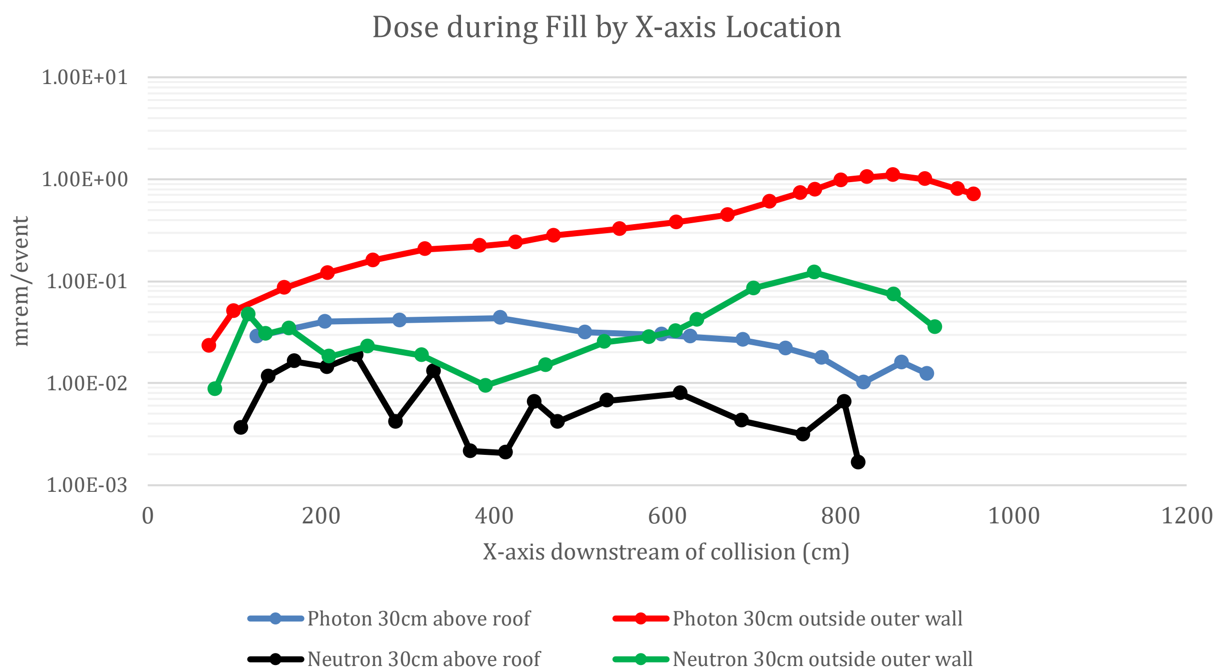

Figure 7.13. *Fill dose per event(mrem/event) following ATS collision by distance*

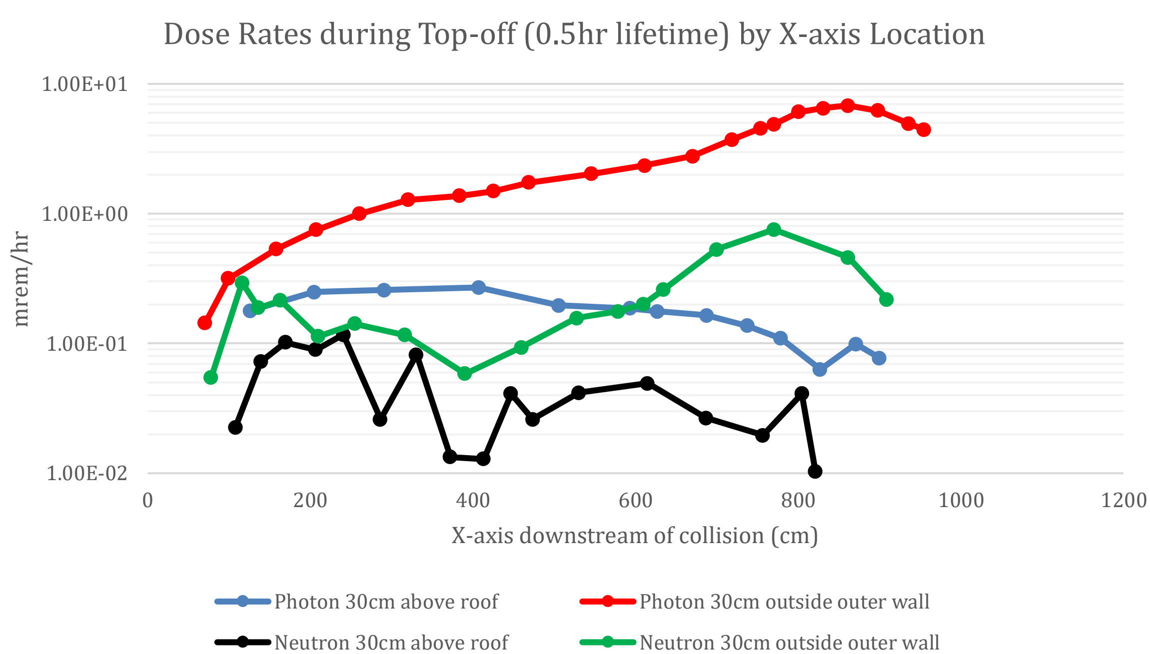

Figure 7.14. Top-off dose rate (mrem/hr) following ATS collision by distance

Table 7.3. ATS Doses and Dose Rates by Loss Scenario and Top-Off Lifetime

Scenario		ATS nC lost	LOC1			LOC2			
			Photon	Neutron	***Total y+n***	Photon	Neutron	***Total y+n***	Unit
SR fill cycle, lasts 0.25 hr		1.9734	0.04	0	0.05	1.1	0.07	1.17	*mrem /event*
Top-off by lifetime (hr) at 500 mA (achieves 1% current stability)	0.1	61.27	1.35	0.06	1.41	34.09	2.3	36.39	*Mrem /hr*
	0.2	30.63	0.67	0.03	0.71	17.04	1.15	18.19	
	0.3	20.42	0.45	0.02	0.47	11.36	0.77	12.13	
	0.4	15.32	0.34	0.02	0.35	8.52	0.57	9.1	
	0.5*	12.25	0.27	0.01	0.28	6.82	0.46	7.28	
	0.6	10.21	0.22	0.01	0.24	5.68	0.38	6.06	
	0.7	8.75	0.19	0.01	0.2	4.87	0.33	5.2	
	0.8	7.66	0.17	0.01	0.18	4.26	0.29	4.55	
	0.9	6.81	0.15	0.01	0.16	3.79	0.26	4.04	
	1	6.13	0.13	0.01	0.14	3.41	0.23	3.64	
	1.1	5.57	0.12	0.01	0.13	3.1	0.21	3.31	
	1.2	5.11	0.11	0.01	0.12	2.84	0.19	3.03	
	1.3	4.71	0.1	0	0.11	2.62	0.18	2.8	
	1.4	4.38	0.1	0	0.1	2.43	0.16	2.6	
	1.5	4.08	0.09	0	0.09	2.27	0.15	2.43	
	1.6	3.83	0.08	0	0.09	2.13	0.14	2.27	
	1.7	3.6	0.08	0	0.08	2.01	0.14	2.14	
	1.8	3.4	0.07	0	0.08	1.89	0.13	2.02	
	1.9	3.22	0.07	0	0.07	1.79	0.12	1.92	
	2	3.06	0.07	0	0.07	1.7	0.11	1.82	

* Shielding design basis

Routine losses for a fill cycle are assumed to be localized to the septum, but may result in dose equivalents of 1.2 mrem at Location 2 on the outside of the storage ring wall, approximately 8 meters downstream from the collision point.

During top-off operations, routine losses with an assumed beam lifetime of 0.5 hours may result in consistent dose rates of 7.3 mrem/hr outside of the storage ring tunnel in areas of continuous occupancy. However, beam lifetimes are expected to be closer to 1 hour. This would produce lower dose rates at a magnitude of approximately 3.6 mrem/hr. Without supplemental shielding along the outer storage ring wall in sectors 1 and 2, radiation areas may be produced and ALARA goals not met. Supplemental shielding outside of the shield wall should be pursed consistent with dose rates measured during operations following input of required equipment into the penetration.

7.3 Storage-to-Accumulator (STA)

7.3.1 STA Geometry

The storage-to-accumulator (STA) transfer line swaps a depleted train in the storage ring to the accumulator ring where it replaces a filled train that has been swapped out via the accumulator-to-storage (ATS) in sector 1. Once the depleted train has reached the end of the STA, it is injected into the accumulator ring via the STA septum, shown in Figure 7.15 The assumed efficiency of this injection process is a factor of 0.998.

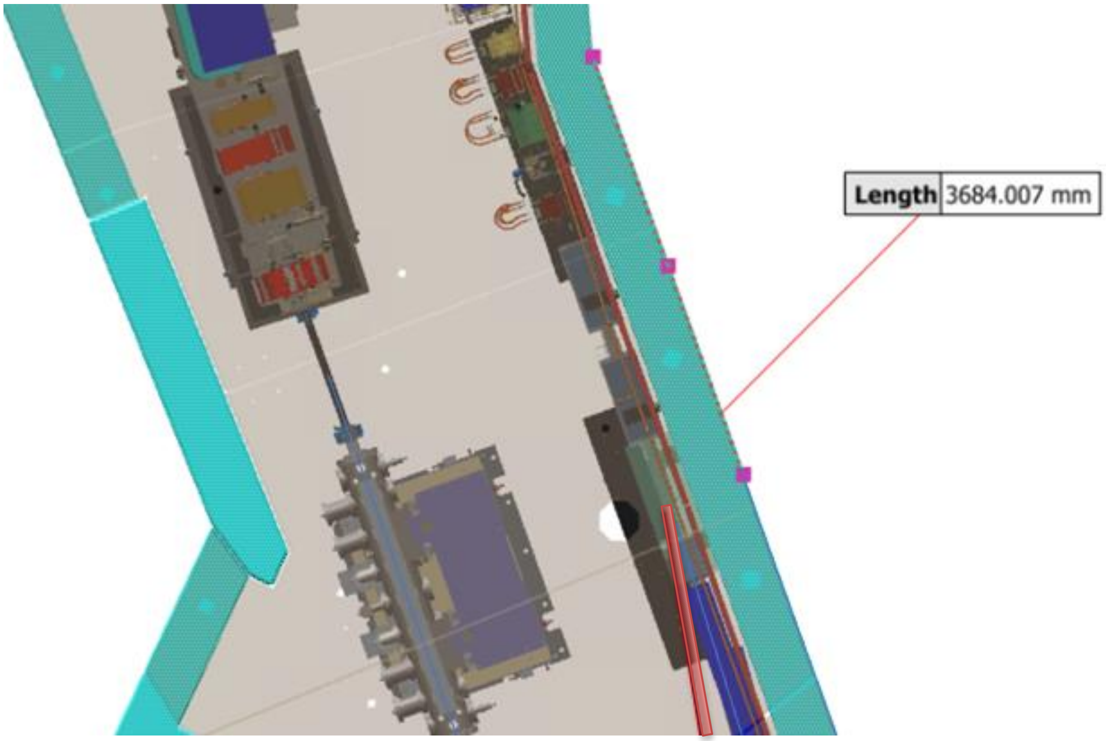

Figure 7.15. The Storage-to-Accumulator transfer line and injection septum (highlighted in red)

The roof block over the top of the STA injection septum are 30-cm thick concrete blocks. The inner storage ring wall adjacent to the STA injection septum is approximately 50-cm thick. The penetration located above and adjacent to the STA septum is 0.3-m in diameter.

7.3.2 STA Source Term Generation

To generate the bremsstrahlung for the simulation, ALS-U's 2-GeV bunch train is collided directly into a target copper block (10cm x 10cm x 5cm) representative of a collision with a magnet following injection due to a routine efficiency-related loss or complete beam loss from the STA.

Prior to entering the injection septum, the STA is angled 10 degrees off from the accumulator ring. This angle is assumed for the simulation collision, resulting in the 0-degree downstream radiation colliding directly into the inner storage ring wall a few meters down the tunnel.

The amount of charge lost in the STA will vary depending on the state of fill of the bunch train and the mode in which the accelerator is operating, whether top-off or fill. Tables 4.5 and 4.6 detail the charge loss per fill cycle and charge loss during top-off operations.

During fill operations, the STA is estimated to lose 1.32 nC of charge over the 0.25-hour long fill. The amount of charge lost varies with the amount of charge being transferred from the SR to the AR as the increased charge resulting in increased inefficiency of the transfer. The filling of the final 20% of the SR capacity has the highest charge loss rate at 0.04784 nC/train over the course of 3 minutes. During fill operations, the STA loses 1.32 nC of charge during the 15-minute fill period. This is equivalent to 8.2×10^9 electrons lost during the fill cycle.

During top-off operations, the STA loses approximately 10.96 nC/hr of charge at an assumed beam lifetime of 0.5 hours. This is equivalent to 1.89×10^7 electrons/s of continuous loss.

7.3.3 STA MCNP6 Environment

To characterize the dose rate resulting from the beam losses, a model was developed using the MCNP6 software. The transport model was based on available schematic and technical data for ALS-U.

The STA injection septum is simulated as a 1 cm thick-walled stainless steel rectangular box under vacuum with the 10cm x 10cm x 5cm-target copper block inside. The roof block over the top of the STA injection septum is modeled as 30-cm thick concrete. The inner storage ring wall adjacent to the STA injection septum is modeled as a consistent 50-cm thick concrete wall. This geometry is shown in Figures 7.16 and 7.17 below.

The e- train is assumed to collide approximately 45-cm away from the center of the penetration but at the same distance downstream in the STA. Moving in the +Z direction, there is 40-cm of air present before reaching the penetration passing through the 30-cm roof block.

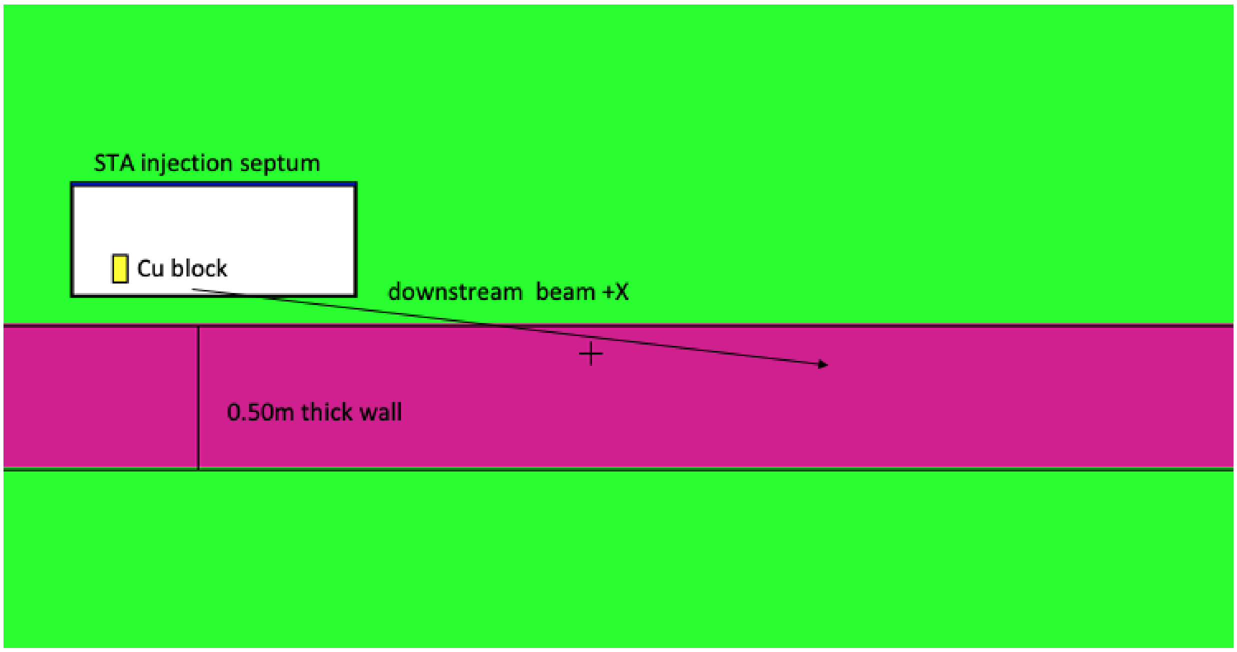

Figure 7.16. STA MCNP6 Environment showing the injection septum in relation to the shield wall X-Y

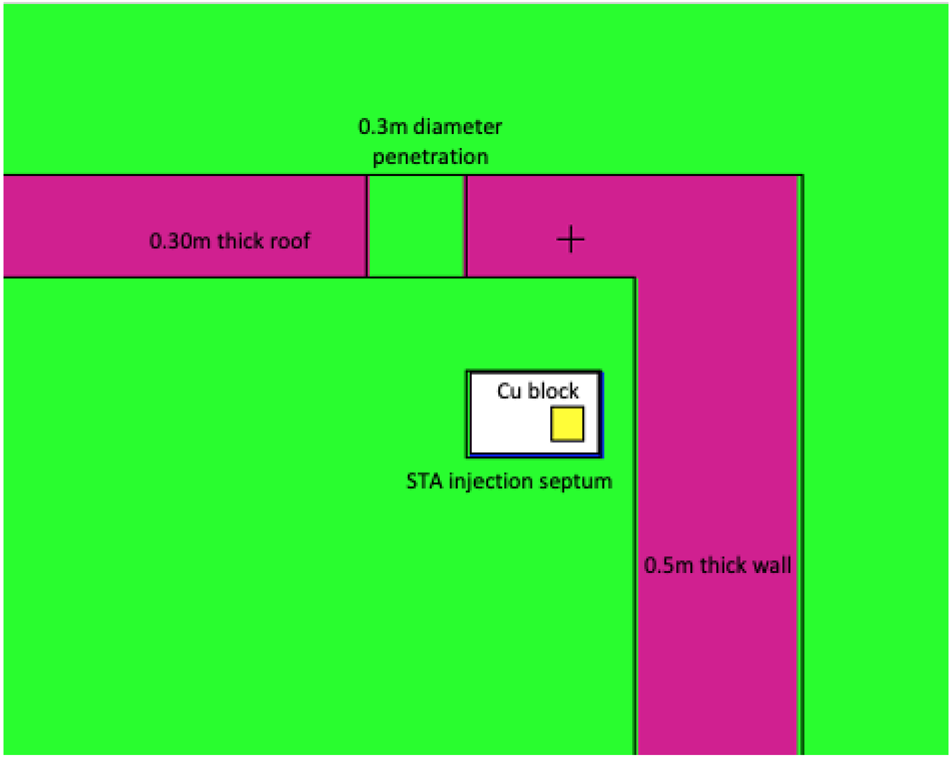

Figure 7.17. STA MCNP6 Environment showing the injection septum in relation to the shield wall Y-Z

7.3.4 STA Simulation Results

Due to the distance downstream through the storage ring tunnel following bremsstrahlung interaction with the Cu block, a number of variance reduction techniques were used to decrease the estimated tally uncertainties for the simulation and the amount of cpu time to conduct the simulation. To produce more efficient runtimes, energy cutoffs for electrons within MCNP6 were set at 0.01-MeV.

The locations of interest are defined as:

- LOC1: Dose/dose rate 30-cm above the roof at the inside of the inner storage ring wall at 1.4-meters downstream of the Cu block collision

- LOC2: Dose/dose rate 30-cm outside of the lateral 1m thick interior wall at 1.7-meters downstream of the Cu block collision

- LOC3: Dose/dose rate 30-cm above the penetration adjacent to the STA collision.

Figures 7.18, 7.19 and 7.20 below shows a MCNP6 photon t-mesh of the STA electron train collision. Associated doses and dose rates by length downstream of the collision are shown in Figures 7.21 and 7.22 for locations outside of the roof and outside of the outer storage ring wall.

Dose rates associated with loss of the electron trains in the STA produce a combination of photon and neutron fields. The neutron fields peak adjacent to major collision areas such as the target Cu block and collision of remaining high-energy photons with the concrete wall.

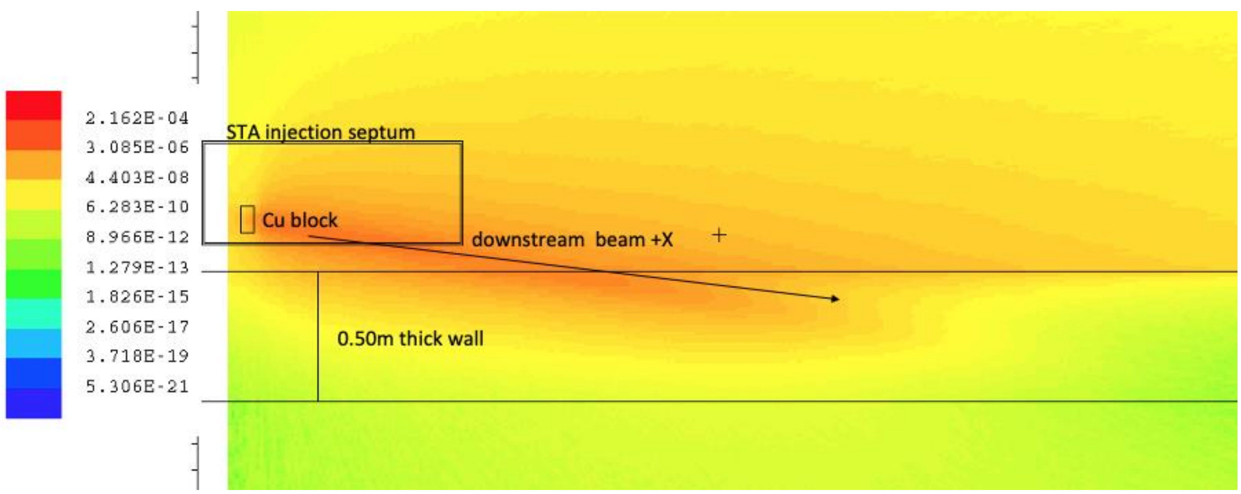

Figure 7.18. Photon dose rate tally result (ICRP21 (rem/hr)/(p/cm2-s)) of STA collision; X-Y

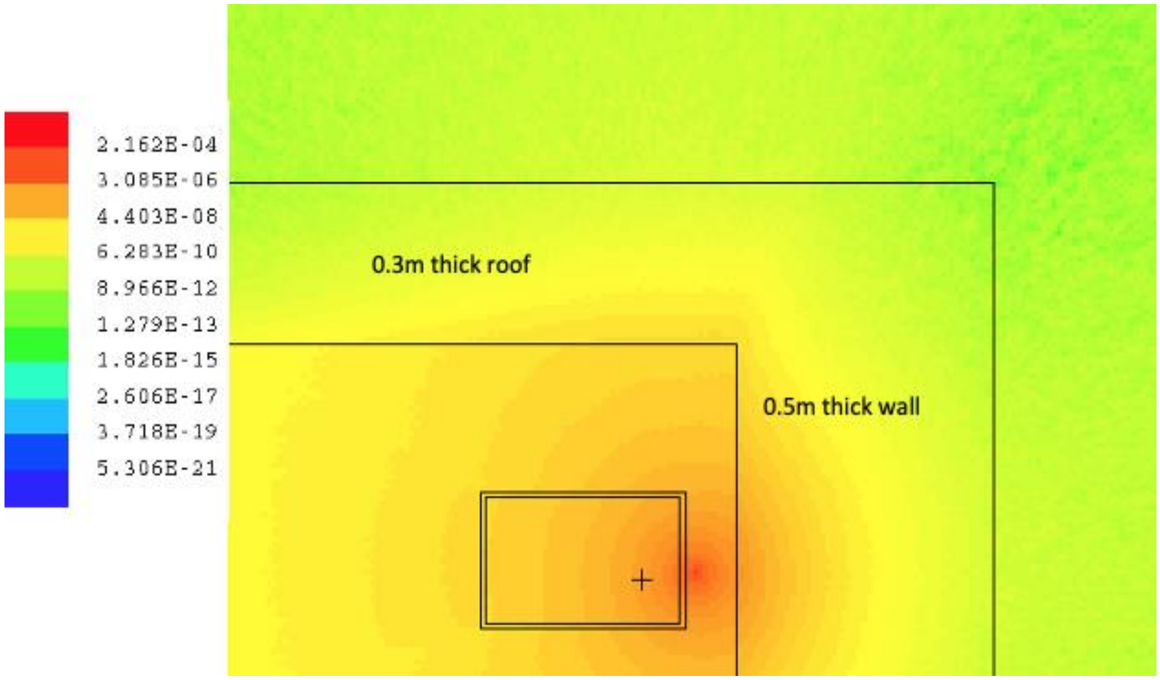

Figure 7.19. Photon dose rate tally result (ICRP21 (rem/hr)/(p/cm2-s)) of STA collision at 1.4m downstream; Y-Z

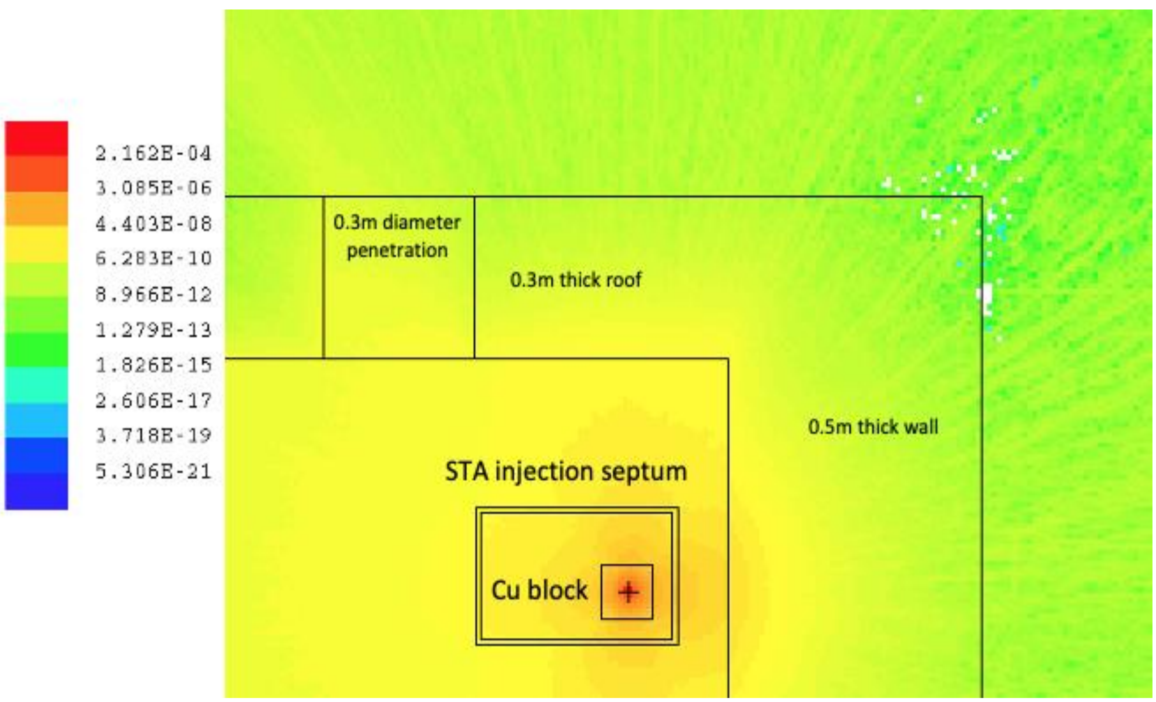

Figure 7.20. Photon dose rate tally result (ICRP21 (rem/hr)/(p/cm2-s)) of STA collision at 0m downstream; Y-Z

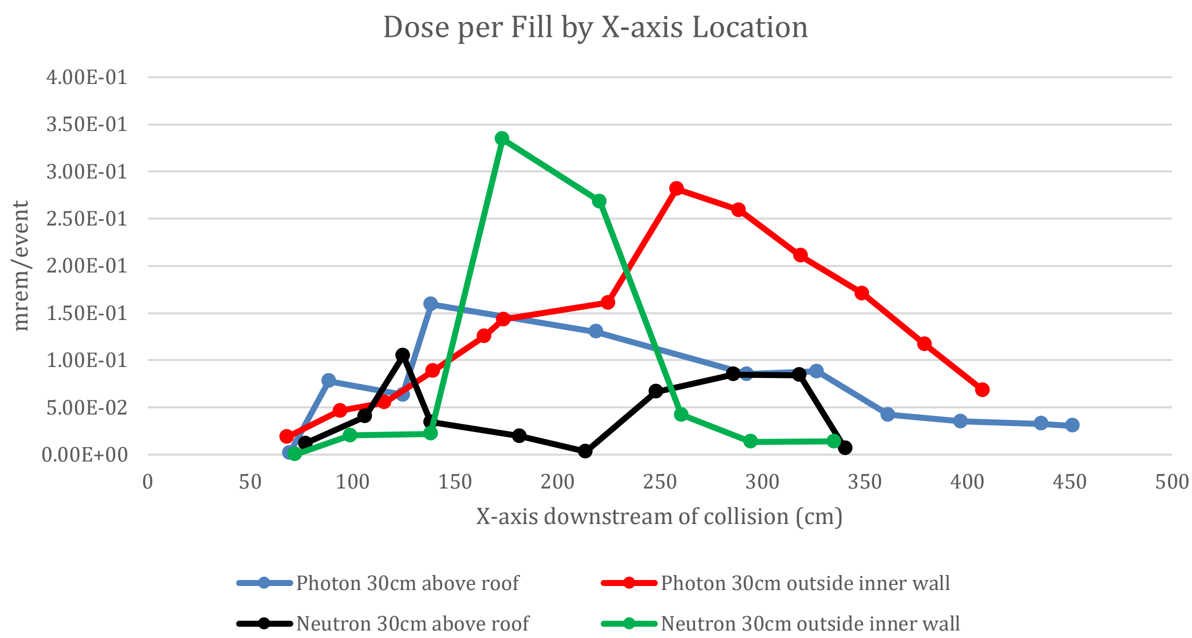

Figure 7.21. Fill dose per event (mrem/event) following STA collision by distance

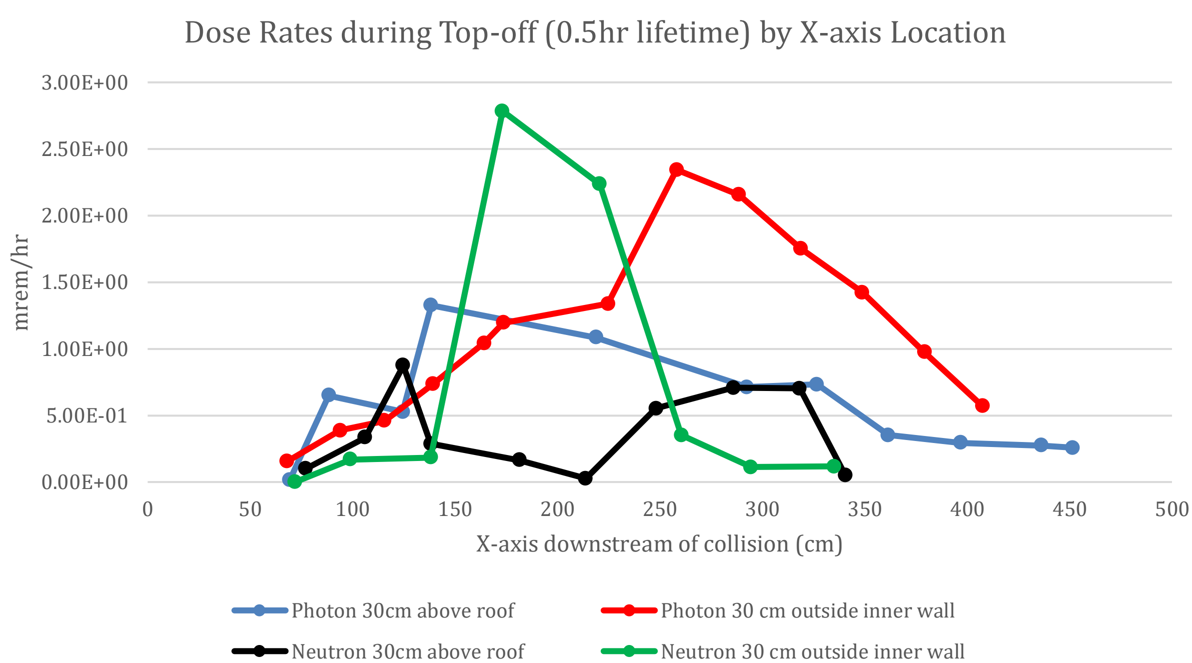

Figure 7.22. Top-off dose rate (mrem/hr) following STA collision by distance

Table 7.4. STA Doses and Dose Rates by Loss Scenario and Top-Off Lifetime

Scenario		STA nC lost	LOC1			LOC2			LOC3			Unit
			Photon	Neutron	Total y+n	Photon	Neutron	Total y+n	Photon	Neutron	Total y+n	
SR fill cycle, lasts 0.25 hr		1.32	0.16	0.03	0.19	0.14	0.33	0.48	0.1	0	0.1	*mrem /event*
Top-off by lifetime (hr) at 500 mA (achieves 1% current stability)	0.1	54.79	6.63	1.43	8.06	5.97	13.92	19.89	4.16	0.19	4.35	
	0.2	27.39	3.32	0.72	4.03	2.99	6.96	9.95	2.08	0.1	2.18	
	0.3	18.26	2.21	0.48	2.69	1.99	4.64	6.63	1.39	0.06	1.45	
	0.4	13.7	1.66	0.36	2.02	1.49	3.48	4.97	1.04	0.05	1.09	
	0.5*	10.96	1.33	0.29	1.61	1.19	2.78	3.98	0.83	0.04	0.87	
	0.6	9.13	1.11	0.24	1.34	1	2.32	3.32	0.69	0.03	0.73	
	0.7	7.83	0.95	0.2	1.15	0.85	1.99	2.84	0.59	0.03	0.62	
	0.8	6.85	0.83	0.18	1.01	0.75	1.74	2.49	0.52	0.02	0.54	
	0.9	6.09	0.74	0.16	0.9	0.66	1.55	2.21	0.46	0.02	0.48	
	1	5.48	0.66	0.14	0.81	0.6	1.39	1.99	0.42	0.02	0.44	*mrem/ hr*
	1.1	4.98	0.6	0.13	0.73	0.54	1.27	1.81	0.38	0.02	0.4	
	1.2	4.57	0.55	0.12	0.67	0.5	1.16	1.66	0.35	0.02	0.36	
	1.3	4.21	0.51	0.11	0.62	0.46	1.07	1.53	0.32	0.01	0.33	
	1.4	3.91	0.47	0.1	0.58	0.43	0.99	1.42	0.3	0.01	0.31	
	1.5	3.65	0.44	0.1	0.54	0.4	0.93	1.33	0.28	0.01	0.29	
	1.6	3.42	0.41	0.09	0.5	0.37	0.87	1.24	0.26	0.01	0.27	
	1.7	3.22	0.39	0.08	0.47	0.35	0.82	1.17	0.24	0.01	0.26	
	1.8	3.04	0.37	0.08	0.45	0.33	0.77	1.11	0.23	0.01	0.24	
	1.9	2.88	0.35	0.08	0.42	0.31	0.73	1.05	0.22	0.01	0.23	
	2	2.74	0.33	0.07	0.4	0.3	0.7	0.99	0.21	0.01	0.22	

* Shielding design basis

Routine losses for a fill cycle assumed to be localized to the septum may result in approximately 0.5 mrem of dose/event at Location 2 on the outside of the storage ring wall, approximately 1.7-meters downstream from the collision point.

Routine losses for top-off operations with an assumed beam lifetime of 0.5 hours may result in consistent dose rates of 4 mrem/hr outside of the storage ring tunnel in areas of continuous occupancy. However, beam lifetimes are expected to be closer to 1 hour. This would produce anticipated dose rates of approximately 2 mrem/hr. The open penetration (LOC3) adjacent to the STA collision area reaches approximately 0.9 mrem/hr during top-off operations. Without supplemental shielding, ALARA goals for continuous occupancy areas will not be met around the STA. Supplemental shielding outside of the shield wall should be pursed consistent with dose rates measured during operations following input of required equipment into the penetration.

7.4 Data Fit

MCNP6 simulation data of dose equivalent rates for the BTA, STA, and STA from Tables 7.2, 7.3, and 7.4 are plotted against top-off operations beam lifetime in Figure 7.23. The power trendline function in Microsoft Excel was used to create fit equations to each location's data. A power trendline is a curved line that is best used with data sets that compare measurements that increase at a specific rate. All equations presented a R^2 of 1, indicating excellent goodness-of-fit to the linear model each presented. In this case, declining beam lifetime indicates increased charge loss from the system and hence increased dose equivalent rates. This represents an inverse-linear relationship of beam lifetime to dose equivalent rate.

Table 7.5. Fit Equations of Location (LOC) Dose Equivalent Rate (mrem/hr) by Beam Lifetime (X) in hr.

Transfer Line	Location	Equation (mrem/hr)	R^2
BTA	1	$335.38x^{-1}$	1
	2	$69.049x^{-1}$	1
STA	1	$8.0647x^{-1}$	1
	2	$19.892x^{-1}$	1
	3	$4.3543x^{-1}$	1
ATS	1	$1.4137x^{-1}$	1
	2	$36.385x^{-1}$	1

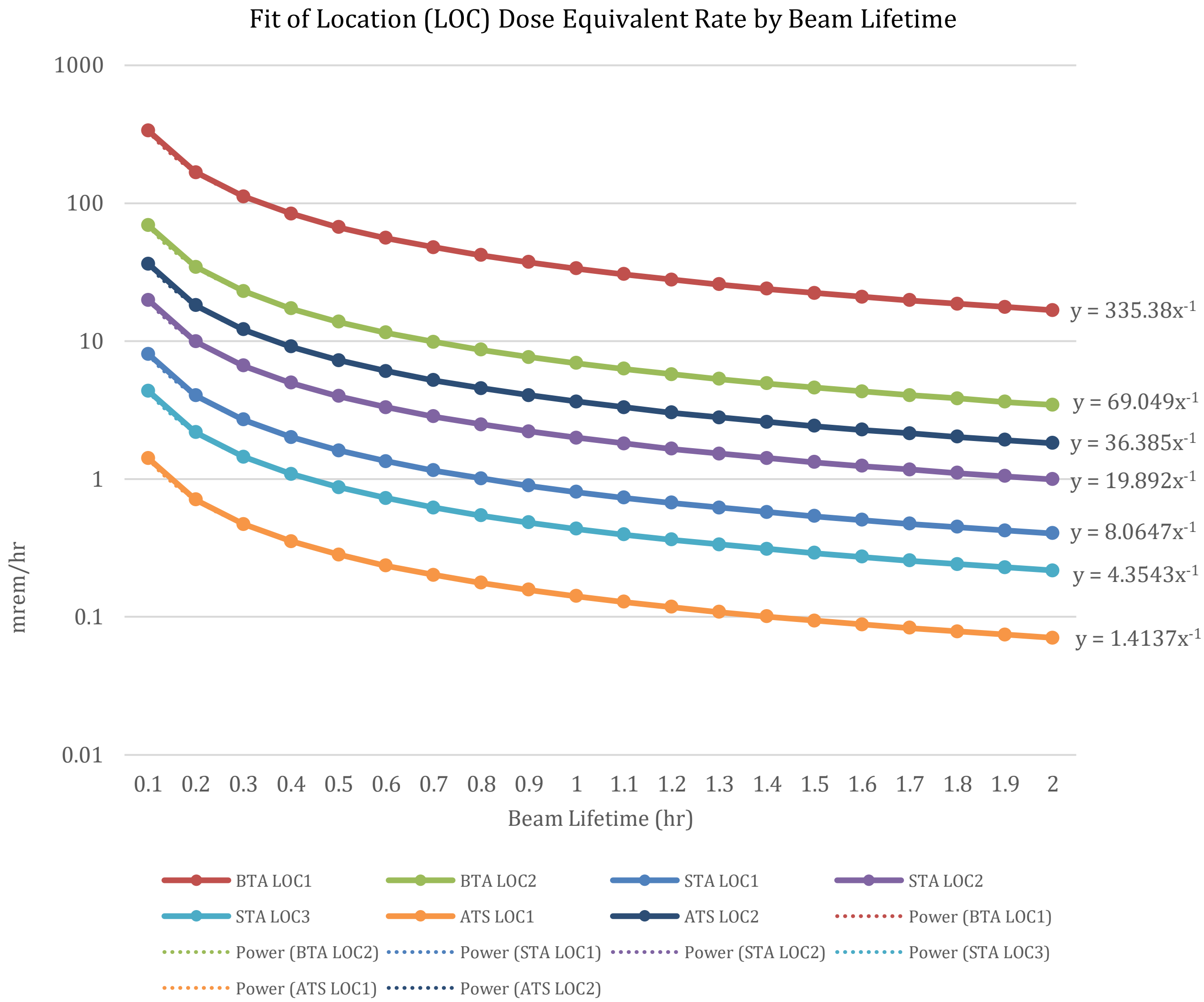

Figure 7.23. Trendline Fit of Location (LOC) Dose Equivalent Rate (mrem/hr) by Beam Lifetime (hr).

8 CONCLUSION

8.1 GB Summary

Table 8.1 provides a summary of the evaluated effective dose rates for ALS-U accumulator-ring due to GB. The MCNP simulations did not account for any areas of additional shielding provided by lead or thicker shield walls already deployed, so the real-life conditions may be even lower. The beam paths in the table refer to those established in Figure 5.6 Gas Bremsstrahlung interaction pathways by beam position. Beam path #2 and beam path #4 represent the highest and therefore most conservative, and lowest and therefore least conservative dose rates as calculated on the opposite side of the storage ring wall.

Table 8.1. Accumulator-Ring Effective Dose Rates Due to GB at Different Locations

Location	Pressure (torr)	Effective Dose Rate (Rem/hr)
Post AR Vacuum Chamber	$4.0\text{x}10^{-07}$	546.3 + 0.01%
Beam Path #1 (no magnet collisions)	$4.0\text{x}10^{-07}$	0.345 + 13%
Beam Path #2 (most conservative within defined aperture)	$4.0\text{x}10^{-07}$	$1.15\text{x}10^{-03}$ + 29%
Beam Path #2 (1000 A-hrs)	$7.7\text{x}10^{-09}$	$2.89\text{x}10^{-05}$ + 22%
Beam Path #4 (least conservative within defined aperture)	$4.0\text{x}10^{-07}$	$3.2\text{x}10^{-05}$ + 25%
Beam Path #4 (1000 A-hrs)	$7.7\text{x}10^{-09}$	$6.15\text{x}10^{-07}$ + 25%

Based on these Monte Carlo results, it is concluded that the current shielding is adequate to meet design specifications and that no special shielding or posting precautions should necessary during ALS-U start-up with regard to the accumulator-ring GB production. This simulation is based on the 72-amp-hour pressures anticipated to exist during startup if the electron beam can be limited to the aperture defined in Figure 5.5.

If the electron beam cannot be limited to the defined aperture, shielding will be need be placed at the exit of the dipole magnet of the achromat. A similar solution is already in place at the ALS storage ring's dipole magnets, see Figure 8.1.

Figure 8.1. ALS Storage Ring Dipole Magnet GB Shielding

A BBREM:1/*k* source spectra comparison of energy, flux, and error indicated the analytical expression approximated the monte-carlo simulation, but the analytical expression was higher than the monte carlo simulation. The monte carlo simulation estimates were only 79.9% of the magnitude of the average bin value over various energy increments of the analytical expression. As a result, the null hypothesis that analytical expressions to derive gas bremsstrahlung fluence can approximate MCNP6 monte-carlo simulations and BBREM variance reduction biasing techniques within MCNP6 to 95% accuracy is rejected and the alternate hypothesis that analytical expressions to derive gas bremsstrahlung fluence can approximate MCNP6 monte-carlo simulations and BBREM variance reduction biasing techniques within MCNP6 to 95% accuracy is supported.

NOTE: Effective dose rates calculated for this simulation represent the gas bremsstrahlung produced by the accumulator ring. They are based on conditions present at 72 amp-hours of accelerator operation. Pressure conditions prior to that remain unknown. By 1,000 amp-hours, dose rates are expected to drop by a factor of 52 ($4x10^{-07}$ torr assuming that pressure drops to an average of $7.7x10^{-09}$ torr). As the pressure drops, dose rates will decrease linearly (LBNL2019).

8.2 HVAC and Electrical Penetration Summary

Based on the Monte Carlo simulations conducted, it appears that shielding is necessary to reduce the photon and neutron dose rates at 1-foot outside the shield wall HVAC penetrations from 3.41 mrem/hr and 1.44 mrem/hr, respectively, to 0.1 mrem/hr combined. This may be accomplished by a variety of shielding materials as presented in Table 6.1 and Table 6.2.

The shielding solution recommended is 3 inches of lead or 5 inches of stainless steel, followed by 9 inches of polyethylene in a two-barrier labyrinth design within the HVAC penetration itself or a total of 12 inches of concrete in a non-labyrinth style design shield block placed outside of the penetration would also suffice. These designs were demonstrated to reduce dose rates to below the requirements for Scenario 2's 100% beam dump and just above Scenario 1 5% continuous loss requirements. This recommendation is consistent with facility ALARA criteria and due to the conservatism of the simulation would likely meet the design goal in reality.

The in-duct shielding design may affect the efficiency of the HVAC system's operation. Therefore, the HVAC Group's concurrence must be sought before any shielding is added inside the HVAC ducts.

Based upon the Monte Carlo simulations conducted, it appears that no shielding for bremsstrahlung radiation is necessary to reduce the dose rates and dose to below facility design requirements as long as the electrical penetrations <6 inches in diameter and have a centerline height of no more than 20 inches from the floor surface.

As Geometric factors in addition to the existing shield wall of the 3rd generation light source is not sufficient to allow for the additional of an accumulator ring and its associated electron losses without supplemental shielding to meet design criteria for limits on radiation field magnitude, the null hypothesis is rejected and the alternate is supported.

8.3 Electron Bunch Swapping Summary

The anticipated dose and dose rates associated with different beam loss scenarios of the BTA, ATS, and STA transfer lines have been simulated using Monte Carlo modeling techniques. The loss rates associated with their respective efficiencies were determined. With these estimates, it was demonstrated in Section 7.4 that the decrease of electron beam lifetimes has an inverse linear relationship with dose.

The BTA transfer line doses and dose rates are expected to routinely create radiation areas on the shield block roof and the penetration will require additional shielding.

This Monte Carlo simulation has modeled the anticipated dose and dose rates associated with different beam loss scenarios of the BTA, ATS, and STA transfer lines. The loss rates associated with their respective efficiencies were derived. It was demonstrated in Tables 7.2, 7.3, and 7.4 that the decrease of electron beam lifetime has an inverse linear relationship with dose. The null hypothesis that the decrease of electron beam lifetime within ALS-U will have an inverse, linear relationship with dose rates resulting from electron losses is accepted and the alternate hypothesis that the decrease of electron beam lifetime within ALS-U will not have an inverse, linear relationship with dose rates resulting from electron losses is rejected.

The anticipated dose and dose rates for the ATS and STA transfer lines are expected to be below radiation area posting requirements for most locations. The BTA transfer line doses and dose rates are expected to routinely create radiation areas and its nearest penetration will require additional shielding to meet ALARA goals.

8.4 Biasing Factors

Section 6.5.1 ALS Measured Data compared measured data from a 100% beam dump event ALS to simulation designed to reproduce that system. The simulated result was approximately 18% lower than that of the simulation which could be attributed to slight differences in geometry or to the assumptions on scraper split efficiencies.

For the problem involving GB production during early operations, the model included sufficient conservatism in the assumed vacuum pressure being the maximum value 4×10^{-7} torr as opposed to the average 2.4×10^{-7} torr. As such an additional adjustment of 18% is not warranted as the value should already be bounding of actual conditions.

For the problem involving losses through HVAC and electrical penetrations, the model included sufficient conservatism in the assumed scraper loss points of AR and SR being immediately next to one another creating an artificially high dose location. From the simulations, it was noted that although the accumulator ring is assumed to run at one-tenth of the current of the storage ring, it contributes approximately 44% of the photon dose and 33% of the neutron dose to the F4 tally cell outside the penetration. Having both beam loss locations be side by side and happy simultaneously is sufficiently conservative such that an additional adjustment of 18% is not warranted.

For the problem involving losses from the transfer lines due to electron bunch swapping, the BTA transfer line represents the highest losses due to an assumed efficiency of 0.96. A more likely but less conservative efficiency value is estimated to be 0.98. This potential 50% reduction in source term is sufficiently conservative such that an additional adjustment of 18% is not warranted.

8.5 Future Research

This research focuses on the definition of initial radiological engineering issues associated with the following accelerator systems: booster-to-accumulator transfer line, accumulator ring, accumulator-to-storage transfer line, and storage-to-accumulator transfer line. Prior to operations at ALS-U commencing, each x-ray beamline will need to be fully characterized and properly shielded for the generated synchrotron radiation. The complete characterization of the x-ray beamlines will be done over the course of the next few years going into operations.

9 REFERENCES

Bruenlin, J. 2016. Emittance related topics for fourth generation storage ring light sources. Lund University.

Chinaka, E.M., 2014 Radiation Shielding Analysis and Optimisation for the Mineral-PET Kimberlite Sorting Facility using the Monte Carlo Calculation Code MCNPX. University of Johannesburg.

Christofilos, N. Focusing system for ions and electrons, 1950. US Patent 2,736,799. Published 1956.

Cockcroft, J.D. and Walton, E. T. S., 1932. Experiments with high velocity positive ions. (I) further developments in the method of obtaining high velocity positive ions. Proceedings of the Royal Society of London A: Mathematical, Physical and Engineering Sciences, 136(830):619–630.

Cossairt, J.D., and K. Vaziri, 2008. *Neutron Dose per Fluence and Weighting Factors for Use at High Energy Accelerators*, FERMILAB-PUB-08-244-ESH-REV.

Cossairt, J.D., FERMILAB-TM-1834, *Radiation Physics for Personnel and Environmental Protection*, November, 2011.

Courant, E. D., Livingston, M. S., and Snyder, H. S. The strong-focusing synchrotron – A new high energy accelerator. Physical Review, 88:1190–1196, 1952.

Elder, F. R., Gurewitsch, A. M., Langmuir, R. V., and Pollock, H. C., 1947. Radiation from electrons in a synchrotron. Physical Review, 71:829–830.

Fassò, A, Goebel,K, Höfert, M, Ranft, J, and Stevenson, G. Landolt-Börnstein numerical data and functional relationships in science and technology new series; Group I: nuclear and particle physics Volume II: *Shielding against high energy radiation* (O. Madelung, Editor in Chief, H. Schopper, Editor, Springer-Verlag, Berlin, Heidelberg, 1990).

Harvey, Z. R., *Advanced light source-Upgrade accumulator-ring gas bremsstrahlung Production.* Nuclear Inst. and Methods in Physics Research, A 983 (2020) 164592

Hettel, R., DLSR design and plans: an international overview. Journal of Synchrotron Radiation, 21(5):843–855, 2014.

International Commission of Radiation Protection (ICRP21), 1973. Data for Protection Against Ionizing Radiation from External Sources: Supplement to ICRP Publication 15. ICRP Publication 21. Pergamon Press, Oxford.

Johansson, M., Anderberg, B. and Lindgren, L.-J. Magnet design for a low-emittance storage ring. Journal of Synchrotron Radiation, 21(5):884–903, 2014.

Koch, H. W., Motz, J. W., *Bremsstrahlung Cross-section Formulas and Related Data*, Reviews of Modern Physics, vol. 31, no. 4, pp. 920–955, Oct. 1959. DOI: 10.1103/RevModPhys.31.920

Lawrence E.O. and Edlefsen, N. E. 1930. Science, 72:376–377.

Lawrence Berkeley National Laboratory, EHS Procedure 718.3, *Radiation Shielding Design and Optimization*

Lawrence Berkeley National Laboratory, 2016 ALS Safety Assessment Document, Rev. 9 (December 14, 2016).

Lawrence Berkeley National Laboratory, 2018. *Advanced Light Source Upgrade Conceptual Design Report*.

Lawrence Berkeley National Laboratory, 2019A. *ALS-U Accumulator: Ring Vacuum System, Technical and Schedule Review of the ALS-U Accumulator*.

Lawrence Berkeley National Laboratory, 2019B. *ALS-U Storage Ring: Particle Loss Studies and Ion Instabilities*, *CD-3A Director's Review.*

Lawrence Berkeley National Laboratory, 2021. *ALS-U Beam Loss (draft),* AL-1407-4385**.**

Lee, T-Y, *Practical Definitions of Beam Lifetimes in an Electron Storage Ring.* Proceedings of 2005 Particle Accelerator Conference, Knoxville, Tennessee Pohang Accelerator Laboratory, San 31, Hyoja-dong, Pohang, Kyungbuk, 790-784 KOREA

Liu, J C, Nelson, W R, & Kase, K R. *Gas bremsstrahlung and associated photon-neutron shielding calculations for electron storage rings*. 1994. United States.

Liu, J. C. and Vylet, V. Radiation Protection at Synchrotron Radiation Facilities, Radiation Protection Dosimetry 96(4), 345-357 (2001).

Los Alamos National Laboratory (LANL), Monte Carlo N-Particle Transport Code (MCNP6) 6.1 software package.

Environmental Protection Agency (EPA) NUREG-1576 Multi-Agency Radiological Laboratory Analytical Protocols (MARLAP) Manual (2004).

Marshall, R[1]., Cully C[2]. *Atmospheric effects and signatures of high-energy electron precipitation*. 1 Ann and H. J. Smead Department of Aerospace Engineering Sciences, University of Colorado, Boulder, CO, United States. 2 Department of Physics and Astronomy, University of Calgary, Calgary, AB, Canada

Mollerach, S., E, Roulet. *Progress in high-energy cosmic ray physics*. Centro Atomico Bariloche, CONICET, Argentina November 1, 2017

National Council on Radiation Protection and Measurements. Protection against Neutron Radiation. NCRP Report No. 38 (Bethesda, MD: NCRP), 1971.

McConn, RJ, Gesh, CJ, Pagh, RT, RA, Williams, RG, *Compendium of Material Composition Data for Radiation Transport Modeling.* Pacific Northwest National Laboratory (PNNL) *Revision 1*, *2011*.

Nelson, W (Feb 2005). The SHIELD11 Computer Code (SLAC-R--737). United States

Rodgers, D.W.O., 1984. Fluence to dose equivalent conversion factors calculated with EGS3 for electrons from 100 keV to 20 GeV and photons from 11 keV to 20 GeV, *Health Physics*, vol. 46, no. 4, pp. 891–914.

Roy,C.J, Oberkampf, W, L. *A comprehensive framework for verification, validation, and uncertainty quantification in scientific computing,* Computer Methods in Applied Mechanics and Engineering, Volume 200, Issues 25–28, 2011, Pages 2131-2144, ISSN 0045-7825

Shultis, J.K., Faw, R.E., *An MCNP Primer.* Dept. of Mechanical and Nuclear Engineering Kansas State University Manhattan, KS 66506 (2011)

SLAC National Accelerator Laboratory, 2017A. *SLAC Radiation Physics Note RP-17-13, Shielding Evaluation for FOE of APS-U ID Beamline*, SLAC Radiation Physics Note RP-17-13.

SLAC National Accelerator Laboratory, 2017B. *Shielding Evaluation for FOE of APS-U BM Beamline*, SLAC Radiation Physics Note RP-17-14.

Xia, Z. *Comparison of Analytical Shielding Calculations for NSLS-II Linac Lateral Wall with FLUKA Monte-Carlo Program.* NSLS II Technical Note Brookhaven National Laboratory Number NSLSII-ESH-TN-133. August 2018.

10 APPENDIX I, Example Gas Bremsstrahlung MCNP6 Input Deck

```
2.0 GeV e- gas brem calculation for AR at
ALS-U
c mcnp6 i=321.txt tasks 5
c mcnp6 ip i=321.txt

c
c
************************************
*********************************
c                    Cell Cards
c
************************************
*********************************
c
1   1 -6.34e-6   -10 12 -13     $ inner AR air,
4e-7 Torr
2   2 -7.9       10 -11 12 -13  $ AR straight
pipe, check SS density
3   2 -7.9       13 -14 -11     $vac tube wall
end
10  0            -20 40          $F4 box
11  0            -21             $SSW box
30  3 -7.9       -30             $suxtupole magnet,
was 3 -7.9
40  4 -2.3       -40 20          $concrete
shieldwall
41  5 -11.35     -41             $pb at shieldwall
998 1 -1.205e-3  -99 #41 #40 30 20 21 #1 #2
#3 $ SR ring air
999 0            99              $Kill'm all

c
************************************
*********************************
c                    Surface Cards
c
************************************
*********************************
c
10 cx   2.5      $AR straight ID
11 cx   2.58     $AR straight OD
12 px   0.0      $AR beginning
13 px   450.0    $AR end
14 px   450.08   $vac tube wall end
c
20 box 1851 -0.5 -0.5  1 0 0  0 1 0  0 0 1
$1cm3 F4 box, 451previous, 518 after sx,
1803 before 1851after wall
21 box 520 -50 -50  0.1 0 0  0 100 0  0 0 100
$ssw write box
22 px 520 $ssw surface
c
30 rcc 475 0 0 18.86 0 0 17 $sextupole mag
c
40 box 1805 -50 -50   45.74 0 0  0 100 0  0 0
100 $shieldwall
41 box 1797 -50 -50   7.62 0 0   0 100 0  0 0
100 $3" pb shield
c
99 box -50 -50 -50 1950 0 0   0 100 0   0 0
100 $universe


c
************************************
*********************************
c                    Data Cards
c
************************************
*********************************
c for material cards -#s indicate wt fraction,
+#s indicate atomic fraction
c
c Air from PNNL Materials document
m1      6012  -0.000124
        7014  -0.755268
        8016  -0.231781
       18040  -0.012827
m2 26000 -0.67 24000 -0.18 25000 -0.0875
28000 -0.05 $stainless steel
m3 26000 -1 $iron magnet
m4 1001 -0.01 8016 -0.532 11023 -0.029
$Concrete, regular
     13027 -0.034 14000 -0.337 20000
     -0.044 26000 -0.014
m5 82000 -1 $pb shielding
```

```
c
imp:e    1   1   1  1   1   1   1   1   1   0
imp:p    1   1   1  1   1   1   1   1   1   0
elpt:e  .1  .1  .1  .1  .1  .1  .1  .1  .1  .1  $cell
by cell E Cut
elpt:p  .1  .1  .1  .1  .1  .1  .1  .1  .1  .1
mode e p
nps 5e6 $1e7 ssw then 1e9 used for ssr
read file=sdef_ALSU_AR_bbrem.txt $ource
info in sdef.txt
c sdef par=3 erg=2000.0 x=0 y=0 z=0 vec=
1 0 0 dir=1.
c bbrem 1.0 1.0 46i 10.0 1
phys:p 2000    $upper limit for p particle E
c phys:e 2000 j j j j j 0 0 1 -1 j j 0.99 j $
phys:e 2000
mphys on
c
c SSW -22(998) $30.2(998) $4 5 11 12 3 7 -
22 $(23)
c SSR old 21.2 $30.2
c
c
c e0 1e-3 110log 2e+3   $
c fc2 'Dose rate 0 degrees, 500mA, 1 ntorr,
9m ID at 14m'
c f2:p 13
c fs2  -10
c sd2  1.4522e-1 1.0 $ vacuum tube area
c df2 iu 1 FAC 1.040e6
c
c fc5 'Scatter Dose rate 0 degrees, 500mA, 1
ntorr, 9m ID at 14m'
c f5:p 30.48 0 1410.0  1.0
c df5 iu 1 FAC 3.701e7
c
c fac1 = (1e-9/760)(.5/1.6e-19)(9/1) =
3.701e7  $fac is log interpolation of E and
dose
c fac2 = 9/(13.95(9+13.95)) = 2.811e-2
c FAC = fac1*fac2 = 1.040e6
c fmesh4:p geom=xyz origin 1850.74 -50 -
50 $mesh for shield wall
c      imesh=1851 iints=1
c      jmesh=50 jints=100
c      kmesh=50 kints=100
fmesh4:p geom=xyz origin 505 -50 -0.5
$mesh for run length
      imesh=1905 iints=1905
      jmesh=50 jints=100
      kmesh=1 kints=1
c mplot file fmesh 4 freq 1
c stop f4 0.05
c f4:p 10
de4 0.01 0.015 0.02 0.03 0.04 0.05 0.06 0.08
    0.1 0.15 0.2 0.3 0.4 0.5 0.6 0.8 1 1.5 2
    3 4 5 6 8 10  20 30 40 50 100 200 500
    1000 2000
c df4 2.78E-06 1.11E-06 5.88E-07 2.56E-07
1.56E-07 1.2E-07 $ICRP21 photon flux to
dose conv factors pg 479 mcnp manual
c     1.11E-07 1.2E-07 1.47E-07 2.38E-07
3.45E-07
c     5.56E-07 7.69E-07 9.09E-07 1.14E-06
1.47E-06
c     1.79E-06 2.44E-06 3.03E-06 4.00E-06
4.76E-06
c     5.56E-06 6.25E-06 7.69E-06 9.09E-06
c
df4 1.54E+02 6.15E+01 3.26E+01
1.42E+01 8.64E+00 $icrp21 photon x
5.54e7 p/s = Rem/hr
      6.65E+00 6.15E+00 6.65E+00 8.14E+00
1.32E+01
      1.91E+01 3.08E+01 4.26E+01 5.04E+01
6.31E+01
      8.14E+01 9.92E+01 1.35E+02 1.68E+02
2.22E+02
      2.64E+02 3.08E+02 3.46E+02 4.26E+02
5.04E+02
      8.64E+02 1.25E+03 1.63E+03 1.97E+03
3.94E+02
      6.01E+02 9.53E+02 1.13E+03 1.29E+03
c e4 0 1 2 3 4 5 6 7 8 9 10 20 30 40 50 60
$For F4 energy bin tally
c     70 80 90 100 110 120 130 140 150 160
c     170 180 190 200 210 220 230 240 250
c     260 270 280 290 300 310 320 330 340
c     350 360 370 380 390 400 410 420 430
c     440 450 460 470 480 490 500 510 520
c     530 540 550 560 570 580 590 600 610
c     620 630 640 650 660 670 680 690 700
```

c 710 720 730 740 750 760 770 780 790
c 800 810 820 830 840 850 860 870 880
c 890 900 910 920 930 940 950 960 970
c 980 990 1000 1010 1020 1030 1040
c 1050 1060 1070 1080 1090 1100 1110
c 1120 1130 1140 1150 1160 1170 1180
c 1190 1200 1210 1220 1230 1240 1250
c 1260 1270 1280 1290 1300 1310 1320
c 1330 1340 1350 1360 1370 1380 1390
c 1400 1410 1420 1430 1440 1450 1460
c 1470 1480 1490 1500 1510 1520 1530
c 1540 1550 1560 1570 1580 1590 1600
c 1610 1620 1630 1640 1650 1660 1670
c 1680 1690 1700 1710 1720 1730 1740
c 1750 1760 1770 1780 1790 1800 1810
c 1820 1830 1840 1850 1860 1870 1880
c 1890 1900 1910 1920 1930 1940 1950
c 1960 1970 1980 1990 2000

11 APPENDIX II, Example HVAC and Electrical Penetration MCNP6 Input Deck

```
ALS-U Accumulator Ring and Storage Ring
Brem through HVAC Penetration
c
***********************************
***********************************
****
c  Cell Cards
c
***********************************
***********************************
****
1 6 -8.96     -1              $SR Cu Target
Collimator
2 6 -8.96     -2              $AR Cu Target
Collimator
c
11 9 -0.001205 11 -12 -13 14 15 -16
$HVAC penetration
12 9 -0.001205 11 -12 -14 23 15 -16  $IMP
cell extension
c
21 9 -0.001205 21 -22 -23 24 25 -26 $F4
box
c
31 9 -0.001205 -31                $elec
penetration
c
90 9 -0.001205 -90 1 2 #11 #12 #21 #31
$SR air
91 1 -2.35 -91 90 #11 #12 #21 #31
$SR concrete
c
98 9 -0.001205 -99 #1 #2 #11 #12 #21 #31
#90 #91 $outside air
99 0          99           $Kill'm all

c
c
***********************************
***********************************
****
c  Surface Cards
c
***********************************
***********************************
****
1  box  70 295 134.7  40 0 0   0 10 0  0 0 10
$SR Cu Target Collimator
2  box  70 63.58 198.2  40 0 0  0 10 0  0 0 10
$AR Cu Target Collimator
c
11 pz 162.56 $HVAC Penetration
12 pz 203.2
13 py 0
14 py -45.72
15 px 50.32
16 px 90.32
c
21 pz 162.56 $F4 box
22 pz 203.2
23 py -75.72
24 py -76.72
25 px 50.32
26 px 90.32
c
31 RCC 70.32 0 35.56  0 -45.72 0  5.08 $4"
dia CY, center at 14"
  c
90 box 0 0 0   600 0 0  0 400 0   0 0 243.84
$inside SR air
91 box -30.48 -45.72 -30.48   660.98 0 0   0
477 0   0 0 304.8   $SR Concrete
c
99 box -250 -250 -250    1000 0 0  0 1000 0
0 0 1000  $Universe

c
***********************************
***********************************
****
c  Data Cards
c
***********************************
***********************************
****
```

```
c
************************************
************************************
****
c  Source
c
************************************
************************************
****
imp:e    1   1   1   1    1    1   1   1   1   0
imp:p    1   1   10  100  100  10  1   1   1   0
imp:n    1   1   10  100  100  10  1   1   1   0
elpt:e  .1  .1  .1  .1   .1   .1  .1  .1  .1  .1 $cell
by cell E Cut
elpt:p  .01  .01  .01  .01   .01   .01  .01  .01
.01  .01
elpt:n  0.001 0.001 0.001 0.001 0.001 0.001
0.001 0.001 0.001 0.001
mode e p n
nps 1e5 $2e5 was good for N-mesh
c read file=sdef_ALSU_AR_bbrem.txt
$ource info in sdef.txt
c sdef par=3 erg=2000.0 pos d1 vec= 1 0 0
dir=1. $x=60 y=300 z=140 SR source
sdef par=3 erg=2000.0 pos d1 vec 0.99995
0.015 0 ara 0.1 dir 1 $0.002999996=2mra
c SI1 L 60 300 140    60 68.58 203.2
SI1 L 57 294.82 140  $only SR source
SP1   1
c bbrem 1.0 1.0 46i 10.0 1
c phys:p 2000 0 0 -1 0 J 0   $Photonnuclear
ON
phys:p 2000 0 0 0 0 J 0    $Photonuclear
OFF
phys:e 2000    $upper limit for p particle E
phys:n 2000    $upper limit for p particle E
MPHYS ON
c
************************************
************************************
****
c  Materials
c
************************************
************************************
****
```

```
C name: Concrete as specified in Chilton, pg
374
C density = 2.35 g/cc
M1      1001  -0.013
        8016  -1.165
        14000  -0.737
        20000  -0.194
        11023  -0.040
        12000  -0.006
        13027  -0.107
        16032  -0.003
        19000  -0.045
        26000  -0.029
C name: Sand (dry)
C density = 1.6 g/cc
M2   14000 1 8016 2
C name: Simple Iron
C density = 7.874 g/cc
M3   26000 1
C name: Aluminum
C density = 2.7 g/cc
M4   13027 1
C name: Copper
C density = 8.96 g/cc
 M6   29063 -.6917 29065 -.3083
C name: Air (dry, sea level)
C density = 0.001205 g/cc
m9    6000       -0.000124
        8016       -0.231781
        7014       -0.755268
        18000      -0.012827
C name: Al
C density = 2.7
m506  13027 1.0000e+00
C name: Pb
C density = 11.3
m510 82204 1.4000e-02
        82206 2.4100e-01
        82207 2.2100e-01
        82208 5.2400e-01
C name: W
C density = 19.25
m512  74182 0.265
        74183 0.1431
        74184 0.3064
        74186 0.2843
```

```
c
************************************
************************************
****
c  Tallies
c
************************************
************************************
****
c
FMESH4:p GEOM=xyz ORIGIN = 0 -46 0
    IMESH=300 IINTS=50
    JMESH=450 JINTS=110
    KMESH=243.84 KINTS=100
c
c FMESH4:n GEOM=xyz ORIGIN = 481 -
14 -14
c      IMESH= 501 515 516 516.5 517 529
540
c      IINTS= 10  14  2   10    1   6   11
c      JMESH= 14 JINTS= 14
c      KMESH= 14 KINTS= 14
c
c F4:p 21
c
c mplot file fmesh 4 freq 1
c stop f4 0.05
de4 0.01 0.015 0.02 0.03 0.04 0.05 0.06 0.08
    0.1 0.15 0.2 0.3 0.4 0.5 0.6 0.8 1 1.5 2
    3 4 5 6 8 10  20 30 40 50 100 200 500
    1000 2000
df4 2.78E-06 1.11E-06 5.88E-07 2.56E-07
1.56E-07 1.2E-07  $ c ICRP21 photon
    1.11E-07 1.2E-07 1.47E-07 2.38E-07
3.45E-07
     5.56E-07 7.69E-07 9.09E-07 1.14E-06
1.47E-06
    1.79E-06 2.44E-06 3.03E-06 4.00E-06
4.76E-06
    5.56E-06 6.25E-06 7.69E-06 9.09E-06
1.56E-05
    2.26E-05 2.94E-05 3.56E-05 7.11E-06
1.09E-05
    1.72E-05 2.04E-05 2.32E-05
```

12 APPENDIX III, Example Booster-to-Accumulator Electron Bunch Swapping MCNP6 Input Deck

```
ALS-U BTA Line charge loss scenarios,
scintillator in beam18
c
************************************
************************************
****
c  Cell Cards
c
************************************
************************************
****
c 1 6 -8.96     -1            $SR Cu Target
Collimator
2 11 -3.97     -2            $AR scintillator
c
c 11 9 -0.001205 11 -12 -13 14 15 -16
$HVAC penetration
c 12 9 -0.001205 11 -12 -14 23 15 -16
$IMP cell extension
c
c 21 9 -0.001205 21 -22 -23 24 25 -26 $F4
box
c
31 9 -0.001205 -31              $elec
penetration
c
34 9 -0.001205  -34 #31   $inner quad air
33 6 -8.96 -33 34 #34 #31          $quad
magnet
35 3 -7.784 -35 33 #33     $yoke
c
40 0 -41 #33 #34 #35 #31 $septum inner vac
41 4 -2.7 -40 #33 #35 #40 #34 #31 $septum
al outer
90 9 -0.001205 -90  2  #31 #33 #34 #35 #40
#41       $SR air
32 9 -0.001205 -32 90 #31 #34 #35 #40 #41
91 1 -2.35 -91 90  #31 #32 #33 #34 #40 #41
$SR concrete
92 1 -2.35 -92 90 91  #31 #32 #33 #34 #35
#40 #41
c
98 9 -0.001205 -99 #2 #31 #32 #33 #34 #35
#40 #41 #90 #91 #92 $outside air
99 0           99          $Kill'm all

c
c
************************************
************************************
****
c  Surface Cards
c
************************************
************************************
****
c 1  box  70 295 134.7  40 0 0   0 10 0  0 0
10  $SR Cu Target Collimator
c 2  box  70 25 198.2  40 0 0  0 10 0  0 0 10
$AR Cu Target Collimator
2 ARB 25 45 198.2  25 55 198.2  35 45
208.2  35 55 208.2  25.1 45 198.2
    25.1 55 198.2  35.1 45 208.2  35.1 55
208.2 1234 5678 1256
    3478 2468 1357
c 63.58
11 pz 162.56 $HVAC Penetration
12 pz 203.2
13 py 0
14 py -45.72
15 px 50.32
16 px 90.32
c
21 pz 162.56 $F4 box
22 pz 203.2
23 py -75.72
24 py -76.72
25 px 50.32
26 px 90.32
c
31 RCC 70.32 0 35.56  0 -100 0  5.08 $elec
pen4" i CY, center at 14"
```

32 RCC 70.32 30 243.84 0 0 46 15 $roof pen 12"dia
c
33 RCC 55 50.22 203.2 20 0 0 12.6 $quad outer 0.1m
34 RCC 55 50.22 203.2 20 0 0 8.21 $quad inner 0.05m
35 RCC 60 50.22 203.2 10.8 0 0 16.8 $yoke
c
40 box 85 45 190 100 0 0 0 20 0 0 0 26 $injection septum box outer
41 box 90 46 191 94 0 0   0 18 0 0 0 24 $inject septum inner 1cm
c 90 box -30.48 0 0   660.98 0 0   0 400 0   0 0 243.84 $inside SR air
c 91 box -30.48 -45.72 -30.48   660.98 0 0 0 477 0   0 0 304.8 $SR Concrete
c
c
90 box -30.48 0 0   660.98 0 0   0 400 0   0 0 243.84 $inside SR air
91 box -30.48 -100 -30.48   130 0 0   0 531.28 0   0 0 320.04 $SR Concrete 406mm roof
92 box 99.52 -100 -30.48   530.98 0 0 0 531.28 0 0 0 304.8 $SR concrete 254mm roof
c
99 box -250 -250 -250   1000 0 0 0 1000 0 0 0 1000 $Universe

c
****
c Data Cards
c
****
c
****
c Source
c
****
imp:e 1 1 1 1 1 1 1 1 1 1 1 1 0
imp:p 1 1 1 1 1 1 1 1 1 1 1 1 0
imp:n 1 1 1 1 1 1 1 1 1 1 1 1 0
c elpt:e .1   .1 .1   .1   .1 .1 .1 $cell by cell E Cut
c elpt:p .1 .1 .1   .1   .1 .1 .1
c elpt:n 0.001 0.001 0.001 0.001 0.001 0.001 0.001
mode e p n
nps 1e7 $2e7 failed after 7hr
PRDMP -100 -100 1 $write MCTAL file at problem completion
c read file=sdef_ALSU_AR_bbrem.txt $source info in sdef.txt
sdef par=3 erg=2000.0 pos d1 vec= 1 0 0 ara 0.1 dir=1 $x=60 y=300 z=140 SR source
c sdef par=3 erg=2000.0 pos d1 vec 1 -0.31125 0.21875 ara 0.1 dir 1 $0.002999996=2mrad,5X = 0.015
c SI1 L 60 300 140   60 68.58 203.2
SI1 L 24 50.22 203.2
SP1   1.0
bbrem 1.0 1.0 46i 10.0 1
phys:p 2000 0 0 -1 0 J 0 $Photonnuclear ON
c phys:p 2000 0 0 0 0 J 0 $Photonuclear OFF
phys:e 2000 $upper limit for p particle E
phys:n 2000 $upper limit for p particle E
MPHYS ON
c
****
c Materials
c
****
C name: Concrete as specified in Chilton, pg 374
C density = 2.35 g/cc

```
M1      1001  -0.013
        8016  -1.165
       14000  -0.737
       20000  -0.194
       11023  -0.040
       12000  -0.006
       13027  -0.107
       16032  -0.003
       19000  -0.045
       26000  -0.029
C name: Sand (dry)
C density = 1.6 g/cc
M2   14000 1 8016 2
C name: Simple Iron
C density = 7.874 g/cc
M3   26000 1
C name: Aluminum
C density = 2.7 g/cc
M4   13027 1
C name: Copper
C density = 8.96 g/cc
M6   29063 -.6917 29065 -.3083
C name: Air (dry, sea level)
C density = 0.001205 g/cc
m9    6000       -0.000124
      8016       -0.231781
      7014       -0.755268
      18000      -0.012827
C name: Pb
C density = 11.34
m10
     82204 -1.4000e-02
     82206 -2.4100e-01
     82207 -2.2100e-01
     82208 -5.2400e-01
C
c name: aluminum oxide doped with
Chromium (~6% wgt)
c density = 3.97 g/cc
m11  8016 -0.470749
     13027 -0.529251
     24000 -0.06
C name: Stainless Steel 409
C density = 7.8
m502
     6012 -7.8085e-04
     6013 -9.1516e-06
     14028 -9.0305e-03
     14029 -4.7515e-04
     14030 -3.2438e-04
     15031 -4.4000e-04
     16032 -4.1675e-04
     16033 -3.3933e-06
     16034 -1.9810e-05
     16036 -4.9355e-08
     22046 -5.8371e-04
     22047 -5.3785e-04
     22048 -5.4424e-03
     22049 -4.0772e-04
     22050 -3.9834e-04
     24050 -4.6453e-03
     24052 -9.3157e-02
     24053 -1.0767e-02
     24054 -2.7306e-03
     25055 -9.8300e-03
     26054 -4.8552e-02
     26056 -7.9035e-01
     26057 -1.8579e-02
     26058 -2.5159e-03
C name: Al
C density = 2.7
m506
     13027 1.0000e+00
C name: Pb
C density = 11.3
m510
     82204 1.4000e-02
     82206 2.4100e-01
     82207 2.2100e-01
     82208 5.2400e-01
C name: W
C density = 19.25
m512
     74182 0.265
     74183 0.1431
     74184 0.3064
     74186 0.2843
C name: Tantalum
C density = 16.654 g/cc
M900  73181 1
C name: Beryllium
C density = 1.848 g/cc
```

```
M901  4009  1
c
****************************************************************************
c  Tallies
c
****************************************************************************
c
c FMESH4:p GEOM=xyz ORIGIN = 0 -200
203.1
c      IMESH=450 IINTS=300
c      JMESH=450 JINTS=300
c      KMESH=203.2 KINTS=1
c
tmesh
rmesh1:p dose 10 $10=icrp21 photon
cora1  0  250i  250.0 $mcnp6 manual 2.8.1
for 18i explan
corb1  0  100i  100.0
corc1  100  220i  320.0
c
c rmesh1:n dose 10 $10=icrp21 neutron
c cora1  0 250i  250.0 $mcnp6 manual 2.8.1
for 18i explan
c corb1  0  100i  100.0
c corc1  100  220i  320.0
c
c rmesh31:p dose 10 $10=icrp21 photon
c cora31  70  71.0 $mcnp6 manual 2.8.1 for
18i explan
c corb31  -150  300i  300.0
c corc31  0  300i  320.0
c
c rmesh41:n dose 10 $10=icrp21 neutron
c cora41  70  71.0 $mcnp6 manual 2.8.1 for
18i explan
c corb41  -150  300i  300.0
c corc41  0  300i  320.0
endmd
c PRDMP mct 1 $write MCTAL file at
problem completion
c
c FMESH4:p GEOM=xyz ORIGIN = 50 24
0  $yz mesh
c      IMESH=250 IINTS=300
c      JMESH=25 JINTS=1
c      KMESH=320 KINTS=300
c
c FMESH4:n GEOM=xyz ORIGIN = 481 -
14 -14
c      IMESH= 501 515 516 516.5 517 529
540
c      IINTS= 10  14  2   10    1   6   11
c      JMESH= 14 JINTS= 14
c      KMESH= 14 KINTS= 14
c
c F4:n 21
c
c mplot file fmesh 4 freq 1
c stop f4 0.05
F5:p 71 31 320   1
F15:n 71 31 320  1
F25:p 150 31 290    1
F35:n 150 -31 290    1
c
c de4 0.01 0.015 0.02 0.03 0.04 0.05 0.06
0.08
c     0.1 0.15 0.2 0.3 0.4 0.5 0.6 0.8 1 1.5 2
c     3 4 5 6 8 10  20 30 40 50 100 200 500
c     1000 2000
c df4 2.78E-06 1.11E-06 5.88E-07 2.56E-07
1.56E-07 1.2E-07  $ c c ICRP21 photon flux
to dose conv factors pg 479 mcp manual
c      1.11E-07 1.2E-07 1.47E-07 2.38E-07
3.45E-07
c      5.56E-07 7.69E-07 9.09E-07 1.14E-06
1.47E-06
c      1.79E-06 2.44E-06 3.03E-06 4.00E-06
4.76E-06
c      5.56E-06 6.25E-06 7.69E-06 9.09E-06
1.56E-05
c      2.26E-05 2.94E-05 3.56E-05 7.11E-06
1.09E-05
c      1.72E-05 2.04E-05 2.32E-05
c
de5 0.01 0.015 0.02 0.03 0.04 0.05 0.06 0.08
     0.1 0.15 0.2 0.3 0.4 0.5 0.6 0.8 1 1.5 2
     3 4 5 6 8 10  20 30 40 50 100 200 500
```

```
   1000 2000
df5 2.78E-06 1.11E-06 5.88E-07 2.56E-07
1.56E-07 1.2E-07  $ c c ICRP21 photon flux
to dose conv factors pg 479 mcp manual
     1.11E-07 1.2E-07 1.47E-07 2.38E-07
3.45E-07
     5.56E-07 7.69E-07 9.09E-07 1.14E-06
1.47E-06
     1.79E-06 2.44E-06 3.03E-06 4.00E-06
4.76E-06
     5.56E-06 6.25E-06 7.69E-06 9.09E-06
1.56E-05
     2.26E-05 2.94E-05 3.56E-05 7.11E-06
1.09E-05
     1.72E-05 2.04E-05 2.32E-05
c
de25 0.01 0.015 0.02 0.03 0.04 0.05 0.06
0.08
    0.1 0.15 0.2 0.3 0.4 0.5 0.6 0.8 1 1.5 2
    3 4 5 6 8 10  20 30 40 50 100 200 500
    1000 2000
df25 2.78E-06 1.11E-06 5.88E-07 2.56E-07
1.56E-07 1.2E-07  $ c c ICRP21 photon flux
to dose conv factors pg 479 mcnp manual
     1.11E-07 1.2E-07 1.47E-07 2.38E-07
3.45E-07
     5.56E-07 7.69E-07 9.09E-07 1.14E-06
1.47E-06
     1.79E-06 2.44E-06 3.03E-06 4.00E-06
4.76E-06
     5.56E-06 6.25E-06 7.69E-06 9.09E-06
1.56E-05
     2.26E-05 2.94E-05 3.56E-05 7.11E-06
1.09E-05
     1.72E-05 2.04E-05 2.32E-05
c
de15 2.5e-8 1e-7 1e-6 1e-5 1e-4 1e-3 1e-2 $
NCRP-38, ANSI6.1.1-1977 neutron flux
      1e-1 5e-1 1 2.5 5 7 10 14 20 40 60 $ to
dose rate conv factors
      100 200 300 400                  $ 20
MeV+ DCFs from D. Coissart, in folder
df15 3.67e-6 3.67e-6 4.46e-6 4.54e-6       $
pg.271 mcnp6 user manual
      4.18e-6 3.76e-6 3.56e-6 2.17e-5
      9.26e-5 1.32e-4 1.25e-4 1.56e-4
      1.47e-4 1.47e-4 2.08e-4 2.27e-4
      2.36E-05 1.86E-05 1.35E-05 1.18E-05
      1.18E-05 1.18E-05
c df4 iu=1 fac=1 log IC=20 $ncrp38
c
de35 2.5e-8 1e-7 1e-6 1e-5 1e-4 1e-3 1e-2 $
NCRP-38, ANSI6.1.1-1977 neutron flux
      1e-1 5e-1 1 2.5 5 7 10 14 20 40 60 $ to
dose rate conv factors
      100 200 300 400                  $ 20
MeV+ DCFs from D. Coissart, in folder
df35 3.67e-6 3.67e-6 4.46e-6 4.54e-6       $
pg.271 mcnp6 user manual
      4.18e-6 3.76e-6 3.56e-6 2.17e-5
      9.26e-5 1.32e-4 1.25e-4 1.56e-4
      1.47e-4 1.47e-4 2.08e-4 2.27e-4
      2.36E-05 1.86E-05 1.35E-05 1.18E-05
      1.18E-05 1.18E-05
c
```

13 APPENDIX IV, Example Accumulator-to-Storage Electron Bunch Swapping MCNP6 Input Deck

```
ALS-U ATS Line charge loss scenarios
c
************************************
************************************
****
c  Cell Cards
c
************************************
************************************
****
c 1 6 -8.96     -1              $SR Cu Target
Collimator
2 6 -8.96     -2              $AR Cu target coll
c
c 11 9 -0.001205 11 -12 -13 14 15 -16
$HVAC penetration
c 12 9 -0.001205 11 -12 -14 23 15 -16
$IMP cell extension
c
c 21 9 -0.001205 21 -22 -23 24 25 -26 $F4
box
c
31 9 -0.001205 -31                $elec
penetration
c
c 34 9 -0.001205  -34 #31   $inner quad air
c 33 6 -8.96 -33 34 #34 #31          $quad
magnet
c 35 3 -7.784 -35 33 #33     $yoke
c
40 0 -41 2 #31 $septum inner vac
41 4 -2.7 -40 #2 #40  #31 $septum al outer
90 9 -0.001205 -90 #2  #31  #40 #41
$SR air
32 1 -2.35 -32 90 #2 #31  #40 #41
91 1 -2.35 -91 90 #2 #31 #32 #40 #41
$arb +y SR concrete
93 1 -2.35 -93 91 90 #2 #31 #32 #40 #41
$arb roof
94 1 -2.35 -94 91 90 #2 #31 #32 #40 #41
$arb floor
92 1 -2.35 -92 90 91 #94 #93 #2 #31 #32
#40 #41 $conc roof
c
98 9 -0.001205 -99 #2 #31 #32 #40 #41 #90
#91 #92 #93 #93 #94 $outside air
99 0            99           $Kill'm all

c
c
************************************
************************************
****
c  Surface Cards
c
************************************
************************************
****
c 1  box  70 295 134.7  40 0 0   0 10 0  0 0
10  $SR Cu Target Collimator
2  box  70 278.7 135  5 0 0  0 10 0  0 0 10
$AR Cu Target Collimator
c
11 pz 162.56 $HVAC Penetration
12 pz 203.2
13 py 0
14 py -45.72
15 px 50.32
16 px 90.32
c
21 pz 162.56 $F4 box
22 pz 203.2
23 py -75.72
24 py -76.72
25 px 50.32
26 px 90.32
c
31 RCC 70.32 0 35.56  0 -100 0  5.08 $elec
pen4" i CY, center at 14"
32 RCC 70.32 65 243.84  0 0 30.48  15
$roof pen 12"dia
c
```

33 RCC 55 50.22 203.2 20 0 0 12.6 $quad outer 0.1m
34 RCC 55 50.22 203.2 20 0 0 8.21 $quad inner 0.05m
35 RCC 60 50.22 203.2 10.8 0 0 16.8 $yoke
c
40 box 55 256 130 100 0 0 0 40 0 0 0 26 $injection septum box outer
41 box 56 257 131 98 0 0   0 38 0 0 0 24 $inject septum inner 1cm
c 90 box -30.48 0 0   660.98 0 0   0 400 0   0 0 243.84 $inside SR air
c 91 box -30.48 -45.72 -30.48   660.98 0 0 0 477 0   0 0 304.8 $SR Concrete
c
c
90 box -30.48 0 0   960.98 0 0   0 400 0   0 0 243.84 $inside SR air
c 91 box -30.48 -50 -30.48   130 0 0   0 481.28 0   0 0 304.8 $320.04 SR Concrete 406mm roof
91 ARB -30.48 540 0 -30.48 510 0 99.52 430 0 99.52 400 0 $+Y wall
       -30.48 540 289.74 -30.48 510 289.74 99.52 430 289.74
       99.52 400 289.74 1234 5678 1256 3478 2468 1357
93 ARB -30.48 510 243.81 -30.48 -50 243.81 99.52 400 243.81 $thick roof block
     99.52 -50 243.81 -30.48 510 289.74 -30.48 -50 289.74
     99.52 400 289.74 99.52 -50 289.74 1234 5678 1256 3478 2468 1357
94 ARB -30.48 540 -30.48 -30.48 -50 -30.48 99.52 430 -30.48 $floor block
     99.52 -50 -30.48 -30.48 540 0 -30.48 -50 0
     99.52 400 0 99.52 -50 0 1234 5678 1256 3478 2468 1357
92 box 99.52 -50 -30.48   830.98 0 0 0 481.28 0 0 0 304.8 $SR concrete 254mm roof
c
99 box -250 -250 -250   1300 0 0 0 1000 0 0 0 1000 $Universe

c
****
c Data Cards
c
****
c
****
c Source
c
****
imp:e 1 1 1 1 1 1 10 10 1 100 100 0
imp:p 1 1 1 1 1 1 10 10 1 100 100 0
imp:n 1 1 1 1 1 1 10 10 1 100 100 0
elpt:e 1 1 1 1 1 1 1 1 1 1 1 1 $cell by cell E Cut
elpt:p 1 1 1 1 1 1 1 1 1 1 1 1
elpt:n .001 .001 .001 .001 .001 .001 .001 .001 .001 .001 .001 .001
mode e p n
nps 1e6 $2e7 failed after 7hr
PRDMP -100 -100 1 $write MCTAL file at problem completion
c read file=sdef_ALSU_AR_bbrem.txt $ource info in sdef.txt
sdef par=3 erg=2000.0 pos d1 vec= 1 0.174533 0 ara 0.1 dir=1 $x=60 y=300 z=140 SR source
c sdef par=3 erg=2000.0 pos d1 vec 1 -0.31125 0.21875 ara 0.1 dir 1 $0.002999996=2mrad,5X = 0.015
c SI1 L 60 300 140   60 68.58 203.2
SI1 L 69 284.29 140
SP1   1.0
bbrem 1.0 1.0 46i 10.0 1
phys:p 2000 0 0 -1 0 J 0 $Photonnuclear ON

```
c phys:p 2000 0 0 0 0 J 0    $Photonuclear
OFF
phys:e 2000    $upper limit for p particle E
phys:n 2000    $upper limit for p particle E
MPHYS ON
c
***********************************
***********************************
****
c  Materials
c
***********************************
***********************************
****
C name: Concrete as specified in Chilton, pg
374
C density = 2.35 g/cc
M1      1001  -0.013
        8016  -1.165
       14000  -0.737
       20000  -0.194
       11023  -0.040
       12000  -0.006
       13027  -0.107
       16032  -0.003
       19000  -0.045
       26000  -0.029
C name: Sand (dry)
C density = 1.6 g/cc
M2   14000 1 8016 2
C name: Simple Iron
C density = 7.874 g/cc
M3   26000 1
C name: Aluminum
C density = 2.7 g/cc
M4   13027 1
C name: Copper
C density = 8.96 g/cc
M6   29063 -.6917 29065 -.3083
C name: Air (dry, sea level)
C density = 0.001205 g/cc
m9    6000       -0.000124
      8016       -0.231781
      7014       -0.755268
      18000      -0.012827
C name: Pb
C density = 11.34
m10
     82204 -1.4000e-02
     82206 -2.4100e-01
     82207 -2.2100e-01
     82208 -5.2400e-01
C
c name: aluminum oxide doped with
Chromium (~6% wgt)
c density = 3.97 g/cc
m11  8016 -0.470749
     13027 -0.529251
     24000 -0.06
C name: Stainless Steel 409
C density = 7.8
m502
     6012 -7.8085e-04
     6013 -9.1516e-06
     14028 -9.0305e-03
     14029 -4.7515e-04
     14030 -3.2438e-04
     15031 -4.4000e-04
     16032 -4.1675e-04
     16033 -3.3933e-06
     16034 -1.9810e-05
     16036 -4.9355e-08
     22046 -5.8371e-04
     22047 -5.3785e-04
     22048 -5.4424e-03
     22049 -4.0772e-04
     22050 -3.9834e-04
     24050 -4.6453e-03
     24052 -9.3157e-02
     24053 -1.0767e-02
     24054 -2.7306e-03
     25055 -9.8300e-03
     26054 -4.8552e-02
     26056 -7.9035e-01
     26057 -1.8579e-02
     26058 -2.5159e-03
C name: Al
C density = 2.7
m506
     13027 1.0000e+00
C name: Pb
C density = 11.3
```

```
m510
    82204 1.4000e-02
    82206 2.4100e-01
    82207 2.2100e-01
    82208 5.2400e-01
C name: W
C density = 19.25
m512
    74182 0.265
    74183 0.1431
    74184 0.3064
    74186 0.2843
C name: Tantalum
C density = 16.654 g/cc
M900  73181 1
C name: Beryllium
C density = 1.848 g/cc
M901  4009  1
c
***********************************
***********************************
****
c  Tallies
c
***********************************
***********************************
****
c
c FMESH4:p GEOM=xyz ORIGIN = 0 -200
203.1
c      IMESH=450 IINTS=300
c      JMESH=450 JINTS=300
c      KMESH=203.2 KINTS=1
c
tmesh
c rmesh1:p dose 10 $10=icrp21 photon
c rmesh1:n dose 10 $10=icrp21 neutron
c cora1   65  935i  1000.0 $mcnp6 manual
2.8.1 for 18i explan
c corb1  395  1i  400.0
c corc1  130  230i  360.0
c cora1  65   935i  1000.0 $mcnp6 manual
2.8.1 for 18i explan
c corb1  250  250i  500.0
c corc1  135  i  145.0
c
rmesh21:n dose 10 $10=icrp21 neutron
cora21   65  935i  1000.0 $mcnp6 manual
2.8.1 for 18i explan
corb21  250  250i  500.0
corc21  135  1i  145.0
endmd
c
c rmesh31:p dose 10 $10=icrp21 photon
c cora31  70  71.0 $mcnp6 manual 2.8.1 for
18i explan
c corb31  -150  300i  300.0
c corc31  0  300i  320.0
c
c rmesh41:n dose 10 $10=icrp21 neutron
c cora41  70  71.0 $mcnp6 manual 2.8.1 for
18i explan
c corb41  -150  300i  300.0
c corc41  0  300i  320.0
c endmd
c PRDMP mct 1 $write MCTAL file at
problem completion
c
c FMESH4:p GEOM=xyz ORIGIN = 50 24
0  $yz mesh
c      IMESH=250 IINTS=300
c      JMESH=25 JINTS=1
c      KMESH=320 KINTS=300
c
c FMESH4:n GEOM=xyz ORIGIN = 481 -
14 -14
c      IMESH= 501 515 516 516.5 517 529
540
c      IINTS= 10  14  2   10    1   6   11
c      JMESH= 14 JINTS= 14
c      KMESH= 14 KINTS= 14
c
c F4:n 21
c
c mplot file fmesh 4 freq 1
c stop f4 0.05
F5:p 250 50 305   1
F15:n 250 50 305  1
F25:p 70 20 320    1
F35:n 70 20 320    1
c
```

```
c de4 0.01 0.015 0.02 0.03 0.04 0.05 0.06
0.08
c     0.1 0.15 0.2 0.3 0.4 0.5 0.6 0.8 1 1.5 2
c     3 4 5 6 8 10  20 30 40 50 100 200 500
c     1000 2000
c df4 2.78E-06 1.11E-06 5.88E-07 2.56E-07
1.56E-07 1.2E-07  $ c c ICRP21 photon flux
to dose conv factors pg 479 mcp manual
c      1.11E-07 1.2E-07 1.47E-07 2.38E-07
3.45E-07
c      5.56E-07 7.69E-07 9.09E-07 1.14E-06
1.47E-06
c      1.79E-06 2.44E-06 3.03E-06 4.00E-06
4.76E-06
c      5.56E-06 6.25E-06 7.69E-06 9.09E-06
1.56E-05
c      2.26E-05 2.94E-05 3.56E-05 7.11E-06
1.09E-05
c      1.72E-05 2.04E-05 2.32E-05
c
de5 0.01 0.015 0.02 0.03 0.04 0.05 0.06 0.08
    0.1 0.15 0.2 0.3 0.4 0.5 0.6 0.8 1 1.5 2
    3 4 5 6 8 10  20 30 40 50 100 200 500
    1000 2000
df5 2.78E-06 1.11E-06 5.88E-07 2.56E-07
1.56E-07 1.2E-07  $ c c ICRP21 photon flux
to dose conv factors pg 479 mcp manual
     1.11E-07 1.2E-07 1.47E-07 2.38E-07
3.45E-07
     5.56E-07 7.69E-07 9.09E-07 1.14E-06
1.47E-06
     1.79E-06 2.44E-06 3.03E-06 4.00E-06
4.76E-06
     5.56E-06 6.25E-06 7.69E-06 9.09E-06
1.56E-05
     2.26E-05 2.94E-05 3.56E-05 7.11E-06
1.09E-05
     1.72E-05 2.04E-05 2.32E-05
c
de25 0.01 0.015 0.02 0.03 0.04 0.05 0.06
0.08
    0.1 0.15 0.2 0.3 0.4 0.5 0.6 0.8 1 1.5 2
    3 4 5 6 8 10  20 30 40 50 100 200 500
    1000 2000
df25 2.78E-06 1.11E-06 5.88E-07 2.56E-07
1.56E-07 1.2E-07  $ c c ICRP21 photon flux
to dose conv factors pg 479 mcnp manual
     1.11E-07 1.2E-07 1.47E-07 2.38E-07
3.45E-07
     5.56E-07 7.69E-07 9.09E-07 1.14E-06
1.47E-06
     1.79E-06 2.44E-06 3.03E-06 4.00E-06
4.76E-06
     5.56E-06 6.25E-06 7.69E-06 9.09E-06
1.56E-05
     2.26E-05 2.94E-05 3.56E-05 7.11E-06
1.09E-05
     1.72E-05 2.04E-05 2.32E-05
c
de15 2.5e-8 1e-7 1e-6 1e-5 1e-4 1e-3 1e-2 $
NCRP-38, ANSI6.1.1-1977 neutron flux
      1e-1 5e-1 1 2.5 5 7 10 14 20 40 60 $ to
dose rate conv factors
      100 200 300 400                 $ 20
MeV+ DCFs from D. Coissart, in folder
df15 3.67e-6 3.67e-6 4.46e-6 4.54e-6       $
pg.271 mcnp6 user manual
      4.18e-6 3.76e-6 3.56e-6 2.17e-5
      9.26e-5 1.32e-4 1.25e-4 1.56e-4
      1.47e-4 1.47e-4 2.08e-4 2.27e-4
      2.36E-05 1.86E-05 1.35E-05 1.18E-05
      1.18E-05 1.18E-05
c df4 iu=1 fac=1 log IC=20 $ncrp38
c
de35 2.5e-8 1e-7 1e-6 1e-5 1e-4 1e-3 1e-2 $
NCRP-38, ANSI6.1.1-1977 neutron flux
      1e-1 5e-1 1 2.5 5 7 10 14 20 40 60 $ to
dose rate conv factors
      100 200 300 400                 $ 20
MeV+ DCFs from D. Coissart, in folder
df35 3.67e-6 3.67e-6 4.46e-6 4.54e-6       $
pg.271 mcnp6 user manual
      4.18e-6 3.76e-6 3.56e-6 2.17e-5
      9.26e-5 1.32e-4 1.25e-4 1.56e-4
      1.47e-4 1.47e-4 2.08e-4 2.27e-4
      2.36E-05 1.86E-05 1.35E-05 1.18E-05
      1.18E-05 1.18E-05
c
```

14 APPENDIX V, Example Storage-to-Accumulator Electron Bunch Swapping MCNP6 Input Deck

```
ALS-U STA Line charge loss scenarios
c
************************************
************************************
****
c  Cell Cards
c
************************************
************************************
****
c 1 6 -8.96     -1              $SR Cu Target
Collimator
2 6 -8.96     -2              $AR Cu target coll
c
c 11 9 -0.001205 11 -12 -13 14 15 -16
$HVAC penetration
c 12 9 -0.001205 11 -12 -14 23 15 -16
$IMP cell extension
c
c 21 9 -0.001205 21 -22 -23 24 25 -26 $F4
box
c
31 9 -0.001205 -31                $elec
penetration
c
c 34 9 -0.001205  -34 #31   $inner quad air
c 33 6 -8.96 -33 34 #34 #31          $quad
magnet
c 35 3 -7.784 -35 33 #33     $yoke
c
40 0 -41 2 #31 $septum inner vac
41 4 -2.7 -40 #2 #40  #31 $septum al outer
90 9 -0.001205 -90 #2  #31  #40 #41
$SR air
32 9 -0.001205 -32 90 #2 #31  #40 #41
91 1 -2.35 -91 90 #2 #31 #32 #40 #41
$SR concrete
92 1 -2.35 -92 90 91 #2 #31 #32  #40 #41
c
98 9 -0.001205 -99 #2 #31 #32 #40 #41 #90
#91 #92 $outside air
99 0          99          $Kill'm all

c
c
************************************
************************************
****
c  Surface Cards
c
************************************
************************************
****
c 1  box  70 295 134.7  40 0 0   0 10 0  0 0
10  $SR Cu Target Collimator
2  box  70 15 195  5 0 0  0 10 0  0 0 10 $AR
Cu Target Collimator
c
11 pz 162.56 $HVAC Penetration
12 pz 203.2
13 py 0
14 py -45.72
15 px 50.32
16 px 90.32
c
21 pz 162.56 $F4 box
22 pz 203.2
23 py -75.72
24 py -76.72
25 px 50.32
26 px 90.32
c
31 RCC 70.32 0 35.56  0 -100 0  5.08 $elec
pen4" i CY, center at 14"
32 RCC 70.32 65 243.84  0 0 30.48  15
$roof pen 12"dia
c
33 RCC 55 50.22 203.2  20 0 0  12.6 $quad
outer 0.1m
34 RCC 55 50.22 203.2  20 0 0  8.21   $quad
inner 0.05m
35 RCC 60 50.22 203.2  10.8 0 0  16.8
$yoke
```

```
c
40 box 55 10 190  100 0 0  0 40 0  0 0 26
$injection septum box outer
41 box 56 11 191  98 0 0   0 38 0  0 0 24
$inject septum inner 1cm
c 90 box -30.48 0 0   660.98 0 0            0
400 0   0 0 243.84  $inside SR air
c 91 box -30.48 -45.72 -30.48   660.98 0 0
0 477 0   0 0 304.8   $SR Concrete
c
c
90 box -30.48 0 0   660.98 0 0            0 400
0   0 0 243.84  $inside SR air
91 box -30.48 -50 -30.48   130 0 0   0 481.28
0   0 0 304.8 $320.04 SR Concrete 406mm
roof
92 box 99.52 -50 -30.48      530.98 0 0  0
481.28 0  0 0 304.8   $SR concrete 254mm
roof
c
99 box -250 -250 -250    1000 0 0  0 1000 0
0 0 1000  $Universe

c
***********************************
***********************************
****
c  Data Cards
c
***********************************
***********************************
****
c
***********************************
***********************************
****
c  Source
c
***********************************
***********************************
****
imp:e  1 1 1 1 1  1 1 1 1  0
imp:p  1 1 1 1 1  1 1 1 1  0
imp:n  1 1 1 1 1  1 1 100 100  0
elpt:e  .1 .1 .1 .1 .1 .1 .1 .1 .1 .1 $cell by cell
E Cut
elpt:p .1 .1 .1 .1 .1 .1 .1 .1 .1 .1
elpt:n  .001 .001 .001 .001 .001 .001 .001
.001 .001 .001
mode e p n
nps 1e6 $2e7 failed after 7hr
PRDMP -100 -100 1 $write MCTAL file at
problem completion
c read file=sdef_ALSU_AR_bbrem.txt
$ource info in sdef.txt
sdef par=3 erg=2000.0 pos d1 vec= 1 -
0.174533 0 ara 0.1 dir=1 $x=60 y=300
z=140 SR source
c sdef par=3 erg=2000.0 pos d1 vec 1 -
0.31125 0.21875 ara 0.1 dir 1
$0.002999996=2mrad,5X = 0.015
c SI1 L 60 300 140    60 68.58 203.2
SI1 L 69 20 200
SP1   1.0
bbrem 1.0 1.0 46i 10.0 1
phys:p 2000 0 0 -1 0 J 0   $Photonnuclear
ON
c phys:p 2000 0 0 0 0 J 0    $Photonuclear
OFF
phys:e 2000    $upper limit for p particle E
phys:n 2000    $upper limit for p particle E
MPHYS ON
c
***********************************
***********************************
****
c  Materials
c
***********************************
***********************************
****
C name: Concrete as specified in Chilton, pg
374
C density = 2.35 g/cc
M1      1001  -0.013
         8016  -1.165
        14000  -0.737
        20000  -0.194
        11023  -0.040
        12000  -0.006
        13027  -0.107
        16032  -0.003
```

```
      19000  -0.045
      26000  -0.029
C name: Sand (dry)
C density = 1.6 g/cc
M2   14000 1 8016 2
C name: Simple Iron
C density = 7.874 g/cc
M3   26000 1
C name: Aluminum
C density = 2.7 g/cc
M4   13027 1
C name: Copper
C density = 8.96 g/cc
M6   29063 -.6917 29065 -.3083
C name: Air (dry, sea level)
C density = 0.001205 g/cc
m9    6000       -0.000124
      8016       -0.231781
      7014       -0.755268
      18000      -0.012827
C name: Pb
C density = 11.34
m10
     82204 -1.4000e-02
     82206 -2.4100e-01
     82207 -2.2100e-01
     82208 -5.2400e-01
C
c name: aluminum oxide doped with
Chromium (~6% wgt)
c density = 3.97 g/cc
m11  8016 -0.470749
     13027 -0.529251
     24000 -0.06
C name: Stainless Steel 409
C density = 7.8
m502
     6012 -7.8085e-04
     6013 -9.1516e-06
     14028 -9.0305e-03
     14029 -4.7515e-04
     14030 -3.2438e-04
     15031 -4.4000e-04
     16032 -4.1675e-04
     16033 -3.3933e-06
     16034 -1.9810e-05
     16036 -4.9355e-08
     22046 -5.8371e-04
     22047 -5.3785e-04
     22048 -5.4424e-03
     22049 -4.0772e-04
     22050 -3.9834e-04
     24050 -4.6453e-03
     24052 -9.3157e-02
     24053 -1.0767e-02
     24054 -2.7306e-03
     25055 -9.8300e-03
     26054 -4.8552e-02
     26056 -7.9035e-01
     26057 -1.8579e-02
     26058 -2.5159e-03
C name: Al
C density = 2.7
m506
     13027 1.0000e+00
C name: Pb
C density = 11.3
m510
     82204 1.4000e-02
     82206 2.4100e-01
     82207 2.2100e-01
     82208 5.2400e-01
C name: W
C density = 19.25
m512
     74182 0.265
     74183 0.1431
     74184 0.3064
     74186 0.2843
C name: Tantalum
C density = 16.654 g/cc
M900  73181 1
C name: Beryllium
C density = 1.848 g/cc
M901  4009  1
c
***********************************
***********************************
****
c  Tallies
c
***********************************
```

```
*************************************
****
c
c FMESH4:p GEOM=xyz ORIGIN = 0 -200
203.1
c      IMESH=450 IINTS=300
c      JMESH=450 JINTS=300
c      KMESH=203.2 KINTS=1
c
tmesh
rmesh1:p dose 10 $10=icrp21 photon
cora1  65   635i  700.0 $mcnp6 manual 2.8.1
for 18i explan
corb1  -85  185i  100.0
corc1  180  130i  310.0
c
rmesh21:n dose 10 $10=icrp21 neutron
cora21   65  285i  350.0 $mcnp6 manual
2.8.1 for 18i explan
corb21  -85  185i  100.0
corc21  180  130i  310.0
endmd
c
c rmesh31:p dose 10 $10=icrp21 photon
c cora31  70  71.0 $mcnp6 manual 2.8.1 for
18i explan
c corb31  -150  300i  300.0
c corc31  0  300i  320.0
c
c rmesh41:n dose 10 $10=icrp21 neutron
c cora41  70  71.0 $mcnp6 manual 2.8.1 for
18i explan
c corb41  -150  300i  300.0
c corc41  0  300i  320.0
c endmd
c PRDMP mct 1 $write MCTAL file at
problem completion
c
c FMESH4:p GEOM=xyz ORIGIN = 50 24
0  $yz mesh
c      IMESH=250 IINTS=300
c      JMESH=25 JINTS=1
c      KMESH=320 KINTS=300
c
c FMESH4:n GEOM=xyz ORIGIN = 481 -
14 -14
c      IMESH= 501 515 516 516.5 517 529
540
c      IINTS= 10  14  2   10    1   6   11
c      JMESH= 14 JINTS= 14
c      KMESH= 14 KINTS= 14
c
c F4:n 21
c
c mplot file fmesh 4 freq 1
c stop f4 0.05
F5:p 250 50 305   1
F15:n 250 50 305  1
F25:p 70 20 320    1
F35:n 70 20 320    1
c
c de4 0.01 0.015 0.02 0.03 0.04 0.05 0.06
0.08
c     0.1 0.15 0.2 0.3 0.4 0.5 0.6 0.8 1 1.5 2
c     3 4 5 6 8 10  20 30 40 50 100 200 500
c     1000 2000
c df4 2.78E-06 1.11E-06 5.88E-07 2.56E-07
1.56E-07 1.2E-07  $ c c ICRP21 photon flux
to dose conv factors pg 479 mcp manual
c      1.11E-07 1.2E-07 1.47E-07 2.38E-07
3.45E-07
c      5.56E-07 7.69E-07 9.09E-07 1.14E-06
1.47E-06
c      1.79E-06 2.44E-06 3.03E-06 4.00E-06
4.76E-06
c      5.56E-06 6.25E-06 7.69E-06 9.09E-06
1.56E-05
c      2.26E-05 2.94E-05 3.56E-05 7.11E-06
1.09E-05
c      1.72E-05 2.04E-05 2.32E-05
c
de5 0.01 0.015 0.02 0.03 0.04 0.05 0.06 0.08
    0.1 0.15 0.2 0.3 0.4 0.5 0.6 0.8 1 1.5 2
    3 4 5 6 8 10  20 30 40 50 100 200 500
    1000 2000
df5 2.78E-06 1.11E-06 5.88E-07 2.56E-07
1.56E-07 1.2E-07  $ c c ICRP21 photon flux
to dose conv factors pg 479 mcp manual
     1.11E-07 1.2E-07 1.47E-07 2.38E-07
3.45E-07
     5.56E-07 7.69E-07 9.09E-07 1.14E-06
1.47E-06
```

```
     1.79E-06 2.44E-06 3.03E-06 4.00E-06
4.76E-06
     5.56E-06 6.25E-06 7.69E-06 9.09E-06
1.56E-05
     2.26E-05 2.94E-05 3.56E-05 7.11E-06
1.09E-05
     1.72E-05 2.04E-05 2.32E-05
c
de25 0.01 0.015 0.02 0.03 0.04 0.05 0.06
0.08
    0.1 0.15 0.2 0.3 0.4 0.5 0.6 0.8 1 1.5 2
    3 4 5 6 8 10  20 30 40 50 100 200 500
    1000 2000
df25 2.78E-06 1.11E-06 5.88E-07 2.56E-07
1.56E-07 1.2E-07  $ c c ICRP21 photon flux
to dose conv factors pg 479 mcnp manual
     1.11E-07 1.2E-07 1.47E-07 2.38E-07
3.45E-07
     5.56E-07 7.69E-07 9.09E-07 1.14E-06
1.47E-06
     1.79E-06 2.44E-06 3.03E-06 4.00E-06
4.76E-06
     5.56E-06 6.25E-06 7.69E-06 9.09E-06
1.56E-05
     2.26E-05 2.94E-05 3.56E-05 7.11E-06
1.09E-05
     1.72E-05 2.04E-05 2.32E-05
c
de15 2.5e-8 1e-7 1e-6 1e-5 1e-4 1e-3 1e-2 $
NCRP-38, ANSI6.1.1-1977 neutron flux
      1e-1 5e-1 1 2.5 5 7 10 14 20 40 60 $ to
dose rate conv factors
      100 200 300 400                 $ 20
MeV+ DCFs from D. Coissart, in folder
df15 3.67e-6 3.67e-6 4.46e-6 4.54e-6       $
pg.271 mcnp6 user manual
      4.18e-6 3.76e-6 3.56e-6 2.17e-5
      9.26e-5 1.32e-4 1.25e-4 1.56e-4
      1.47e-4 1.47e-4 2.08e-4 2.27e-4
      2.36E-05 1.86E-05 1.35E-05 1.18E-05
      1.18E-05 1.18E-05
c df4 iu=1 fac=1 log IC=20 $ncrp38
c
de35 2.5e-8 1e-7 1e-6 1e-5 1e-4 1e-3 1e-2 $
NCRP-38, ANSI6.1.1-1977 neutron flux
      1e-1 5e-1 1 2.5 5 7 10 14 20 40 60 $ to
dose rate conv factors
      100 200 300 400                 $ 20
MeV+ DCFs from D. Coissart, in folder
df35 3.67e-6 3.67e-6 4.46e-6 4.54e-6       $
pg.271 mcnp6 user manual
      4.18e-6 3.76e-6 3.56e-6 2.17e-5
      9.26e-5 1.32e-4 1.25e-4 1.56e-4
      1.47e-4 1.47e-4 2.08e-4 2.27e-4
      2.36E-05 1.86E-05 1.35E-05 1.18E-05
      1.18E-05 1.18E-05
c
c e4 0 5.00E-10 2.00E-09 5.00E-09 1.00E-
08 $h histogram linear interpolation of E
within bin boundary
c     1.45E-08 2.10E-08 3.00E-08 4.00E-08
$MeV bins
c     5.00E-08 7.00E-08 1.00E-07 1.25E-07
c     1.50E-07 1.84E-07 2.25E-07 2.75E-07
c     3.25E-07 3.67E-07 4.14E-07 5.00E-07
c     5.32E-07 6.25E-07 6.83E-07 8.00E-07
c     8.76E-07 1.00E-06 1.04E-06 1.08E-06
c     1.13E-06 1.30E-06 1.45E-06 1.86E-06
c     2.38E-06 3.06E-06 3.93E-06 5.04E-06
c     6.48E-06 8.32E-06 1.07E-05 1.37E-05
c     1.76E-05 2.26E-05 2.90E-05 3.73E-05
c     4.79E-05 6.14E-05 7.89E-05 1.01E-04
c     1.30E-04 1.67E-04 2.14E-04 2.75E-04
c     3.54E-04 4.54E-04 5.83E-04 7.49E-04
c     9.61E-04 1.23E-03 1.58E-03 2.03E-03
c     2.25E-03 2.49E-03 2.61E-03 2.75E-03
c     3.04E-03 3.35E-03 3.71E-03 4.31E-03
c     5.53E-03 7.10E-03 9.12E-03 1.06E-02
c     1.17E-02 1.50E-02 1.93E-02 2.19E-02
c     2.36E-02 2.42E-02 2.48E-02 2.61E-02
c     2.70E-02 2.85E-02 3.18E-02 3.43E-02
c     4.09E-02 4.63E-02 5.25E-02 5.66E-02
c     6.74E-02 7.20E-02 7.95E-02 8.25E-02
c     8.65E-02 9.80E-02 1.11E-01 1.17E-01
c     1.23E-01 1.29E-01 1.36E-01 1.43E-01
c     1.50E-01 1.58E-01 1.66E-01 1.74E-01
c     1.83E-01 1.93E-01 2.02E-01 2.13E-01
c     2.24E-01 2.35E-01 2.47E-01 2.73E-01
c     2.87E-01 2.95E-01 2.97E-01 2.98E-01
c     3.02E-01 3.34E-01 3.69E-01 3.88E-01
c     4.08E-01 4.50E-01 4.98E-01 5.23E-01
```

c 5.50E-01 5.78E-01 6.08E-01 6.39E-01
c 6.72E-01 7.07E-01 7.43E-01 7.81E-01
c 8.21E-01 8.63E-01 9.07E-01 9.62E-01
c 1.00E+00 1.11E+00 1.16E+00
1.22E+00
c 1.29E+00 1.35E+00 1.42E+00
1.50E+00
c 1.57E+00 1.65E+00 1.74E+00
1.83E+00
c 1.92E+00 2.02E+00 2.12E+00
2.23E+00
c 2.31E+00 2.35E+00 2.37E+00
2.39E+00
c 2.47E+00 2.59E+00 2.73E+00
2.87E+00
c 3.01E+00 3.17E+00 3.33E+00
3.68E+00
c 4.07E+00 4.49E+00 4.72E+00
4.97E+00
c 5.22E+00 5.49E+00 5.77E+00
6.07E+00
c 6.38E+00 6.59E+00 6.70E+00
7.05E+00
c 7.41E+00 7.79E+00 8.19E+00
8.61E+00
c 9.05E+00 9.51E+00 1.00E+01
1.05E+01
c 1.11E+01 1.16E+01 1.22E+01
1.25E+01
c 1.28E+01 1.35E+01 1.38E+01
1.42E+01
c 1.46E+01 1.49E+01 1.57E+01
1.65E+01
c 1.69E+01 1.73E+01 1.96E+01
2.00E+01
c 3.00E+01 4.00E+01 5.00E+01
6.00E+01
c 7.00E+01 8.00E+01 9.00E+01
1.00E+02
c 2.00E+02 3.00E+02 4.00E+02
5.00E+02
c 6.00E+02 7.00E+02 8.00E+02
9.00E+02
c 1.00E+03 2.00E+03